UNIVERSITY OF CALIFORNIA SAN DIEGO

SAN DIEGO STATE UNIVERSITY

Dissecting the cellular biology of the model methanotroph *Methylotuvimicrobium alcaliphilum* 20Z^{R} through multi-omics, mutagenesis, and microscopy

A dissertation submitted in partial satisfaction of the
requirements for the degree Doctor of Philosophy

in

Biology

by

David Andrew Inniss Collins

Committee in charge:

San Diego State University

Professor Marina G. Kalyuzhnaya, Chair
Professor Terrence Frey
Professor Nicholas Shikuma

University of California San Diego

Professor Joe Pogliano
Professor Kit Pogliano

2021

The dissertation David Andrew Inniss Collins is approved, and it is acceptable in quality and form for publication on microfilm and electronically.

_____

_____

_____

_____

_____
Chair

University of California San Diego

San Diego State University

2021

DEDICATION

A substantial portion of this work is dedicated to my husband, John Inniss Collins. I'm thankful for his patience, support, and exuberance for my research during graduate school. I'm lucky to have a partner in life who can interrogate my scientific passions as well as enjoy debates about music, movies, and politics with me.

My family is also due a portion of this dedication. I can always count on my parents Shawn and Melanie to pepper me with important questions about bacteria during every family gathering. My siblings Timothy, Matthew, Christian, Jonathan, and Katie likewise will never grow tired of my answer to questions outside of my writ of "I don't know I'm just a microbiologist". For their support and love I am very grateful.

Lastly, I'd like to also dedicate part of this work to Dr. Veronica Casas & Dr. Stanley Maloy who were inspirational to me as younger scientist and introduced me to the wonders of the bacteriophage lifecycle. They are both incredible communicators of their passions for microbiology, easily captivating me with the wonders of unseen life on the planet.

EPIGRAPH

"The most merciful thing in the world, I think, is the inability of the human mind to correlate all its contents. We live on a placid island of ignorance in the midst of black seas of infinity, and it was not meant that we should voyage far. The sciences, each straining in its own direction, have hitherto harmed us little; but some day the piecing together of dissociated knowledge will open up such terrifying vistas of reality, and of our frightful position therein, that we shall either go mad from the revelation or flee from the deadly light into the peace and safety of a new dark age."

-H.P. Lovecraft,

February 1928

47°9′S 123°43′W

TABLE OF CONTENTS

LIST OF FIGURES

LIST OF TABLES

LIST OF GRAPHS

ACKNOWLEDGEMENTS

I would like to acknowledge Professor Marina G. Kalyuzhnaya for her support as the chair of my committee and PI of the C_1 Biocatalysis lab at San Diego State University. Her guidance and insights have been appreciated throughout my years with her in the lab. I am grateful for her passion of microbial metabolism and for introducing me to a wide world of microorganisms that I began knowing very little about.

I also must acknowledge the other scientists of the C_1 Biocatalysis lab who are an exceptional group of researchers, students, and friends. They are an incredibly patient and supportive lot whose helpfulness and talents will be missed. Particularly I must acknowledge Richard Hamilton III for help with many aspects of my research as it truly takes a team to run a bioreactor and with whom I can commiserate in double and triple checking for methane leaks in the lab.

Chapter 1 contains material published by Collins DA & Kalyuzhnaya MG. (2018) “Navigating methane metabolism: Enzymes, compartments, and networks” in Methods in Enzymology **613**:349-383. doi: 10.1016/bs.mie.2018.10.010. The dissertation author was the primary investigator and author of this paper.

Chapter 2, in part is currently being prepared for submission for publication of the material by Collins, D., Hamilton, R., Krutkin, D.D., Kalyuzhnaya, M.G. (2021) as “Copper availability controls cell structure, cell energetics and MxaF/XoxF expression in *Methylotuvimirobium alcaliphilum* $20Z^R$, a model methanotroph possessing only

particulate methane-monooxygenase". The dissertation author is the primary investigator and author of this material.

Chapter 3, in full, contains material and data that will be submitted as "Genetic elements of surface layer protein" in Molecular Microbiology (2021) by Collins, D., Vazquez, A.V., Kalyuzhnaya, M. The dissertation author is the primary investigator and author of this material.

Chapter 4, in part references data published by Ortega, D., Subramanian, P., Mann, P., Kjaer, A., Watts, K., Pirbadian, S., Collins, D., Kooger, R., Kalyuzhnaya, M., Pilhofer, M., Ringgaard, S., Briegel, A., Jensen, G. as "Repurposing a chemosensory macromolecular machine" (2020) in Nature Communications. The dissertation author was a contributing investigator and author of this material.

VITA

2015	Bachelor of Sciences, Microbiology
	San Diego State University, Summa cum Laude
2016-2019	Teaching Assistant, San Diego State University
	General Microbiology, Electron Microscopy, Cell & Molecular Biology
2017-2018	Graduate Research Fellow, Intrexon
2018-2019	Graduate Research Fellow, San Diego State University
2019	NSF iCorps Summer Sprint Fellow, San Diego State University
2021	Doctor of Philosophy, Biology
	University of California San Diego, San Diego State University

PUBLICATIONS

Collins, D., Hamilton, R., Krutkin, D.D., Akberdin, I., Adkins, J., Kalyuzhnaya, M. (2021). Copper availability controls cell structure, cell energetics and MxaF/XoxF expression in *Methylotuvimirobium alcaliphilum* 20Z^{R}, a model methanotroph possessing only particulate methane-monooxygenase. In Preparation

Collins, D., Vazquez, A.V., Kalyuzhnaya, M.G. (2021). Genetic elements of surface layer protein. In Preparation.

Ortega, D., Subramanian, P., Mann, P., Kjaer, A., Watts, K., Pirbadian, S., **Collins, D.**, Kooger, R., Kalyuzhnaya, M., Pilhofer, M., Ringgaard, S., Briegel, A., Jensen, G. (2020). Repurposing a chemosensory macromolecular machine. Nature Communications.

Chistersodova, L., **Collins, D**., Kalyuzhnaya, M. (2019). Microbial Cycling of Methane. Reference Module in Life Sciences. Elsevier https://doi.org/10.1016/B978-0-12-809633-8.90670-8.

Collins, D., Kalyuzhnaya, M. (2018). Navigating methane metabolism: enzymes, compartments, and networks. Methods in Enzymology. Vol 613.

Akberdin, I., **Collins, D**., Hamilton, R., Oshchepkov, D., Shukla, A., Nicora, C., Nakayaku, E., Adkins, J., Kalyuzhanaya, M. (2018). Rare Earth Elements Alter Redox Balance in *Methylomicrobium alcaliphilu*m 20Z^R. Frontiers in Microbiology doi: 10.3389/fmicb.2018.02735

Collins, D., Akberdin, I., Kalyuzhnaya, M. (2017). Methylobacter. Bergey's Manual of Systematics of Archaea and Bacteria. Wiley. https://doi.org/10.1002/9781118960608.gbm01179.pub2

FIELDS OF STUDY

Major Field: Cell and Molecular Biology of Bacteria
Professor Marina G. Kalyuzhnaya

Expertise in Transmission and Scanning Electron Microscopy
Under Dr. Ingrid Niesman, Dr. Steve Barlow, Dr. Rick Bizzoco

ABSTRACT OF THE DISSERTATION

Dissecting the cellular biology of the model methanotroph *Methylotuvimicrobium alcaliphilum* 20Z^{R} through multi-omics, mutagenesis, and microscopy

by

David Andrew Inniss Collins

Doctor of Philosophy in Biology

University of California San Diego, 2021

San Diego State University, 2021

Professor Marina G. Kalyuzhnaya, Chair

Methane levels have rapidly increased in concentration in the atmosphere due to anthropogenic inputs making it a crucial abatement target against global climate change. The aerobic methanotrophs are bacteria capable of growth solely on methane as substrate and are genetically tractable and amenable to large scale fermentation making them ideal model system for the engineering of C_1- biocatalysts. In this dissertation I examine the effects of trace minerals and substrate on the cell performance of *Methylotuvimicrobium alcaliphilum* 20Z^{R} by contextualizing multi-omics with structural characterization through electron microscopy. This reveals the development of the intracytoplasmic membrane network within the cell which is affected

by metals and leads to the increased gas consumption. Occupying the cell volume with membranes leads to an overflow metabolic state in conditions with sufficient substrate and oxygen in which fermentation products such as formate are excreted.. The nature of structural features revealed by microscopy is explored to determine the genetic elements for expression and transport of the surface layer protein. Genes responsible for the large and small proteins of the surface layer protein matrix are identified and a Type 1 Secretion System is explored as the potential mechanism of export for this cell surface feature. Concluding with an exploration of a novel methane chemotactic phenotype, which was identified by structural modelling and confirmed through a methane-based chemotaxis assay. This work demonstrates the importance of tying systems-level data such as proteomics with structural information gathered by electron microscopy to explain and explore phenotypes of performance such as growth rate and substrate consumption to cell biology of a model organism used as a methane-based biotechnology strain.

INTRODUCTION

Methane, Man, and the Atmosphere

Methane (CH_4) is the smallest hydrocarbon and a powerful greenhouse gas that escapes into the atmosphere from many natural sources from the biosphere (Case, *et al.* 2015) and increasingly anthropogenic sources (Nazaries, *et al.* 2013). The largest natural sources of methane are dominated by the saturated anaerobic wetland ecosystem production (Kirschke *et al.* 2013), emissions from lakes, and the large biomass of pelagic microbes such as SAR11 in the open ocean (Carini, *et al.* (2014).)

There also exists a large amount of methane which is captured in frozen forms in the ocean and within continents in the form of submarine gas hydrates and within Arctic permafrost (McCalley, *et al.* 2014). Hydrates sequester methane within crystalline cages of water and are subject to release during geological upheaval or due to increasing ambient water temperatures. Ocean seeps of methane that also occur along continental margins can originate from these hydrates (Skarke, *et al.* 2014), hydrocarbon deposits or from geological processes such as mud volcanism such as those seen the Haakon Mosby mud volcano (Niemann, *et al.* 2006). Reports of craters and chasms in melting permafrost point to evidence of methane release from the subsurface as these deposits appear to be more sensitive to changes in global temperature then with compared to the deep-sea methane hydrates (Moskvitch 2014).

These natural sources do not explain why the Global atmospheric methane concentrations have been increasing (Figure 0.1) since the mid 1980's (Dlugokencky, 2021). The steadily rising concentrations of add methane in the atmosphere are a clear indictment of the role of man in contributing today increase of the global carbon budget

(Jackson, *et al.* 2020). These emissions are known to contribute to the greenhouse effect by altering composition of the atmosphere and Methane is a the second most abundant greenhouse gas after CO_2. The contributions of modern society have resulted in about 3 times as higher concentration in the atmosphere since the 1750's due to industrialization and modernization of society (Montzka, *et al.* 2011). It should be appreciated that methane usage as a fossil fuel impacts the lives of people across the globe as it constitutes a cheap heating and cooking fuel. This reliance on methane in energy infrastructure is not without consequences (Conley, *et al.* 2016), leaks are increasingly common in aging gas distribution systems and cataclysmic failures can result in massive emissions which can have regional disruptions to the lives of residents (Pandey, *et al.* 2019). The impacts from agriculture also have increased as the demand for livestock has increased globally it is predicted to increase as the standard of living and demands for animal products increase (Jackson, *et al.* 2020). Methane gas concentrations are increasing in the atmosphere unequivocally contributes to global temperature increases. This presents a feedback in which warming will result in greater release of sequestered methane sinks like permafrost and oceanic hydrates, resulting in increased atmospheric greenhouse gas release (Yvon-Durocher, *et al.* 2014).

Of methane and microbes

Fugitive methane is not solely a waste product, the carbon derived from it drives productivity in many ecosystems such as in the deep sea by chemosynthetic microbe communities within invertebrates (Kiel & Hansen 2015) as well as and in aquatic communities on in the arctic (He, *et al.* 2015). Many clades of microbes such as

bacteria and Archaea have the capability to grow on C_1 compounds like methane as their carbon and energy source, collectively those that utilize methane are known as Methanotrophs (Anthony 1982).

These microbes often are the basis of many food chains in ecosystems, converting methane to biomass as a form of primary microbial productivity (Ho, *et al* 2014). These microbes can be free living organisms, living as epibionts of invertebrates such as arthropods (Watsuji, *et al.* 2014), and remarkably have been observed as endosymbionts. These endosymbiotic methanotrophs reside within specialized bacteriocytes of deep ocean organisms such as bivalves *Bathymodiolus* (Fiala-Medioni, *et al.* 2002). The abundance of methane within the biosphere has enabled methanotrophic clades of bacteria and archaea to become ubiquitous throughout terrestrial biomes as varied as deserts to wetlands (Bull, *et al.* 2000), oceanic niches (Ruff, *et al.* 2015), and extreme environments such as (halo)alkaline lakes (Trotsenko & Khmelenina, 2001).

Diversity of Methanotrophs

Methane oxidation is aerobically tied to oxygen reduction or anaerobically to electron acceptors such as sulfate and nitrate by bacteria in the Alphaproteobacteria, Gammaproteobacteria, Verrucomicrobia, NC10 phyla and among consortia *Archaea* species as well. Gammaproteobacteria constitute the largest group of methanotrophs, throughout several aerobic and anaerobic ecosystems such as freshwater (Trimmer, *et al.* 2015), marine (Tavormina, *et al.* 2010), and terrestrially among the rhizosphere of plants (Lee, *et al.* 2015), and associated with human microbiomes (Clemente, *et al.*

2015). Alphaproteobacteria have been isolated from diverse environments as well and can electron acceptors such as oxygen or nitrate for anaerobic methane oxidation (Dam, *et al.* 2013). Veruccomicrobia methanotrophs have been identified across many ranges of pH including extremely acidic environments (Pol, *et al.* 2007) and are capable of methanotrophy aerobically and anaerobically (van Teeseling, *et al.* 2014).

The candidate phylum NC10 have been identified in wastewater treatment plants and as well as marine environments but have not been isolated in pure cultures (Gonzalez-Gil, *et al.* 2015), and are capable of anaerobic methane oxidation utilizing nitrate (Ettwig, *et al.* 2009).

Members of *Archaea* such as ANME1 and ANME2 are perform anaerobic methane oxidation but often grow in consortia with various bacteria (McGlynn, *et al.* 2015). This consortia approach involves a modular metabolism between the closely growing Archaea and bacterial partner where electrons are passed from archaeon to bacterium through extracellular cytochromes which function as intercellular wires (Wegener, *et al.* 2015). This association is not essential for the archaeal partner as it can be performed *in vitro* as a pure culture of ANME Archaea when supplied with an appropriate chemical electron acceptor (Scheller, *et al.* 2016).

Membranes and metabolism

Ultrastructure is a crucially the unifying feature among the proteobacterial methanotrophs as their intracellular features are easy identifiable via transmission electron microscopy (Weaver & Dugan, 1975). Oxidation of methane was seen to coincide with compact stacks of membranous organelles called intracytoplasmic

membranes (ICMs) observed within many bacterial methanotrophs, largely absent in Veruccomicrobia and NC10 phyla and entirely absent in ANME. These ICMs form in various orientations, either as sheets parallel (type II) or perpendicularly (type I) to the cytoplasmic membrane. Investigations of these intracytoplasmic membranes as they function in relationship to culture conditions in *M. alcaliphilum* $20Z^R$ is further examined within Chapter 2.

M. alcaliphilum possess membrane bound particulate methane monooxygenase (pMmo) to aerobically oxidize methane into methanol (CH_3OH), which is then oxidized to formaldehyde (CH_2O) by methanol dehydrogenase. Formaldehyde can then be incorporated into biomass via hexulose-phosphate synthase (hps) and hexulose-phosphate isomerase (hpi) or used to generate NADH through formate dehydrogenase (Kalyuzhnaya, *et al.* 2013). Coupling of redox potential in which NADH acts as the reductant to supply pMMO with electrons is not supported by growth rates or substrate consumption rates (de la Torre, *et al.* 2015). Direct coupling of methane oxidation to methanol oxidation posits an interaction between pMMO and MDH that is supported by some biochemical associations between the two enzymes (Culpepper & Rosenzweig, 2014). The possible mechanisms of reducing power supplied to pMMO to begin methane oxidation warrants additional research considering the distribution of methane oxidation. A schematic summary of the metabolism in *M. alcaliphilum* $20Z^R$ is displayed in Figure 0.1. It should be noted that compartmentalization of major reactions and methane metabolism depicted in the figure of *M. alcaliphilum* $20Z^R$ is also addressed in chapter 2. Other structural features unrelated to metabolism are important among methanotrophs including the observation of a surface layer protein which are structures

examined further in Chapter 3. Other unanswered aspects about the cell biology of *M. alcaliphilum* 20Z^R include how these bacteria sense substrates in their environment which is the topic of Chapter 4.

Methanotrophs are a potentially powerful biocatalyst for the mitigation of emissions as well as a potential platform to produce value-added chemical precursors that can be produced from methane or biogas feedstock (Kalyuzhnaya, *et al.* 2015). Deciphering the metabolic networks and proteomic changes in cells under various conditions is crucial to understanding the conditions for optimal biotechnologies involving production of biomass or metabolites using a microbe like *M. alcaliphilum* 20Z^R. The goal of the research presented in my dissertation is to examine the cell biology of the model methanotroph *M. alcaliphilum* 20Z^R using multi-omics paired with structural analysis of cells using microscopy (Chapter 1) to answer questions related to growth performance in response to trace minerals and substrate and during culturing conditions (Chapter 2), the genetic elements responsible for the surface layer protein (Chapter 3) and concluding in an examination of chemotaxis towards methane (Chapter 4).

References

Anthony, C. (1982). The Biochemistry of Methylotrophs. Academic Press.

Brantner, C.A., Buchholz, L.A., Remsen, C.C., Collins, M.P. (2000). Isolation of intracytoplasmic membrane from the methanotrophic bacterium *Methylomicrobium album* BG8. Current Microbiology **40**:132–134.

Bull, I.D., Parekh, N.R., Hall, G.H., Ineson, P., Evershed, R.P. (2000). Detection and classification of atmospheric methane oxidizing bacteria in soil. Nature **405**:175–178.

Carini, P., White, A.E., Campbell, E.O., Giovannoni, S.J. (2014). Methane production by phosphate-starved SAR11 chemoheterotrophic marine bacteria. Nature Communications **5**:4346.

Case, D.H., Pasulka, A.L., Marlow, J.J., Grupe, B.M., Levin, L.A., Orphan, V.J. (2015). Methane seep carbonates host distinct, diverse, and dynamic microbial assemblages. MBio **6**(6):e01348-15. doi:10.1128/mBio.01348-15.

Clemente, J.C., Pehrsson, E.C., Blaser, M.J., Sandhu, K., Gao, Z., Wang, B., Magris, M., Hidalgo, G., Contreras, M., Noya-Alarcon, O., Lander, O., McDonald, J., Cox, M., Walters, J., Oh, P.L., Ruiz, J.F., Rodriguez, S., Shen, N., Song, S.J., Metcalf, J., Knight, R., Dantas, G., Dominguez-Bello, M.G. (2015). The microbiome of uncontacted Amerindians. Science Advances **1**(3):e1500183 (2015).

Conley, S., Franco, G., Faloona, I., Blake, D.R., Peischl, J., Ryerson, T.B. (2016). Methane emissions from the 2015 Aliso Canyon blowout in Los Angeles, CA. Science **351**(6279):1317-1320. DOI: 10.1126/science.aaf2348.

Culpepper, M.A., Rosenzweig, A.C. (2014). Structure and protein-protein interactions of methanol dehydrogenase from *Methylococcus capsulatus* (Bath). Biochemistry **53**:6211–6219.

Dam, B., Dam, S., Blom, J. & Liesack, W. (2013). Genome analysis coupled with physiological studies reveals a diverse nitrogen metabolism in *Methylocystis sp.* Strain SC2. PLoS One. doi:10.1371/journal.pone.0074767.

de la Torre, A., Metivier, A., Chu, F., Laurens, L.M., Beck, D.A.C., Pienkos, P.T., Lidstrom, M.E., Kalyuzhnaya, M.G. (2015). Genome-scale metabolic reconstructions and theoretical investigation of methane conversion in *Methylomicrobium buryatense* strain 5G(B1). Microbial Cell Factories **14**:188.

Dlugokencky, E.J., NOAA/ESRL. Global monthly mean CH_4. www.esrl.noaa.gov/gmd/ccgg/trends_ch (2021).

Ettwig, K.F., van Alen, T., van de Pas-Schoonen, K.T., Jetten, M.S.M., Strous, M. (2009). Enrichment and molecular detection of denitrifying methanotrophic bacteria of the NC10 phylum. Applied Environmental Microbiology. doi:10.1128/AEM.00067-09

Fiala-Médioni, A., McKiness, Z., Dando, P., Boulegue, J., Mariotti, A., Alayse-Danet, A., Robinson, J., Cavanaugh, C. (2002) Ultrastructural, biochemical, and immunological characterization of two populations of the mytilid mussel *Bathymodiolus azoricus* from the Mid-Atlantic Ridge: Evidence for a dual symbiosis. Marine Biology **141**:1035-1043 doi:10.1007/s00227-002-0903-9

Gonzalez-Gil, G., Sougrat, R., Behzad, A.R., Lens, P.N.L., Saikaly, P.E. (2015). Microbial community composition and ultrastructure of granules from a full-scale anammox reactor. Microbial Ecology **70**:118–131.

He, R., Wooller, M.J., Pohlman, J.W., Tiedje, J.M. & Leigh, M.B. (2015). Methane-derived carbon flow through microbial communities in arctic lake sediments. Environmental Microbiology. doi:10.1111/1462-2920.12773.

Ho, A., de Roy, K., Thas, O., de Neve, J., Hoefman, S., Vandamme, P., Heylen, K., Boon, N. (2014). The more, the merrier: heterotroph richness stimulates methanotrophic activity. ISME Journal **8:**1945–1948.

Jackson, R.B., Saunois, M., Bousquet, P., Canadell, J.G., Poulter, B., Stavert, A.R., Bergamaschi, P., Niwa, Y., Segers, A., Tsuruta, A. (2020). Increasing antropogenic methane emissions arise equally from agricultural and fossil fuel sources. Environmental Research Letters **15**:071002.

Kalyuzhnaya, M.G., Yang, S., Rozova, O.N., Smalley, N.E., Clubb, J., Lamb, A., Nagana Gowda, G.A., Raftery, D., Fu, Y., Bringel, F., Vuilleumier, S., Beck, D.A.C., Trotsenko, Y.A., Khmelenina, V.N., Lidstrom, M.E. (2013). Highly efficient methane biocatalysis revealed in a methanotrophic bacterium. Nature Communications **4**:2785.

Kalyuzhnaya, M.G., Puri, A.W., Lidstrom, M.E. (2015) Metabolic engineering in methanotrophic bacteria. Metabolic Engineering **29:**142–152.

Kiel, S., Hansen, B. (2015). Cenozoic methane-seep faunas of the Caribbean region. PLoS One. DOI:10.1371/journal.pone.0140788.

Kirschke, S., Bousquet, P., Ciais, P., Saunois, M., Canadell, J.G., Dlugokencky, E.J., Bergamaschi, P., Bergmann, D., Blake, D.R., Bruhwiler, L., Cameron-Smith, P., Castaldi, S., Chevallier, F., Feng, L., Fraser, A., Heimann, M., Hodson, E.L., Houweling, S., Josee, B., Fraser, P.J., Krummel, P.B., Lamarque, J.F., Langenfelds, R.L., Quere, C.L., Naik, V., O'Doherty, S., Palmer, P.I., Pison, I., Plummer, D., Poulter, B., Prinn, R.G. Rigby, M., Ringeval, B., Santini, M., Schmidt, M., Shindell, D.T. Simpson, I.J., Spahni, R., Steele, P., Strode, S.A. Sudo, K., Szopa, S., van der Werf, G., Voulgarakis,

A., van Weele, M., Weiss, R.F., Williams, J.E., Zeng, G. (2013). Three decades of global methane sources and sinks. Nature Geoscience **6**:813–823.

Lee, H.J., Jeong, S.E., Kim, P.J., Madsen, E.L., Jeon, C.O. (2015). High resolution depth distribution of Bacteria, Archaea, methanotrophs, and methanogens in the bulk and rhizosphere soils of a flooded rice paddy. Frontiers in Microbiology 6:639. doi: 10.3389/fmicb.2015.00639

Mccalley, C.K., Woodcraft, B.J., Hodgkins, S.B., Wehr, R.A., Kim, E.H., Mondav, R., Crill, P.M., Chanton, J.P., Rich, V.I., Tyson, G.W., Saleska, S.R. (2014). Methane dynamics regulated by microbial community response to permafrost thaw Permafrost contains about 50% of the global soil carbon. Nature **514**:478–481.

McGlynn, S.E., Chadwick, G.L., Kempes, C.P., Orphan, V.J. (2015). Single cell activity reveals direct electron transfer in methanotrophic consortia. Nature **526**:531–535.

Montzka, S.A., Dlugokencky, E.J., Butler, J.H. (2011). Non-CO_2 greenhouse gases and climate change. Nature **476**:43–50.

Moskvitch, K. (2014). Mysterious Siberian crater attributed to methane. Nature https://doi.org/10.1038/nature.2014.15649

Nazaries, L., Murrell, J.C., Millard, P., Baggs, L., Singh, B.K. (2013) Methane, microbes and models: Fundamental understanding of the soil methane cycle for future predictions. Environmental Microbiology **15**:2395–2417.

Niemann, H., Loesekann, T., de Beer, D., Elvert, M., Nadalig, T., Knittel , K., Amann, R., Sauter, E.J., Schlueter, M., Klages, M., Foucher, J.P., Boetius, A. (2006). Novel microbial communities of the Haakon Mosby mud volcano and their role as a methane sink. Nature 443, 854–858.

Pandey, S., Gautam, R., Houweling, S., van der Gon, H.D., Sadavarte, P., Borsdorff, T., Hasekamp, O., Landgraf, J., Tol, P., van Kempen, T., Hoogeveen, R., van Hees, R., Hamburg, S.P., Maasakkers, J.D., Aben, I. (2019). Satellite observations reveal extreme methane leakage from a natural gas well blowout. Proceedings of the National Academy of Sciences **116**(52):26376-26381. DOI: 10.1073/pnas.1908712116.

Pol, A., Heijmans, K., Harhangi, H.R., Tedesco, D., Jetten, M.S.M., Op den Camp, H.J.M. (2007). Methanotrophy below pH 1 by a new Verrucomicrobia species. Nature **450**:874–878.

Ruff, S.E., Biddle, J.F., Teske, A.P., Knittel, K., Boetius, A, Ramette, A. (2015). Global dispersion and local diversification of the methane seep microbiome. Proceedings of the National Academy of Sciences **112**(13):4015–4020.

Scheller, S., Yu, H., Chadwick, G.L., Mcglynn, S.E. (2016). Artificial electron acceptors decouple archaeal methane oxidation from sulfate reduction. Science **351**:703–707.

Skarke, A., Ruppel, C., Kodis, M., Brothers, D., Lobecker, E. (2014) Widespread methane leakage from the sea floor on the northern US Atlantic margin. Nature Geoscience **7**:1–5.

Tavormina, P.L., Hatzenpichler, R., McGlynn, S., Chadwick, G., Dawson, K.S., Connon, S.A., Orphan, V.J. (2015). *Methyloprofundus sedimenti gen. nov., sp. nov*., an obligate methanotroph from ocean sediment belonging to the 'deep sea-1' clade of marine methanotrophs. International Journal of Systematic and Evolutionary Microbiology **65**(1) doi:10.1099/ijs.0.062927-0.

Trimmer, M., Shelley, F.C., Purdy, K.J., Maanoja, S.T., Chronopoulou, P.M., Grey, J. (2015). Riverbed methanotrophy sustained by high carbon conversion efficiency. ISME Journal **9**:2304–2314.

Trotsenko, Y.A., Khmelenina, V.N. (2002). Biology of extremophilic and extremotolerant methanotrophs. Archives of Microbiology. doi:10.1007/s00203-001-0368-0

van Teeseling, M.C.F., Pol, A., Harhangi, H.R., van der Zwart, S., Jetten, M.S., Op den Camp, H.J.M., van Niftrik, L. (2014). Expanding the verrucomicrobial methanotrophic world: Description of three novel species of *Methylacidimicrobium gen. nov*. Applied and Environmental Microbiology. doi:10.1128/AEM.01838-14

Watsuji, T.O., Yamamoto, A., Takaki, Y., Ueda, K., Kawagucci, S., Takai, K. (2014). Diversity and methane oxidation of active epibiotic methanotrophs on live *Shinkaia crosnieri*. ISME Journal **8**:1020–31.

Weaver, T.L. & Dugan, P.R. (1975). Ultrastructure of Methylosinus trichosporium as Revealed by Freeze Etching. Journal of Bacteriology **121**:704–710.

Wegener, G., Krukenberg, V., Riedel, D., Tegetmeyer, H.E., Boetius, A. (2015). Intercellular wiring enables electron transfer between methanotrophic archaea and bacteria. Nature **526**: 587–590.

Yvon-Durocher, G., Allen, A.P., Bastviken, D., Conrad, R., Gudasz, C., St-Pierre, A., Thanh-Duc, N., del Giorgio, P.A. (2014). Methane fluxes show consistent temperature dependence across microbial to ecosystem scales. Nature 507, 488–91 .

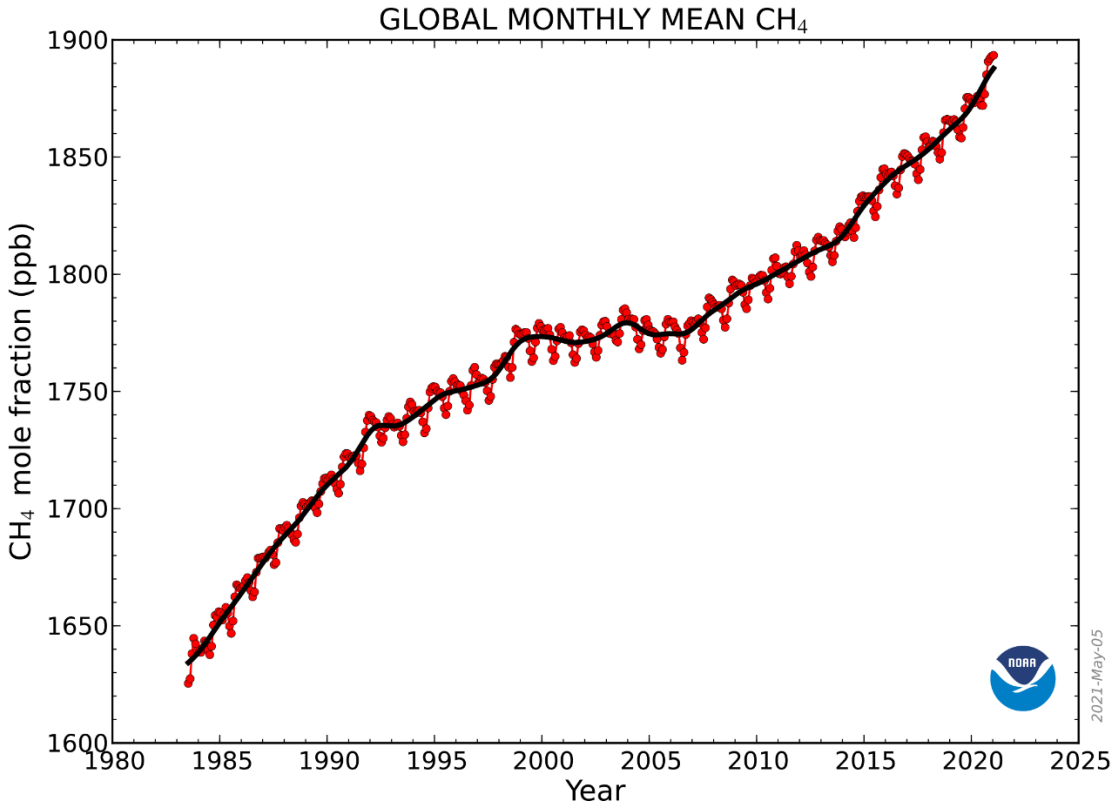

Figure 0.1: Global monthly mean CH_4. Data from NOAA (Dlugokencky, 2021).

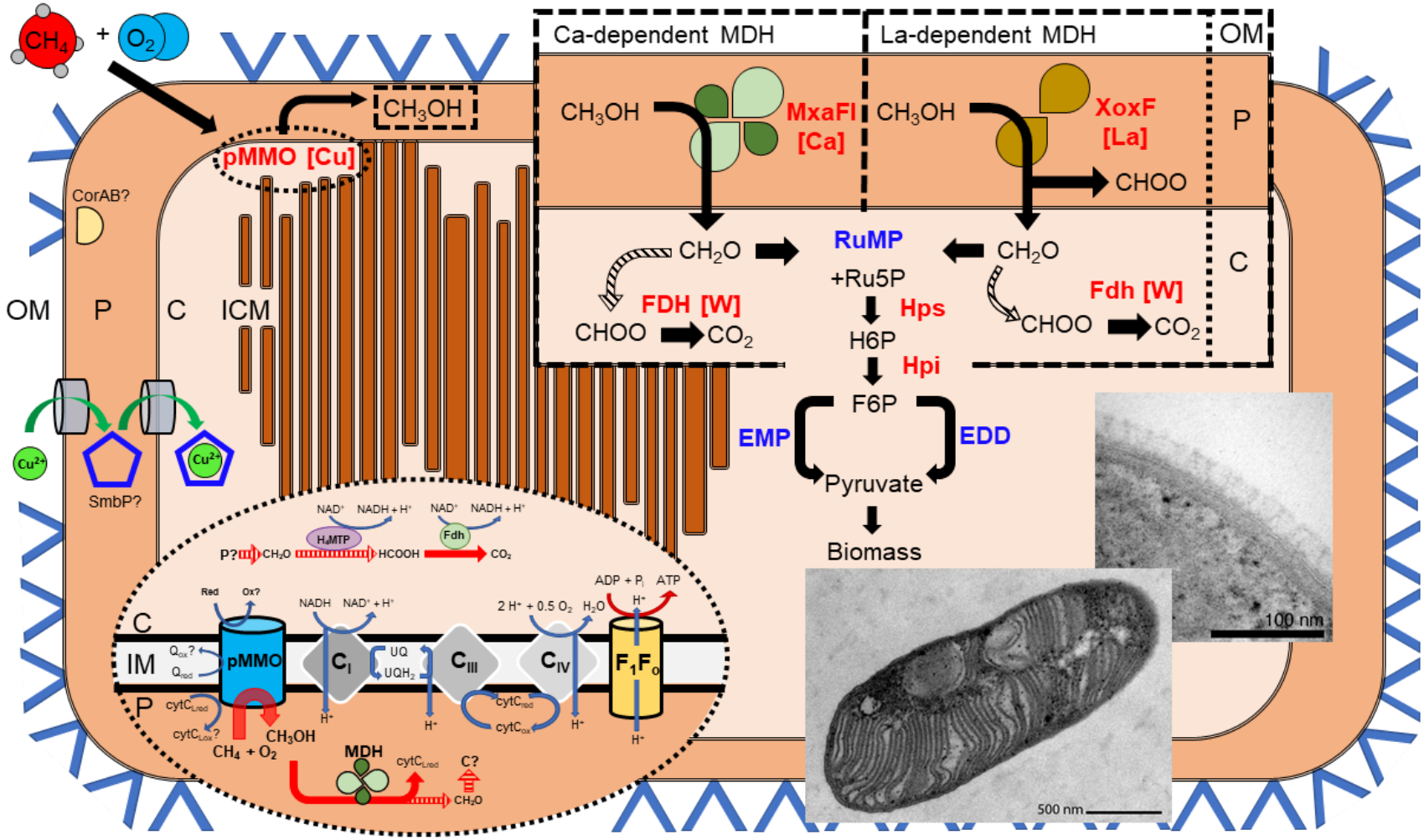

Figure 0.2: Cellular schematic of metabolism in *M. alcaliphilum* 20Z^{R}.
OM: outer membrane, P: periplasm, C: cytosol, ICM: intracytoplasmic membranes. Dashed arrows: multistep formaldehyde reactions.

CHAPTER 1
METHODS

Navigating methane metabolism: Enzymes, compartments, and networks

Adapted from manuscript:

Collins DA, Kalyuzhnaya MG. Navigating methane metabolism: Enzymes, compartments, and networks. (2018). Methods Enzymology **613**:349-383. doi: 10.1016/bs.mie.2018.10.010. PMID: 30509473.

Abstract

Microbial methane utilization—a key node in the global carbon cycle—controls and often eliminates emission of methane into the atmosphere. The diversity and distribution of microbes capable of methane oxidation is astounding. However, from a biochemical point of view, only a very narrow set of unique enzymes underlies their metabolic capabilities. Despite this restriction, the successful integration of the enzymes into non-methanotrophs, if judged by the ability of the trait to grow on methane, remains to be achieved. Failures and small victories with heterologous expression have highlighted a set of challenges linked to structure, compartmentalization, and regulation of the methanotrophic metabolic network. A better understanding of how these challenges are handled by cells of native methane-consuming bacteria is required. In this chapter we focus on key experimental aspects of working with native methanotrophic bacteria, including routine cultivation strategies, lab-scale bioreactor setups, genetic alteration, imaging, and basic -omic-level approaches.

1.1 Culturing methanotrophs

1.11 Growth medium

The original nitrate mineral medium (NMS) described by Whittenbury, Phillips, and Wilkinson (1970) is always a good starting point for the growth or isolation of many methanotrophic strains. However, several aspects of methanotrophic physiology must be considered for further optimization. In addition to obvious modifications, such as pH, salinity/osmolarity, and temperature, several factors can impact and improve growth parameters. Media commonly used for methanotrophic bacteria growth are summarized in Table 1. Some key minerals are typically supplemented as trace elements (Table 1). They include copper, which is an essential element for optimal growth and activity of membrane-bound methane monooxygenase (Semrau, *et al.* 2018; Sirajuddin & Rosenzweig, 2015) as well as electron transport systems, such as terminal cytochrome oxidases; iron, which is critical for methane and methanol oxidation and respiration (Gayazov & Mshenskii, 1991; Semrau *et al.*, 2018); molybdenum and tungsten, which control the type of formate oxidation system used (Chistoserdova, *et al.* 2004); lanthanides, which modulate the expression and activity of two forms of methanol dehydrogenase (Chistoserdova & Kalyuzhnaya, 2018; Chu & Lidstrom, 2016; Gu, *et al* 2016). The range of key microelements is also listed in Table 1.1.

While numerous growth trials are always a good way to optimize cultivation medium, genome mining of methanotrophic bacteria enables additional strategies for further improvements. For example, many species of alkaliphilic methanotrophic bacteria accumulate formate in their growth medium when grown on standard NMS medium. The concentration of formate in the growth medium of *Methylomicrobium spp*.

grown with methane can reach 5–10 mM. Genome mining indicated that the strain possesses a single tungsten-dependent formate dehydrogenase (Akberdin, *et al.* 2018). Incorporation of tungsten in the culture medium almost eliminates formate excretion and improved overall growth and carbon utilization.

1.12 Solid medium cultivation

When possible, solid media cultivation can provide a reliable approach for routine cultivation, verification of purity, counting colony-forming units, or isolating mutants. Some species of methanotrophic bacteria are highly sensitive to agar contaminants but use of Bactoagar (BD Difco) typically eliminates that problem. Since methane is a gas at ambient temperature, the cultivation of methane-consuming bacteria requires special techniques and dedicated instrumentation, which help to control the gas supply in incubation chambers. Anaerobic jars, which are designed for growth of anaerobic and microaerobic organisms, are typically used. Anaerobic jar refill systems, such as Anoxomat (Advanced Instruments), can be adapted for plate incubation in desired environments. The typical atmosphere for incubation of plates comprises 10%–20% CH_4 and air.

1.13 Batch cultivation

Liquid cultures are used for media optimization, validation of mutant phenotypes, or initial trials for sourcing nutrients (e.g., biogas, coal gas, nitrogen fixation). Additionally, batch cultures are used as inocula for bioreactor continuous cultures and for experiments involving growth rates, protein expression, genomic DNA extraction, and initial transcriptomic studies. However, due to the gaseous nature of methane,

which requires the use of closed vials, batch culture experiments are not optimal for investigating the kinetics of methane consumption or estimating biomass yield and carbon conversion efficiencies. The limitations of the batch cultures are due to the highly dynamic changes of both methane and oxygen concentrations in closed settings. Thus, to obtain steady-state data, continuous cultures should be used.

1.14 Continuous bioreactor cultivation

Numerous studies have been carried out to optimize the cultivation of methanotrophic bacteria in continuous culture (Muelemeier, *et al.* 2018). Continuous cultivation requires additional optimizations (Gilman *et al.*, 2017; Mshensky, 1979; Zhivotchenko, *et al.* 1995), and some examples of growth media optimized for single cell protein production with low (up to 5 g CDW/L) and high (up to 30 g CDW/L) cell densities are provided in Table 1.1. Furthermore, the cultivation setup itself poses several challenges. Most of the systems have been custom-built and, due to the flammable nature of methane, should be replicated with caution. One optimal solution for routine lab cultivation is the use of safe mixtures of methane and oxygen, which typically range between 0%–5% CH_4 and 0%–3.5% O_2 (see Ma, 2015 for additional recommendations). A continuous culture setup diagram is shown in Figure 1.1.

In general, any bioreactor system can be converted to a gas-fermentation system with just a few modifications. The gas inputs should be controlled by calibrated mass-transfer systems to provide a reliable estimation of substrate consumption. The concentrations of methane and oxygen in input and output gases should be monitored by gas chromatography or sensor systems (BlueSens; www.bluesens.com/products/all-gas-sensors).

1.15 Routine protocol for continuous bioreactor cultivation

The protocol described below is adapted for working with a mini-parallel bioreactor system, such as DASbox (Eppendorf). The system could be connected to a custom-built gas-distribution system, which controls the gas mixture input. Only nonflammable mixtures of methane (< 5% CH_4) and oxygen (< 3.5% O_2) should be used, and output gases must be connected to exhaust vents. The DASbox system offers single use plastic vessels, which are crucial for small-scale analyses of minerals (Cu, Fe, La, etc.), effects on cell growth, and/or methane oxidation. Four parallel experiments are operated in one run, providing sufficient statistical data for analysis. Examples of a continuous culture parameters setup are shown in Figure 1.2.

1.16 Setting up bioreactor batch and continuous culture experiments

Preparing media and the bioreactor vessel

Media for batch culture must be sterilized by autoclaving within the bioreactor vessel for large-scale experiments. All probes [oxygen probe (DO), pH, redox] must be sterilized in situ with the media and should be carefully covered with silicon caps as well as aluminum foil to protect the electronic connections. All pH and redox probes and pump flow rates must be calibrated prior to sterilization. The pH probe should be calibrated by attaching the probe to the control panel and following the calibration parameters on the control panel. Briefly, low pH 4.0 and high pH 10.0 buffers are measured by the probe and reading value set at the known pH of each buffer, and the slope between the two points is used to determine intermediate pHs. After calibration the probe is cleaned and installed into the reactor before sterilization. Peristaltic pumps

onboard the unit control the supply of additional media, waste outflow, or the addition of acids/bases during an experiment.

Each pump must be calibrated using the same type and diameter of tubing that will be used during the experiment, prior to autoclaving them with the media. Pumps are calibrated by pumping at 100% output for each pump for 30 s to 1min, and measuring the volume pumped. The flow rate in mL/h can then be calculated for each pump. Any ports (sample, addition, harvest, and level controllers) of the vessel should be closed and capped in foil as well.

The gas supply line should have a 0.2μm filter attached and be sealed in foil without blocking the filter to prevent over-pressurization during autoclaving. Autoclaving should be performed at 121°C and 100 kPa (15 psi) above ambient pressure for at least 2 h to sterilize the vessel and media. Any other media (base, acid, buffers, and trace solutions) for continuous culture phases should also be autoclaved with the same settings and duration. Supply lines should be autoclaved with the media as well, so they can be connected to media inflow pumps directly into the fermenter.

Comment: Vessels for the DASbox system are available as disposable, presterilized units which benefit from being virgin materials for trace mineral experiments or comparative conditions.

Preparing the run

It is first necessary to connect the motor and set up the agitation rate. Due to the nature of the carbon source, high agitation is essential. The system should run at 500–1000 rpm. Dissolved oxygen (DO) is measured during fermentation to adjust gas flow

into the reactor. The DO probe must be calibrated prior to activating the gas flow. The probe is autoclaved with the vessel and calibrated afterward once the gas flow lines are connected to the bioreactor.

To calibrate the probe, the reading value of the unattached probe is defined as 0% DO and the probe then is connected to the control panel to begin measuring DO. The agitation is set to maximum speed, and to deliver at least 1 SLPM (standard liter per minute) of room air through the sparger into the media for several hours (or overnight) to saturate the media with oxygen. Once the probe reading has stabilized the value is set to 100% DO to finalize calibration. After the gas is connected, the DO parameter will drop due to O_2 stripping, but it should stabilize at 10%–20% DO for a standard gas mixture. A gas mix for standard experiments consists of 5% methane, 3.5% oxygen, nitrogen balance, and is delivered from the tank at no more than 30 psi through mass flow controllers to the control unit. The control unit additionally is supplied with 30 psi room air and the ratio between the two gases can be controlled on the control panel to adjust the amount of oxygen delivered to the culture. During an experiment, the gas flows from the control unit to the culture through a 0.2μm filter and is dispersed into bubbles by the sparger. The gas composition can be analyzed using an automated sampling gas chromatograph (GC) or by real-time monitoring using a dedicated BlueSens sensor for each gas to be measured: O_2, CO_2, CH_4 (https://www.bluesens.com). Initial data on flow rate and gas composition for at least two agitation rates (500, 750, or 1000 rpm) when operating with an uninoculated bioreactor should be collected. The data will be used as blank parameters for gas consumption calculations.

Inoculation

Once all probes and conditions on the bioreactor are stable, an inoculum is added aseptically through the addition port of the vessel. For standard experiments a 1:100 inoculum is prepared beforehand (i.e., 150mL to 1.5 L batch culture) and added to the bioreactor at the start of the experiment.

Monitoring cell growth

Parameters such as pH, DO, gas flow, and temperature will be monitored and displayed on the bioreactor control panel. Additionally, samples of cells should be withdrawn to monitor optical density and possible contamination. Check for contamination at least daily during an experiment by removing a sample from the culture, such as during measurement of optical density. Plate an aliquot on a solid media that will permit growth of contaminating microbes but not the reactor organism, such as the base media of the reactor supplemented with 10% rich media such as Difco nutrient broth (NB) media (VWR). Incubate the plate at the temperature used for bioreactor culture for 2–3 days to ensure no contaminant CFUs. Finally, the volume of media remaining in the reactor should be recorded daily along with media inflow/outflow volumes. The gas consumption data must be collected during the steady-state phase of the bioreactor run. Exhaust gases should be analyzed for changes in composition compared with inflow gas composition and normalized to the decrease in flow rate.

Like inflow gases, an automated sampler connected to a GC system or real-time BlueSens sensor can be used to determine the consumption of O2 or CH4 and production of CO2 during the experiment. At 25°C and 14.696 psi, the densities of

methane and oxygen are 0.6569 and 1.3088g/L, respectively. The typical output of the continuous culture is shown in Figure 1.2.

Completing a bioreactor run

When an experiment is finished, biomass and spent media are harvested by centrifugation and frozen for downstream analyses. Any remaining culture should be decontaminated, and the bioreactor vessel components disassembled and cleaned. Probes should be washed and stored in manufacture's recommended storage solutions. Waste collection vessels should be emptied and decontaminated with bleach before discarding large volumes.

1.2 Genetic manipulation of methanotrophs

The most recent tools for genetic alterations in methanotrophic bacteria have recently been summarized by Henard and Guarnieri (2018). In general, each genetic modification starts with a set of routine steps including the identification of the chromosomal locus for insertion or deletion and the design of primers for PCR amplification of genomic DNA that are of sufficient length and specific for the desired locus (which can be confirmed by a BLASTn of the primer sequence), the construction of a genetic vector, and the incorporation of the genetic construct via conjugation or electroporation. The procedure used for gene transfer might require further optimization, including selection of the recipient and donor strains. For conjugation-based protocols, the use of E. coli S17-1 strain has proven to be successful for many species of methanotrophic bacteria (Ojala, *et al.* 2011; Puri, *et al.* 2015; Simon, *et al.* 1984). In some cases, the transfer of plasmid could also be facilitated by a triparental conjugation

with strains harboring a pRK2013-helper plasmid (Figurski & Helinski, 1979). A counterselection strategy for eliminating *E. coli* cells after conjugation should also be developed. Initial screening of isolates for antibiotic resistance is a good starting point. Many methanotrophs are naturally resistant to chloramphenicol and ampicillin (Ojala *et al.*, 2011). However, if resistance is not observed, strains resistant to rifamycin can be selected for by a simple plating of cell biomass (typically 10^9–10^{10} cells) on optimal medium supplemented with the antibiotic (*M. alcaliphilum* $20Z^R$; ^{R} = Rif^R).

The procedure will typically yield 2–5 colonies which have a mutation in RNA polymerase and thus the resistance will be stable over generations. Many methanotrophic strains show surprisingly high immunity against foreign DNA, which can severally restrict application of genetic approaches to studying cell physiology. Given below is a protocol for selecting methanotrophic traits with improved accessibility for genetic alterations and protocols for constructing a GFP-tagged protein and deleting a gene. Similar approaches could be used for other genetic modifications, such as a promoter swap, changing a ribosome binding site, or the integration of novel genes or gene clusters.

1.21 Genetic alterations

It is generally assumed that homologous recombination is the main mechanism for making genetic alterations in methanotrophic bacteria. The genetic tools for the constructions of mutants include suicide vectors, such as pCM184 (Marx & Lidstrom, 2002), pCM433 (Marx, 2008), and ZeoCassette (Yan, *et al.* 2016). While it has never been studied specifically, it has been observed that upstream and downstream flanks for gene/genetic region incorporation or deletion should be in the range of 600–800 bp.

Although various strategies can be used for plasmid construction, we found that Gibson assembly (Gibson *et al.*, 2009) is one of the fastest routes to achieve that goal. The resulting constructs can then be incorporated into methanotrophic cells via conjugation or electroporation (Table 1.2).

1.22 Recombination-mediated mutagenesis by suicide vectors in methanotrophs

Flanking region preparation

PCR amplify the upstream and downstream homology region (flanks) of the target gene. The optimal range of the flanking regions should be 600–800 bp. The primers should include at least 20 bp homology to the cloning site of the fragment (e.g., vector being used) or a restriction enzyme recognition site.

For insertions

PCR amplify the insertion sequence, such as GFP, with a forward primer that has 20 bp 5’ complementarity to the 3’ sequence of the gene of interest. This primer is the reverse complement to the reverse primer for the upstream region. The reverse primer for the insertion should have 5’ complementarity for the gene of interest’s downstream homology region and is the reverse complement of the downstream region forward primer.

Assembly

Gel purify PCR products and assemble all fragments using a gene assembly protocol, based on Gibson assembly, such as NEBuilder® HiFi DNA Assembly Master

Mix (NEBiolabs). After the final plasmid is validated by sequencing, proceed with transfer into a methanotroph strain by conjugation or electroporation.

1.23 Conjugation

Recipient culture preparation

Prepare a lawn of methanotrophic culture on an optimal mineral media and incubate with methane until a sufficient density of biomass has grown (3–5 days).

Donor preparation

Prepare chemically competent E. coli S17-1 using a high-efficiency method, such as rubidium chloride (Green & Rogers, 2013), and transform them with a plasmid such as pCM433, pCM184, or pAWP89 containing the desired sequences (for insertion or deletion). Resistant clones are then grown as a lawn on rich selective media (LB agar plate with streptomycin and specific selectable marker on the plasmid being used). This lawn should be started as an overnight culture before mating.

Mating

Conjugation is performed by mixing the donor *E. coli* and recipient methanotrophic culture on mating media (mineral medium, such as NMS or P, supplemented with 10% LB media or nutrient broth). Scrape a full loopful of *E. coli* S17-1 and smear it in a small area on mating media (approximately 1–2 cm in diameter) and then, with a new loop, scoop up an equal amount of biomass from methanotrophic culture and smear it in the same area as the *E. coli*. The two strains should be evenly mixed on the mating media to ensure adequate cell-to-cell contact between the two

species. Mating plates with the two strains are then incubated at 30°C with methane to support growth of both species for at least 2 days, but no more than 4 days.

Selection

Cell biomass should be scraped off the mating plate and transferred to selective media. The entire mating mixture should be transferred to 2–3 plates and spread into a thin layer with a cell spreader. Allow resistant colonies to grow by incubating with methane at 30°C for 5–7 days on mineral medium containing the selective antibiotic. Resulting clones can be purified from residual donor *E. coli* by patch plating colonies onto fresh medium with an appropriate antibiotic for the recipient strain, such as rifamycin. Selected colonies should then be screened by PCR or phenotype depending on the plasmid being used.

Counterselection (if applicable)

Resistant colonies post conjugation that are merodiploid for the homology sequence introduced can then be counter selected to generate double crossover mutants. For example, in the case of pCM433 which contains sacB, selected resistant clones should be transferred onto optimum growth medium plates containing 2%–2.5% sucrose and incubated with methane, allowing for colonies to grow. Patch these sucrose-resistant colonies onto media with and without a selective antibiotic. Clones which are sucrose-resistant and antibiotic-sensitive should then be screened by PCR for the desired deletion or insertion as well as sequenced to confirm the desired double crossover mutation. For insertions, use primer sets that amplify from the chromosome and the inserted sequence. For deletions, use primers which span the deleted

sequence. It is good practice to further validate the resulted constructs by sequencing the amplified fragments.

1.24 Generating a GFP translational fusion with a putative S-layer protein in *M. alcaliphilum*.

In order to construct a transcriptional fusion between a C-terminus of a putative S-layer protein *Methylotuvimicrobium alcaliphilum*: MALCv4_0971, 1102328-1108873, 6546 bp (2181aa), and sfGFP (Pedelacq, Cabantous, Tran, Terwilliger, & Waldo, 2006), two sets of primers were designed: forward primers Malcv4_0971F'1 and Malcv4_0971F'2 (lowercase) with 5' complementarity to the suicide vector pCM433 (uppercase) or GFP (uppercase, bold); reverse primers Malcv4_0971R'1 and Malcv4_0971R'2 (lowercase) with 5' complementarity to GFP coding sequence (uppercase, bold) or to pCM433 (uppercase).

Malcv4_0971F'1: 5' GTGCCACCTGACGTCTAGATCTcgatgtgttgagcaacttcactg 3'

Malcv4_0971R'1: 5' **CAGCTCTTCGCCTTTACGCAT**agcgaggacgaagttatcaac 3'

Malcv4_0971F'2: 5' **GTACAAATAATCTAGACTAG**tcccacttttaaagtgag 3'

Malcv4_0971R'2: 5' GCTGGATCCTCTAGTGAGCTCgccatcctgttgagctggc 3'

GFP F': 5' gttgataacttcgtcctcgct**ATGCGTAAAGGCGAAGAGCTG** 3'

GFP R': 5' ctcactttaaaagtggga**CTAGTCTAGATTATTTGTAC** 3'

pCM433 F'1: 5' gccagctcaacaggatggcGAGCTCACTAGAGGATCCAGC 3'

pCM433 R'1: 5' cagtgaagttgctcaacacatcgAGATCTAGACGTCAGGTGGCAC 3'

The upstream and downstream MALCv4_0971 flanking regions are amplified from M. alcaliphilum 20Z^R DNA using Phusion (NEBiolabs), a high-fidelity polymerase. The sfGFP fusion insert and the suicide vector pCM433 backbone were amplified using GFP F' and GFP R' and pCM433F'1 and pCM433 R'1, respectively. The PCR products were separated by gel electrophoresis and purified. The assembly of the fragments was carried out using a NEBuilder® HiFi DNA assembly mix, according to the NEBlab manufacturer's directions. The reaction mixture was transformed into competent *E. coli* S17-1 and kanamycin-resistant clones were selected. The clones were regrown in liquid culture, and then the plasmid was isolated and sequenced to confirm correct assembly.

The resultant strain was used for biparental mating with *M. alcaliphilum* 20Z^R. Sucrose-resistant, kanamycin-sensitive clones were confirmed as double crossover mutants by PCR and sequencing. The clones were examined by epifluorescent microscopy to localize the putative S-layer protein (see Section 1.3 for details). The image of *M. alcaliphilum* 20Z^R cells harboring the sfGFP fusion is shown in Figure 1.2C.

1.3 Microscopy methods

The unique cell structure of methanotrophic bacteria is commonly associated with their metabolic capabilities. Over the years numerous techniques have been developed and tested on methanotrophic bacteria to study the connection between cellular protein localization and in vivo function (Figure 1.2). Here we summarize the most common strategies to generate fixed or in vivo images of methanotrophic cells.

1.31 Transmission electron microscopy

Transmission electron microscopy (TEM) is one of the most widely used techniques for the investigation of methanotrophic cell structure. Methanotrophs are known for their ability to produce intracytoplasmic membranes (ICMs), which are envisioned as dedicated compartments for methane oxidation. The structure and amount of ICMs can be linked to the type of methane oxidation system (i.e., membrane-bound methane monooxygenase) and cell physiological state (starvation vs active growth). Additional information obtained from TEM might include the amount of carbon storage compounds (polyhydrobutyrate or glycogen), motility (flagella and pili), accumulation of polyphosphates, and surface structures (S-layers, nanowires, fibrils). Cells from both liquid culture and solid medium can be examined for ultrastructure such as the formation and dynamics of ICMs, surface layer proteins, and storage granules. Cells are fixed and then prepared for embedding in resin to stabilize sections for microscopy using a well-established protocol (Hayat, 1981).

Primary fixation

Caution: Aldehydes are toxic and carcinogenic; arsenic buffers are also toxic.

Cell cultures of adequate density (10^6–10^8 cell/mL) should be mixed with 4% glutaraldehyde and 0.2M Cacodylate buffer (1:1, v:v) and incubated for a period of 1 h to overnight on ice or at 4°C. After incubation, wash cells in 0.1 M Cacodylate buffer.

Secondary fixation

Caution: Osmium compounds are volatile, toxic, and carcinogenic; arsenic buffers are also toxic.

Mix washed primary fixed cells 1:1 (v:v) with 2% osmium tetroxide in 0.2M Caco buffer and incubate for 1–2 h on ice or 4°C. The cells should turn black. Wash cells 3 in water by spinning down gently in a tabletop centrifuge, and resuspending in 1mL filtered deionized distilled (dd)H2O. Fixing samples with osmium should be carried out in a chemical fume hood.

Embedding

Gently spin down fixed cell biomass at low g-force and remove supernatant by pipette. Mix cells in 50µL of 1%–2% agarose in water. Quickly dispense cells in small aliquots as beads or a layer of agarose onto a clean glass slide and allow agar to solidify.

Vapor fixation

Colonies grown on agar plates can be processed for TEM without disturbing them by using vapor fixation. Draw a circle on the lid above the colony and invert the plate. Open the plate and dispense a small droplet (50 µL) of stock 8% glutaraldehyde solution in the marked area of the lid beneath the colony. Allow to fix overnight. Pipette off the fixative after 12 h and dispose of properly. Repeat with the stock 4% osmium solution for an additional 12 h overnight fixation. A margin of agar containing the fixed colony can then be excised and placed into a clean Petri dish to begin the dehydration process.

Dehydration

Dehydrate agar-embedded cells to remove water from the sample by transfer

through a graded ethanol series for at least 1 h each. The steps of the graded series can be used as holding points during processing if time does not permit proceeding through them directly. Only absolute ethanol (200 proof) should be used to make the solutions for the dehydration series. It is easiest to put samples into microfuge tubes so that they can be mixed throughout dehydration using a rotary mixer or shaking table. Start with samples in 35%–50% ethanol in water for at least 1 h. Move samples to the next solution 75% ethanol in water and then 90%–95% ethanol in water for at least 1 h. Complete the dehydration by three exchanges in 100% ethanol.

En bloc staining

Depleted uranium is typically used as a heavy metal stain during sample preparation to enhance the inherently low contrast of biological materials. Caution in the use of uranium solutions: dispose of this staining solution and all contaminated dry waste generated with it appropriately in a radioactive waste stream. Uranyl acetate solutions are light sensitive and solutions with precipitate should not be used. During the dehydration in 75% ethanol in water add 1% uranyl acetate for *en bloc* staining (3 volumes of 100% ethanol to 1 volume of 4% uranyl acetate stock solution). Continue with subsequent dehydration steps (95% ethanol, etc.).

Infiltration

During infiltration, the ethanol solvent is exchanged for another solvent compatible with an embedding resin. Multiple resins are available from commercial suppliers and compatible solvents may vary; Epon 812 is routinely used and is compatible with acetone or propylene oxide as a solvent. Stock Epon can be stored in a

freezer for intermediate time periods (approximately 1–2months) but should be prepared as a graded series with the solvent of choice immediately before use. The infiltration can be performed in microfuge tubes, but they should be tightly sealed or clamped closed to prevent lids from popping open or leaking due to the high vapor pressure of acetone. Switch solution from ethanol to 100% acetone for at least 1 h for three exchanges of acetone. Transfer to a prepared 33% Epon:66% acetone solution for at least 6 h or overnight with constant movement in a rotary mixer or shaking table. Then transfer to 66% Epon:33% acetone for the same time with constant movement of the sample within the solution. Lastly transfer the samples to 100% Epon resin for at least 8 h to (preferably) overnight.

Polymerization

Transfer infiltrated samples from 100% Epon into silicon molds and cover with 100% Epon. Create labels in a word processor document containing sample description and date written in font size <3. Cut out labels and add to each mold. Degas them at room temperature under vacuum (few hours to overnight). This will minimize drift of samples and labels within the mold during the baking process. Bake Epon resin at 60°C under vacuum for at least 48 h. Solidified Epon will have a hard, glassy surface that is not tacky and will resist pressure applied to the surface.

Sectioning

Reproducible preparation of sections having uniform thickness is the most critical step of sample preparation for TEM. Specialized tools such as ultramicrotome, glass knives, and a diamond knife are critical for quality sectioning of microbial samples.

Several resources for proper sample sectioning are available from ultramicrotome and diamond knife manufacturers such as Leica. Remove samples from molds and begin sectioning by trimming excess Epon with a razor blade. Samples should be trimmed into square or trapezoidal faces having slightly pyramidal sides to support the sample. Using a glass knife, cut the face of the block down to 100 nm sections until the surface is level and reflective. Move to cutting on a diamond knife down to 65–100 nm sections for the final sections. The surface of the sample face should be mirror-like and highly reflective when viewed under the microtome. Sections can then be picked up using forceps by submerging a copper grid in the diamond knife water boat and picking up the sections from below. Blot excess water from the grid and place into a grid box.

Section staining

Sections can be imaged after sectioning and drying but benefit from enhanced sample contrast generated by staining. The simplest combination of stains uses a uranium solution as previously used during *en bloc* staining as well as a lead solution. Stain samples post-sectioning in 1% uranyl acetate for approximately 1min. Overstaining is not a concern with uranium solutions. Briefly (5–10 s) rinse sections with deionized water and blot dry with filter paper. Stain sections in a 40mM lead nitrate solution for 30 s to 1min. Additional time in lead solutions can result in overstaining. Rinse in deionized water again and blot dry. Let grids dry in fume hood for approximately 1 h and store in a grid box until imaged.

TEM imaging

Examine sections with TEM after drying under high vacuum at accelerating voltages of at least 100 keV and high magnification 10–270k times.

1.32 Scanning electron microscopy

Scanning electron microscopy (SEM) allows the observation of surface features of methanotrophs. One of the unique applications is the investigation of cell surface layers (Fig. 4), or nanowires. Sample preparation involves many similar reagents to TEM sample preparations but is simpler due to the preservation of exterior structures.

Fixation

Caution: Aldehydes and osmium are toxic and carcinogenic; the arsenic buffer is also toxic and requires a dedicated waste stream. Bacterial culture fixation is performed in a single step using a solution of 2% glutaraldehyde and 0.5%–1% osmium tetroxide in 0.1 M cacodylate buffer (final concentrations) for 1 h on ice.

Deposition

Wash cells by spinning down them gently in a tabletop centrifuge at low speed and resuspending in 1 mL of 0. 2μm filtered ddH_2O. Dilute an aliquot of fixed cells 1:100 in 0.2μm filtered ddH_2O (i.e., 50μL into 5mL) and deposit cells onto a nucleopore membrane (Millipore) by passing the diluted cell solution from a Luer lock syringe into a Swinnex filter unit device (Millipore) holding the nucleopore membrane. These filters have a very clean background in SEM and come in various pore sizes. Bacterial samples should be deposited on 1 or 5μm pore filters.

Dehydrate filters containing cells in a graded ethanol series (50%, 70%, 95%, 100% ethanol) for approximately 5min at each concentration. Filters should not be allowed to be exposed to the air and must be always submerged in ethanol during dehydration. Ethanol can then be removed by CO2 critical point drying or by replacing the ethanol by three exchanges with hexadimethylsilazane (HMDS) and allowing it to evaporate in a chemical fume hood.

Dried filters must then be mounted on SEM stubs with adhesive carbon tape or colloidal graphite solution and made conductive by sputter coating. A HiRes sputter coater with a film thickness monitor should be used to apply at least 6 nm of nonreactive metal such as Pt or Au to the filters.

Imaging

View coated filters in SEM under high vacuum conditions ($<10^3$ Pa) with low accelerating voltage (<10 keV) and at a short working distance (10 mm) to optimize determination of cell surface ultrastructure.

1.33 Fluorescence microscopy

Bacterial cell biology has benefited using epifluorescence to track the development of structures and localization of tagged proteins in the context of live cells. This technique involves many routine reagents that differentially stain cellular components such as DAPI for DNA and use of lipophilic dyes such as FM4-64, FM1-43, and Mitotracker (Invitrogen, ThermoFisher) to stain cellular membranes. Consideration must be given to excitation and emission wavelengths for each stain used to determine accurate cellular localization. Fluorophores for protein fusions, such as GFP, mCherry,

and mVenus, also can be used provided they maintain intracellular fluorescence. Below describes the main steps for preparation of live, stained methanotrophic bacterial cells.

Slide preparation

Prepare a 1% agarose solution in optically clear media such as P3% or in phosphate-buffered saline. Pipette agarose solution onto a clean microscope slide and sandwich between another clean microscope slide to allow agarose to harden for at least 30–40min. Do not allow agarose to dry longer than this as it may become brittle. Slowly remove the cover microscope slide by sliding it off the agarose pad to maintain the smooth surface of the agarose.

Cell preparation

Stain cells by mixing an aliquot of cells with each dye as directed by the manufacturer in culture media or cells resuspended in phosphate-buffered saline. The working concentration for many dyes is generally between 1 and 5 μg/mL and can be used in combination to stain cells simultaneously. Cells of membrane-rich methanotrophs are stained with 0.5–1 μg/mL Fm4-64 for at least an hour along with 0.5–1 μg/mL of DAPI and incubated at optimal growth temperature.

Cell loading

Seat cells onto the prepared agarose pad by pipetting 5–10μL of stained cells onto the agarose and allowing to stand for approximately 10min. Apply a clean coverslip to the agarose pad on top of the seated cells and proceed to imaging with a fluorescence microscope.

Imaging

Locate deposited cells at low magnification using brightfield transmitted light before increasing objective magnification up to oil immersion and reflected light using an appropriate emission/excitation filter set. Capture images using each filter set for the dyes used to stain the cells (Fm4-64: 515 nm excitation, 640 nm emission; DAPI: 341nm excitation, 452 nm emission; GFP: 488 nm excitation, 510 nm emission) and merge images for each channel using a software package such as ImageJ to create composites.

1.4 Systems level characterization

It is difficult to carryout microbial physiology research without -omics data. Typical data sets include whole-genome transcriptomics, proteomics, and nontargeted metabolomics. The data enable further improvements of in silico tools, such as metabolic flux modeling. Below we summarize our approaches for the preparation of cell samples for large-scale -omic analyses. Many of the analyses can be outsourced and carried out by dedicated and centralized facilities, such as Metabolon (https://www.metabolon.com).

1.41 Proteomic studies

Samples collected from steady-state cells generally provide a good overview of expressed functions which are essential for the given conditions. Typically, such samples also provide good reproducibility. Some additional insights might be obtained from transition experiments; however, those experiments tend to be less reproducible, and thus require large numbers of replicates, as well as multiple time points. We

recommend at least three biological replicates (BR), with two technical replicates per BR.

Cell harvesting

Grow cells in continuous culture under the desired test conditions (i.e., O_2 limitation, methanol, La vs Ca, without copper, etc.). Collect key parameters, such as growth rate and oxygen and methane consumption rates. Harvest biomass by centrifuging 50 mL of culture for each technical replicate at 4000 rpm for 20 min. Discard supernatant and freeze cell pellets at 80°C. Samples can be stored for 3–6 months.

Cell lysis

Resuspend biomass in lysis buffer [4% sodium dodecyl sulfate (SDS), 100 mM Tris/HCl pH 7.6, 100 mM dithiothreitol (DTT)] by vortexing. Transfer 100 µL fractions into 1.5 mL centrifuge tubes and incubate at 95°C for 5 min to complete cell lysis and fully reduce and denature proteins. Cool samples at 4°C for 30 min and centrifuge at 15,000 x g and 4°C for 10 min to pellet the remaining cell debris. Use a Filter-Aided Sample Preparation (FASP) (Wisniewskiet, Zougman, Nagaraj, & Mann, 2009) kit for protein digestion (Expedeon, San Diego, CA) according to the manufacturer's instructions. Add 400µL of 8M urea to each 500 µL 30k molecular-weight cut-off (MWCO) FASP spin column along with 50 µL of the sample in lysis buffer. Centrifuge at 14,000 x g for 30 min to reduce the sample to the dead volume. Remove waste from the collection tube, add another 400 µL of 8 M urea to the column, and centrifuge again at 14,000 x g for 30 min. Repeat the 8 M urea wash one additional time. Add 400 µL of 50

mM ammonium bicarbonate to each column and centrifuge for 30 min; repeat ammonium bicarbonate wash twice. Place column in a new, clean, and labeled collection tube. Prepare digestion solution by dissolving 4 µg trypsin in 75 µL 50 mM ammonium bicarbonate solution and incubate with the sample for 3 h at 37°C, using a Thermotop (Eppendorf, Hamburg, Germany). Centrifuge digested peptides through the filter unit and into the collection tube at 14,000 x g for 15 min. Snap freeze the collection tube in liquid N_2 and place the column into a new collection tube and digest again overnight with 150 µL of digestion solution. Centrifuge the peptides the following day at 14,000 x g for 15 min and add to the 3 h peptide collection tube and concentrate the sample to approximately 30 µL using a SpeedVac.

Protein estimation

Determine final peptide concentrations using a bicinchoninic acid (BCA) assay (Thermo Scientific, Waltham, MA, USA). Dilute samples with water to 200 ng/µL for subsequent mass spectrometry analysis.

LC–MS/MS analyses

Peptides dissolved in water with a total mass of 500 ng can then be analyzed by liquid chromatography–tandem mass spectrometry (LC–MS/MS). Process LC–MS/MS data with parameters: (1) tryptic digestion in at least one terminus of the peptide (Lys/Arg), (2) 20 ppm parent ion mass error tolerance, and (3) methionine oxidation and lysine trimethylation as variable modifications. Filter identifications with an appropriate probability score $<1^{-9}$ with a false-discovery rate <1% at the protein level. The number of observed peptides can then be determined using their relative abundances as a proxy.

Average the number of peptides observed across replicates and consider a fold-change of greater than 2 as significant.

1.42 Transcriptomics

Whole-genome gene expression studies are becoming a routine approach for investigating metabolic states. Furthermore, new generation sequencing provides massive amounts of information, which can be used for the identification of transcription start sites and promoter regions. When coupled with proteomics, the data can deliver additional insights into posttranscriptional regulation. Finally, we found that integration of transcriptomic data, metabolomic data, and flux balance analysis (FBA) enables identification of novel metabolic arrangements (summarized in Akberdin, *et al.* 2018; Kabimoldayev, *et al*. 2018).

Cell harvesting

Collect samples (45 mL) of bacterial cultures and immediately add 5 mL of stop solution (5% water-equilibrated phenol in ethanol). Pellet cells by centrifugation at 4700 rpm for 15 min, extract RNA using an RNeasy kit (Qiagen), and treat cells with PureLink DNaseI (ThermoFisher Scientific) to digest genomic DNA according to the manufacturer's instructions.

References

Akberdin, I. R., Thompson, M., Hamilton, R., Desai, N., Alexander, D., Henard, C. A., *et al.* (2018). Methane utilization in Methylomicrobium alcaliphilum 20Z^{R}: A systems approach. Scientific Reports, 8, 2512.

Akberdin, I. R., Thompson, M., & Kalyuzhnaya, M. G. (2018). Systems biology and metabolic modeling of C1-metabolism. In M. G. Kalyuzhnaya & X. H. Xing (Eds.), Methane biocatalysis: Paving the way to sustainability (pp. 99–115). Switzerland: Springer International Publishing.

Chistoserdova, L., & Kalyuzhnaya, M. G. (2018). Current trends in methylotrophy. Trends in Microbiology, 26, 703–714.

Chistoserdova, L., Laukel, M., Portais, J.-C., Vorholt, J. A., & Lidstrom, M. E. (2004). Multiple formate dehydrogenase enzymes in the facultative methylotroph Methylobacterium extorquens AM1 are dispensable for growth on methanol. Journal of Bacteriology, 186, 22–28.

Chu, F., & Lidstrom, M. E. (2016). XoxF acts as the predominant methanol dehydrogenase in the Type I methanotroph Methylomicrobium buryatense. Journal of Bacteriology, 198, 1317–1325. https://doi.org/10.1128/JB.00959-15.

Crombie, A., & Murrell, J. C. (2011). Development of a system for genetic manipulation of the facultative methanotroph Methylocella silvestris BL2. Methods in Enzymology, 495, 119–133.

Dedysh, S. N., Panikov, N. S., & Tiedje, J. M. (1998). Acidophilic methanotrophic communities from Spagnum peat bogs. Applied and Environmental Microbiology, 64, 922–929.

de la Torre, A., Metivier, A., Chu, F., Laurens, L. M., Beck, D. A., Pienkos, P. T., Lidstrom, M.E., Kalyuzhnaya, M.G. (2015). Genome-scale metabolic reconstructions and theoretical investigation of methane conversion in Methylomicrobium buryatense strain 5G(B1). Microbial Cell Factories, 14, 188.

Figurski, D. H., & Helinski, D. R. (1979). Replication of an origin-containing derivative of plasmid RK2 dependent on a plasmid function provided in trans. Proceedings of the National Academy of Sciences of the United States of America, 76, 1648–1652.

Gibson, D. G., Young, L., Chuang, R. Y., Venter, J. C., Hutchinson, C. A., III, & O'Smith, H. (2009). Enzymatic assembly of DNA molecules up to several hundred kilobases. Nature Methods, 6, 343–345.

Gilman, A., Fu, Y., Hendershott, M., Chu, F., Puri, A. W., Smith, A. L., Pesesky, M., Lieberman, R., Beck, D.A.C., Lidstrom, M.E. (2017). Oxygen-limited metabolism in the methanotroph Methylomicrobium buryatense 5GB1C. PeerJ, 5, e3945. https://doi.org/10.7717/peerj.3945.

Green, R., & Rogers, E. J. (2013). Transformation of chemically competent. Methods in Enzymology, 529, 329–336.

Gu, W., Haque, F. M. U. I., DiSpirito, A. A., & Semrau, J. D. (2016). Uptake and effect of rare earth elements on gene expression in Methylosinus trichosporium OB3b. FEMS Microbiology Letters, 363. pii: fnw129.

Gayazov, R. R., & Mshenskii, Y. N. (1991). Growth of Methylococcus capsulatus at various concentrations of ammonium nitrogen and inorganic phosphates. Microbiologiya (Moscow, Russia), 60, 171–174.

Haque, M. U. I., Gu, W., DiSpirito, A. A., & Semrau, J. D. (2016). Marker exchange mutagenesis of mxaF, encoding the large subunit of the Mxa methanol dehydrogenase, in Methylosinus trichosporium OB3b. Applied and Environmental Microbiology, 82, 1549–1555.

Hayat, M. A. (1981). Fixation for electron microscopy. Academic Press.

Henard, C. A., & Guarnieri, M. T. (2018). Metabolic engineering of methanotrophic bacteria for industrial biomanufacturing. In M. G. Kalyuzhnaya & X. Xing (Eds.), Methane biocatalysis: Paving the way to sustainability (pp. 117–132). Springer.

Henard, C. A., Smith, H., Dowe, N., Kalyuzhnaya, M. G., Pienkos, P. T., & Guarnieri, M. T. (2016). Bioconversion of methane to lactate by an obligate methanotrophic bacterium. Scientific Reports, 6, 21585.

Kabimoldayev, I., Nguyen, A. D., Yang, L., Park, S., Lee, E. Y., & Kim, D. (2018). Basics of genome-scale metabolic modeling and applications on C1-utilization. FEMS Microbiology Letters, 365. https://doi.org/10.1093/femsle/fny241.

Kalyuzhnaya, M.G., Khmelenina, V.N., Eshinimaev, B.Ts.,Suzina, N.E., Nikitin, D., Solonin, A., Lin, J.L.,McDonald, I.R., Murrell, J.C., and Trotsenko, Yu.A., (2001). Taxonomic Characterization of New Alkaliphilic and Alkalitolerant Methanotrophs from Soda Lakes of the Southeastern Transbaikal Region and Description of *Methylomicrobium buryatense sp. nov*., Systmatics and Applied Microbiology **24(**2):166–176.

Ma, T. (2015). Ignitability and explosibility of gases and vapors (p. 212). New York: Springer Science. https://doi.org/10.1007/978-1-4939-2665-7.

Marx, C. J. (2008). Development of a broad-host-range sacB-based vector for unmarked allelic exchange. BMC Research Notes, 1, 1. https://doi.org/10.1186/1756-0500-1-1.

Marx, C. J., & Lidstrom, M. E. (2002). Broad-host range cre-lox system for antibiotic marker recycling in Gram-negative bacteria. BioTechniques, 33, 1062–1067.

Mshensky, Y. N. (1979). PhD thesis: Growth of methanotrophic bacteria. Pushchino: IBPM RAS.

Muhlemeier, M. I., Speight, R., & Strong, P. J. (2018). Biogas, bioreactors and bacterial-methane oxidation. In M. G. Kalyuzhnaya & X. Xing (Eds.), Methnane biocatalysis: Paving the way to sustainability (pp. 213–235). Springer.

Ojala, D. S., Beck, D. A., & Kalyuzhnaya, M. G. (2011). Genetic systems for moderately halo (alkali) philic bacteria of the genus Methylomicrobium. Methods in Enzymology, 495, 99–118.

Pedelacq, J. D., Cabantous, S., Tran, T., Terwilliger, T. C., & Waldo, G. S. (2006). Engineering and characterization of a superfolder green fluorescent protein. Nature Biotechnology, 24, 79–88.

Pol, A., Heijmans, K., Harhangi, H. R., Tedesco, D., Jetten, M. S. M., & Op den Camp, H. J. M. (2007). Methanotrophy below pH 1 by a new Verrucomicrobia species. Nature, 450, 874–878.

Puri, A. W., Owen, S., Chu, F., Chavkin, T., Beck, D A C., Kalyuzhnaya, M.G., Lidstrom, M.E. (2015). Genetic tools for the industrially promising methanotroph Methylomicrobium buryatense. Applied and Environmental Microbiology, 81, 1775–1781.

Semrau, J. D., DiSpirito, A. A., Gu, W., & Yoon, S. (2018). Metals and methanotrophy. Applied and Environmental Microbiology, 84, e02289-17. https://doi.org/10.1128/AEM.02289-17.

Semrau J.D., Jagadevan S., DiSpirito A.A., Khalifa A., Scanlan J., Bergman B.H., Freemeier B.C., Baral B.S., Bandow N.L., Vorobev A., Haft D.H., Vuilleumier S., Murrell J.C. (2013). Methanobactin and MmoD work in concert to act as the 'copper-switch' in methanotrophs. Environmental Microbiology **15**(11):3077-86. doi: 10.1111/1462-2920.12150.

Simon, R., Priefer, U., & Puhler, A. (1984). A broad host range mobilization system for in vivo genetic engineering: Transposon mutagenesis in Gram-negative bacteria. Biotechnology, 1, 784–791.

Sirajuddin, S., & Rosenzweig, A. C. (2015). Enzymatic oxidation of methane. The Biochemistry, 54, 2283–2294.

Whittenbury, R., Phillips, K. C., & Wilkinson, J. F. (1970). Enrichment, isolation and some properties of methane-utilizing bacteria. Journal of General Microbiology, 61, 205–218.

Wisniewskiet, J. R., Zougman, A., Nagaraj, N., & Mann, M. (2009). Universal sample preparation method for proteome analysis. Nature Methods, 6, 359–362.

Yan, X., Chu, F., Puri, A. W., Fu, Y., & Lidstrom, M. E. (2016). Electroporation-based genetic manipulations in type I methanotrophs. Applied and Environmental Microbiology, 82, 2062–2069.

Zhivotchenko, A. G., Nikonova, E. S., & Jørgensen, M. H. (1995). Copper effect on the growth kinetics of Methylococcus capsulatus (Bath). Biotechnology Techniques, 9, 163.

Table 1.1: Composition of media routinely used for cultivating methanotrophic bacteria.

Component*	K_s/K_I[1] mg [ion]	Whittenbury[2]	SCP fermentation[3] LD# //HD $	DSMZ[4] #632 NMS	Alcaliphiles[5-6]	Acidiphiles[7]	*Verrucomicrobia* [8]
Nitrogen Source							
KNO_3	-	1	-	1	1	1	5 mM
NH_4Cl	380/0.7 [NH_4^+]	0.5	as needed^	-	-	-	-
Sulfur Source							
$MgSO_4$ x 7 H_2O	-	1	0.2 // 0.8	1	0.2	0.1	-
Na_2SO_4	-	-	-	-	-	-	0.14
K_2SO_4	-	-	-	-	-	-	0.35
Other							
$CaCl_2$	-	0.15	0.02 // 0.08	0.1	0.015	0.015	0.02
$LaCl_3$ x 7 H_2O**	-	-	-	--	-	**0.06**	
NaCl	-	-	-	-	30-Jan	-	-
Fe(III) EDTA	-/0.1 [Fe^{2+}]	4 mg		4 mg	-	-	-
$MgCl_2$ x 6 H_2O	-	-		-	-	-	0.2 mM
1000x Trace Element solution***		0.5 ml l^{-1}	-	0.5 ml l^{-1}	1 ml l^{-1}	1 ml l^{-1}	1 ml l^{-1}
Phosphorous source and pH buffering							
KH_2PO_4	700/0.8	0.1	0.2 // 0.8	0.272	0.109	0.2	-
Na_2HPO_4	[PO_4^{3-}]	0.1	0.12 // 0.5	0.717	0.114	-	0.14
High pH buffering: carbonate buffer							
$NaHCO_3$	-	-		-	3.02	-	-
Na_2CO_3	-	-		-	0.42	-	-
Low pH Buffering							
H_3PO_4	-					as needed	
H_2SO_4 (1M)	-						1 ml l^{-1}
Final pH	-	6.8		6.8	8.6-9	4.5-5	2.7
Solid media							
Bacto agar	-	12.5		12.5	14.6		-

*Salt are listed as g per litter, unless otherwise stated; ** Addition of la is optional; it could be used alone or with $CaCl_2$. ***Prepared as a 1000x stock solution in 1 liter volume of ddH_2O and added to media before sterilization. Chelating agents such as EDTA and NTA should be dissolved into solution first before adding additional salts. **In bold:** cultures grown with the compound listed exhibit increased growth.[1]Gyazov r., 1992; [2] Whittenbury *et al.* 1970; [3]Mshenskii, 1979, media optimized for high density fermentation for # for Low Cell density (LD, 5g CDW/L) or $ for High Density (HD, 25-30g CDW /L; **^**ammonium is used as a source of N and pH stabilizing agent (pH =6.6). [4]DSMZ GmbH (2007). NMS medium; [5]Kalyuzhnaya *et al.*, 2001; [6]Akberdin *et al.*, 2018; [7]Dedysh *et al.*, 1998; [8]Pol *et al.*, 2007. CDW, cell dry weight; SCP, single cell protein.

Table 1.2: Composition of trace element solutions used for cultivating methanotrophic bacteria.

1000x Trace Element solution* **							
Na_2EDTA	-	3		0.5	5	5	-
$FeSO_4$ x 7 H_2O	-/0.1 [Fe^{2+}]	1.1	8 // 40	0.2	2	2	1.39
$ZnSO_4$ x7 H_2O	-/0.042	-	0.5 // 2	0.01	0.3	0.1	0.3
$ZnCl_2$	[Zn^{2+}]	0.042	-	-	-	-	-
$MnCl_2$ x 4 H_2O	-/1.72 [Mn^{2+}]	0.04	0.03 // 1.2	0.03	0.03	0.03	1
$CoCl_2$ x 6 H_2O	-/0.046	0.19	0.1 // 0.4	0.02	0.2	0.02	0.24
$CuSO_4$ x 5 H_2O	-/0.054	-	2 // 8	-	1.2	0.1	2.5
$CuCl_2$ x 2 H_2O	[Cu^{2+}]	0.002	-	-	-	-	-
Na_2O_4W x $2H_2O$		-	-	-	**0.3**	-	-
$NiCl_2$ x 6 H_2O		0.024	-	0.002	0.05	0.02	0.23
Na_2MoO_4 x 2 H_2O	-/0.12 [$MoO4^{2-}$]	0.018	0.3 // 1.2	0.003	0.05	0.03	0.24
H_3BO_3		0.3	-	0.03	0.03	-	-
$CeCl_3$		-	-	-	-	-	**0.25**
H^2SO (ml)			0.05 // 0.2				
Nitrilotriacetic acid (NTA)		-	-	-	-	-	9.5

Table 1.3: Commonly used genetic tools for methanotrophic bacteria.

Plasmid / Construct	**Applications**	**Genus**	**Selectable markers [Reference]**
pAWP89, pAWP78	Broad-host range, replicating plasmids with constitutive gene expression	*Methylomicrobium*, *Methylobacter*, *Methylomonas*	Kanamycin [1,2]
pCM433	*oriT*-mobilized allelic exchange	*Methylomicrobium,*	Tetracycline [3], or kanamycin [1], or gentamycin [4] Sucrose
ZS	Linear DNA construct for gene knock out with selection (Zeo) and counter selection (*sacB*) cassettes	*Methylomicrobium*	Zeocin and sucrose [2]
pKiKo	*oriT*-mobilized site-specific gene knock-in, gene knock-out	*Methylomicrobium*	Kanamycin [Demidenko O. Unpublished]
pCM184	Broad-host range *cre-lox* gene knock-out	*Methylobacterium*, *Methylocella*	Ampicillin, kanamycin and tetracycline [5-6]
pK18mob sacB	Allelic exchange, gene knock out	*Methylosinus*	Kanamycin and sucrose [7-8]
pCAH01	Replicating pAWP78 derived broad-host range aTc-inducible gene expression	*Methylomicrobium*	Ampicillin and kanamycin [9]

[1] Puri, *et al.* 2015; [2] Yan, *et al.* 2016; [3] Marx, 2008; [4] Henard, *et al.* 2018; [5] Marx and Lidstrom, 2002; [6] Crombie and Murrell, 2011; [7] Semrau, *et al.* 2013. [8] Haque, *et al.* 2016; [9] Henard, *et al.* 2016.

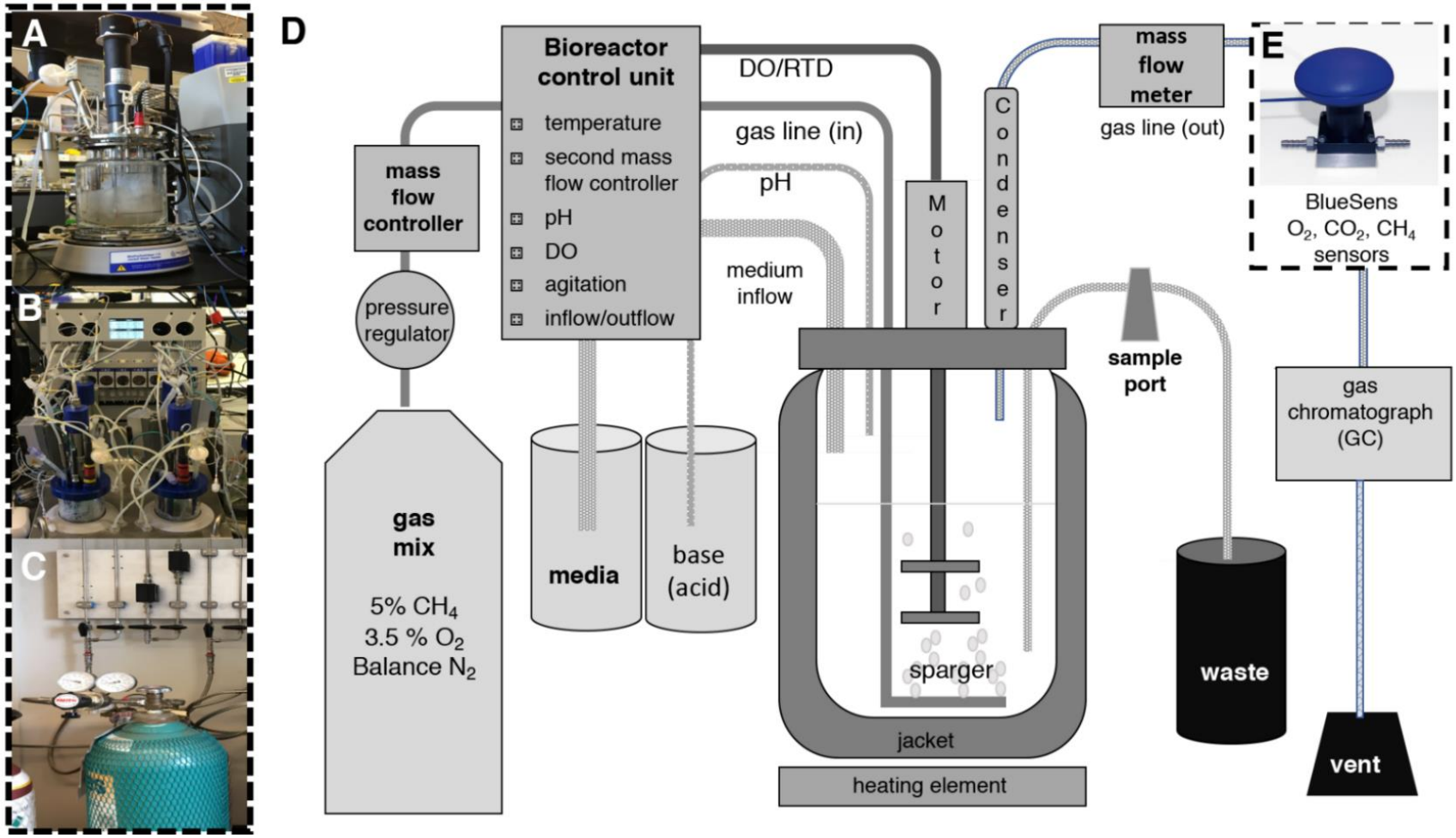

Figure 1.1: Typical lab-scale bioreactor setup for cultivating methane-consuming bacteria.
(A, B) Benchtop fermenter and bioreactor unit. (C) Gas mass-transfer system. (D) Schematic components of a continuous culture bioreactor. (E) Gas composition continuous analysis unit from BlueSens.

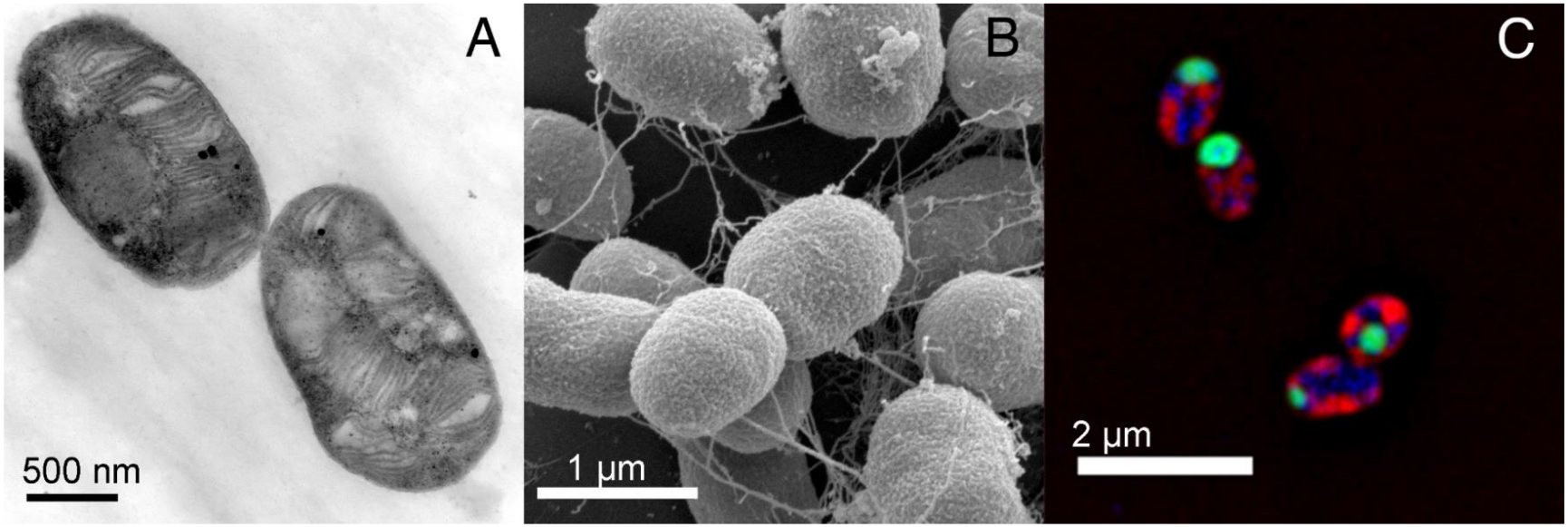

Figure 1.2: Examples of microscopy in *M. alcaliphilum* 20Z^{R}.
(A) Transmission electron micrograph. (B) Scanning electron micrograph. (C) Epifluorescent micrograph with DAPI(blue), Fm4-64 (red), sfGFP (green).

Chapter 1 contains material published by Collins DA & Kalyuzhnaya MG. (2018) “Navigating methane metabolism: Enzymes, compartments, and networks” in Methods in Enzymology **613**:349-383. doi: 10.1016/bs.mie.2018.10.010. The dissertation author was the primary investigator and author of this paper.

CHAPTER 2

Microminerals and Metabolism: Cell Structure, Energetics and Cell Performance Are Steered by Copper Availability

Abstract

Compartmentalization of reactions in higher level structures such as organelles enables the diverse metabolic capacities and is best studied in multi-cellular organisms. Metabolic pathways compartmentalization is increasingly recognized in prokaryotes and warrants the union of structural studies that are paired to systems level analysis of cellular function. Methanotrophic bacteria are known for their ability to form an array of intracytoplasmic membrane (ICMs) to house the key enzymes involved in primary metabolic network for methane oxidation. It has been seen before that in methanotrophs Cu availability modulates membrane formation, and improves the efficiency of methane utilization, mostly due to the activation of pMMO. The impacts of structural changes on cell energetics are not well understood. In this study multi-omics was paired to structural analysis of *M. alcaliphilum* 20Z^R while monitoring core physiological parameters (respiration, fermentation, cell growth and carbon conversion efficiency), during growth on methanol and methane in conditions of varied trace element (copper, calcium, and lanthanum) availability. Here I show that cell performance changes in growth conditions containing copper is due to the internal remodeling of the cell ultrastructure. Induction of the intracytoplasmic membrane network results in higher growth rate, increases to substrate & oxygen consumption ratios and a shift in the energetic network of the cell. This change occurs in conditions contain both calcium and lanthanum and on

substrates methanol and methane. The impacts of this effect changed cell output in the presence of copper towards enhanced growth rate but reveals a phenotype of overflow metabolism in which fast growing cells secrete fermentation products such as formate or acetate during growth on methanol. The integration of cellular morphology and phenotypes with metabolomic, proteomic and transcriptomic data reveals the tradeoffs between intracellular space for biosynthetic and catabolic reactions in a model system which is easily shifted between cellular ‘modes’ by changes in growth conditions.

2.1 Introduction

The metabolic capacity of cells, either free-living or in tissues, is typically defined by the sum of all the energy producing reactions and anabolic costs like synthesis and maintenance of the enzymes involved in them (Diaz & Vazquez, 2018). Energy also must be spent on functional and structural features such as the secretion of proteins. Extrapolating this principle follows that proteins and structural features determine cellular functions which defines the physiological capability of an organism or tissue. The spatial organization of metabolism in cells begins with membrane compartments such as the cell itself and the organelles within it.

In prokaryotes as well as higher cellular life it is established that the simplest function of membranes occurs in acting as capacitors (Ray, *et al.* 2016), separating charge or chemiosmotic potential on either side of lipid-rich microdomains such as the cellular membrane bilayer. Membranes also function to partition the cell for reactions in specific sites. Glycolytic reactions take place in the cytosol for eukaryotes and prokaryotes, but with further downstream reactions with the products of glycolysis are subject to spatial separation from the cytosol. In eukaryotes, the products are directed to energy recovery in membrane-rich organelles, i.e., mitochondria. In the mitochondria integral membrane proteins establish a charge differential through the pumping of protons as part of the electron transport chain, which terminally results in generation of ATP by Complex V gating this built-up potential for ATP synthesis (Sanadi 1965). The ability to localize multiple reactions, maintaining their directionality, avoiding kinetic bottlenecks is crucial in eukaryotes and prokaryotic cells. The mitochondria, characterized as the source of a eukaryotic cell's energy, is distinguished by the internal

membrane network within the organelle. This unique ultrastructure is a hallmark of the important metabolic functions it carries out within cells, but it also functions as the locus for metals such as Fe and Cu in eukaryotes: each Complex of the electron transport chain contains Fe-S clusters, heme prosthetic groups or Cu center active sites in the case of Complex IV (Xu, *et al.* 2013). This positions the mitochondria at a crossroads for structurally compartmentalized metabolism and metal homeostasis for the cell.

Membrane sub-compartmentalization within cytosol is observed in several unrelated clades of prokaryotes with highly specialized metabolic functions such as phototrophs *Rhodopseudomonas* (Varga & Staehelin 2021), anaerobic ammonium-oxidizing 'anammox' bacteria in the *Planctomycetes* phylum (van Niftrik & Jetten, 2012), and in methane-oxidizing bacterial methanotrophs (Suzina, *et al.* 1985). Intracytoplasmic membranes had sporadically been identified in heterotrophic microbes such as *E. coli* $O111_{a1}$ as membrane 'mesosomes' (Schaitman & Greenawalt, 1966), but ultimately result from a regulatory mutation instead of metabolic function (Altenburg and Suit, 1970). The volume of the cell for these bacteria is sub-compartmentalized by formation of intracytoplasmic membranes subtracting from the remaining cytosol which must house the genome, protein synthesis machinery such as ribosomes, cytoskeleton, as well as catabolic enzymes to support the cell. This tradeoff between cell components, the formation of membranes, and the portioning of metabolic function between them and the cytosol results in a rationing of the energetic economy of the cell (Zhuang, *et al.* 2011). membranes had sporadically been identified in heterotrophic microbes such as *E. coli* $O111_{a1}$ as membrane 'mesosomes' (Schaitman & Greenawalt,

1966), but ultimately result from a regulatory mutation instead of metabolic function (Altenburg and Suit, 1970).

The contemporary multi-omics approaches (metabolomics, proteomics, transcriptomics) to not preserve cell structure information and thus have limited potential for studying these specialized metabolic functions in microbial systems. Transcriptomics and proteomic methods generate important datasets in deciphering the changes in metabolism for microbes but are necessarily destructive of cellular structures. The nature of multi-omics losing structural data on cell compartmentalization has resulted in analytical methods which infer much about cell state (Parca*, et al.* 2018). Without preservation of prokaryotic subsystems and compartmentalization this method and can only make inferences from global changes generated by data analysis. Pairing subcellular structural characterization through electron microscopy studies with multi-omics links changes in cellular structure to physiology for microbes and can refine the creation of flux models for these organisms when structure is tied to existing knowledge of cell physiology and new multi-omics data (Almaas, *et al.* 2004).

Early studies of methanotrophs identified the unique ultrastructural feature of the intracytoplasmic membrane network in cells (Davies & Whittenbury, 1970). Structural characterizations came to classify methanotrophs based on the orientation of the ICM networks to the cell membrane; observed as perpendicular to the cell membrane in stacked bundles (Type I; *Methylomonas*, *Methylococcus*, *Methylobacter*) or parallel to the cell membrane in less organized layers (Type II; *Methylosinus*, *Methylocystis*). It was speculated in these characterizations that methane solubility would be higher in the

network of membranes present compared to the aqueous medium and may be important structure for methanotrophic metabolism.

Intracytoplasmic membranes in methanotrophs enable ‘specialized’ metabolisms such as those seen in phototrophs and ammonium or nitrite oxidizing bacteria (Smith and Ribbons, 1970). The formation and maintenance of membranes in different orientations for intracytoplasmic membranes is still unclear but presumed to originate from invaginations of the cellular membrane ultimately (de Boer & Hazeu, 1972). The ICM network is dynamic throughout the entire cell volume; freeze etched models of *M. trichosporium* identify ICMs to be analogous in 3-dimensions to mitochondrial cristae having enclosed volumes within them and extending in multiple planes (Weaver and Dugan, 1975).

Explorations of the effect of copper on *Methylococcus capsulatus* (Bath) identified a switch between the type of methane monooxygenase present in cells, in which the soluble enzyme was replaced by a membrane bound particulate form (Stanley, *et al.* 1983). This has further been codified into the paradigm of the “copper switch” for methanotrophs having both sMMO and pMMO in which extracellular copper is imported through dedicated transporters and results in an enzymatic switch to the membrane bound methane monooxygenase (Semrau, *et al.* 2013).

Copper has typically been identified as a toxic cation to most bacterial species, which must have a way to oxidize or chelate the metal before it enters the cytoplasm. Studies of the proteome in betaproteobacteria has involved identification of potential detoxification proteins or transporters for genera such as *Burkholderia*, *Bordetella* and

Neisseria, but the role of copper does not extend to specialized metabolism in this class (Antoine, *et al.* 2019). To manage the acquisition of copper and deliver it to enzymes such as pMMO, specialized copper binding cytosolic proteins such as Csp1 in *M. trichosporium* OB3b bind multiple equivalents of Cu (I) ions (Vita, *et al.* 2015). The importance of metals beyond copper for aerobic methanotrophs has continued to reveal additional 'switches' in response to rare earth elements (REEs) (Semrau, *et al.* 2018). The REE lanthanum was identified to induce and be the source of activity for an alternative methanol dehydrogenase XoxF (Hibi, *et al.* 2011). This has led to expand the importance of REEs beyond Lanthanum to genera outside of the aerobic methanotrophs to the phyla Verrucomicrobia (Pol, *et al.* 2013) as well as the importance of metals such as manganese and iron for the anerobic methane oxidizing Archaea (Beal, *et al.* 2009).

These switches apply to the model organism of this work, *Methylotuvimicrobium alcaliphilum* 20Z^R, in which metals and micronutrients unite metabolism and structure. These structural dynamics impact the physiology for cells which is captured by multi-omics and electron microscopy to complete a picture of the 'black box' of metabolism in a prokaryotic system. Previous studies show that metals such as lanthanum impact the metabolism and redox balance of the cell (Akberdin, *et al.* 2018). These changes were discovered through global multi-omics but do not explain aspects of the cell's biology which led to measurable physiological changes such as growth rate or substrate. I hypothesize that metals induce changes in *M. alcaliphilum* at the structural level which enable the cell performance improvements. To test this *M. alcaliphilum* was grown through transitions of metals and substrate while monitoring cell performance. During

these transitions cells were also examined for structural changes using transmission electron microscopy to explain the effect on cellular output. The importance of cellular real estate of both cytosolic volume and membrane will have impacts on metabolism as cells shift between respiration and fermentation during growth in which I predict ICMs will generate increased reliance on respiration as they house the electron transport chain and pMMO.

2.2 Methods

Growth media

M. alcaliphilum $20Z^R$ was grown in P medium as described in Chapter 1 with 0.02 $g*L^{-1}$ $CaCl_2$ x 2 H_2O or 0.06 $g*L^{-1}$ $LaCl_3$ x 7 H_2O as specified, with or without 1.2 $g*L^{-1}$ $CuSO_4$ x 5 H_2O in conditions where specified (Akberdin, *et al.*, 2018; Collins & Kalyuzhnaya 2018). Substrate was supplied as methane gas in gas inflow or methanol in stock media feed bottles when indicated.

Cultivation in bioreactor system

Continuous cultivation took place in DasBox mini bioreactor BioBLU® f Single-Use Vessels (Eppendorf) in 150ml of P media as described in Chapter 1. Control unit set points for temperature (°C), agitation (RPM), gas flow (slh), media in flow and out flow ($mL*hr^{-1}$) are described in Table 2.1. Growth of cultures was monitored through periodic sampling to measure optical density (OD_{600nm}).

BlueSens gas sensors were used to measure the percent gas composition of O_2, CO_2, and CH_4 released from the system to calculation consumption. Samples were removed from bioreactors for multi-omics studies as well as for electron microscopy

during turbidostatic growth phases. For transition experiments cultures are started in P media with no copper containing methanol before transitioning to P media with copper containing methanol and then to P media with copper and methane. Samples of inflow media were removed to determine initial methanol concentrations. After all the samples were obtained for initial no copper conditions, the bioreactors were transitioned to media with copper through the media inflow pumps, and later methane added to inflow gas during the final stage of transition.

Starvation of cultures and subcellular fractionation targeting membranes

The effect of starvation from substrate was examined using proteomics by collecting bioreactor cultures during chemostat growth phase in media containing copper and methane as substrate. The collected samples were transferred to sterilized bottles and sealed with no additional methane or oxygen added to the headspace of the bottle. These samples were then incubated at 30°C with 200 RPM rotation in an orbital shaker for 4 or 7 days of starvation from methane. To resume feeding on methane for the cultures the headspace was equilibrated with fresh room air through a 0.22 μm filter before sealing and adding methane gas (20% headspace). Samples from starved state and during recovery with methane were collected for methanol concentration assays as well as subcellular fractionation.

To fractionate actively growing, starved, and recovered cultures 50 mLs of each culture (in duplicate) were centrifuged at 5000 x g to pellet cells. After discarding supernatant, the pellets were washed by resuspending in half-volume of 20 mM Tris pH8 (1% NaCl). The washed cells were centrifuged again and resuspended in 5 mL in

20 mM Tris pH8. The resuspended cells were then disrupted by French press by passage twice at 1000 psi. Unbroken whole cells and cell debris was then pelleted by centrifuge at 2,500 x g for 15 min. The supernatant was then centrifuged at high speed to pellet S-layers, outer membranes, and cell wall materials at 20,000 x g for 1 hour. To purify ICMs the supernatant was ultracentrifuged at 257,000 x g for 2.5 hr at 4°C to pellet membranes from cytosolic supernatant. To fractionate the total membranes further the pellet was centrifuged on a 20-70% Sucrose gradient in 20 mM Tris pH 8 at 116,000 x g for 2.5 hr at 4°C. These fractions were then recovered at 257,000 g for 2.5 hr for downstream proteomics.

Multi-omics workflow

Proteomics

As described in Akberdin, *et al*. 2018 and Chapter 1, 50 ml samples from bioreactors were collected in technical replicates from each condition for total protein extraction before digestion and quantification. 500 ng samples of peptides in water were subjected to liquid chromatography-tandem mass spectrometry (LC-MS/MS).

Transcriptomics

RNA preparation

RNA extraction and preparation protocol was adapted from Johnson, *et al.* (2020): To 2 mL screw-cap tubes (1 tube per sample) 0.5 g of 0.1 mm zirconia-silica beads (BioSpec Products) are added. Samples of batch or bioreactor cultures (45 ml, with OD =0.3-1) are transferred into tubes containing 5 mL of the ‘stop solution’ (5%

water-equilibrated phenol in ethanol). Cells were collected by centrifugation at 2500g for 15 min at 4^{o}C; the supernatant is removed and discarded. Collected cell pellets are resuspended in 350 µL of RLT buffer (RNeasy Mini Kit) and transferred into the prepared 2 mL screw-cap tubes. Samples were homogenized using TissueLyser for 1 min, then cooled on ice for 2 min (repeated 2-3 times). Homogenized samples were centrifuged for 2 min; the supernatant was transferred into a new tube.

One volume of ethanol is added to the supernatant, mixed and transferred to a RNeasy spin column and centrifuged according to the kit. An on-column DNase digestion (ThermoFisher) was utilized before returning to the kit protocol to elute with 50 µL RNase-free water by centrifuging for 1 min at 8000g. For quality control RNA concentration is determined using nanodrop spectrophotometer and purity of RNA preparations confirmed by negative PCR and positive RT-PCR. The RNA library samples were then sequenced on an Illumina HiSeq2500 with ~50 million/sample SR50 reads by IGM Genomics Center, University of California, San Diego.

Metabolomics

In collaboration with Metabolon for untargeted metabolomics cell pellet samples from no copper/methanol, copper/methanol, and copper/methane conditions were extracted at a constant weight per volume of extraction solvent and equally split for analysis on LC/MS/MS and Polar LC platforms. Detected ions were matched to an in-house library of standards in collaboration with Metabolon for metabolite identification of 325 total compounds and for quantitation by peak area integration. Welch's two sample

t-tests were performed using natural log-transformed scaled imputed data to identify biochemicals that were significantly different ($p \leq 0.05$) based on culture condition.

Enzymatic methanol measurement

Samples were removed from Bioreactor vessels or from methane recovering starved cultures and centrifuged at 14,000 x g to pellet cells before collecting supernatant for use in the methanol test. An enzymatic methanol quantification test (Mangos & Haas, 1996) was used on sample which causes a change of color from clear to green in the presence of methanol for the chromogen 2,2'-azino-bis-(3-ethylbenzothiazoline-6-sulfonic acid) (ABTS). The assay combines ABTS, peroxidase, alcohol oxidase, and the sample in 0.1 M potassium phosphate buffer, pH 7.5. The development of color is measured during the assay on a spectrophotometer (Jenway) at a wavelength of 405 nm and for a duration of 1 min to calculate the rate of the reaction. A methanol standard curve of known concentration was created at a range of 0.025 mM – 2.5 mM to generate linear equation for rate to concentration and compared to the samples to determine their concentration of methanol. The samples from the bioreactors were diluted 1,000-fold to fit into the range of the standard ladder, which is within the limits of the enzymatic assay.

HPLC mixed acid measurement

Supernatant from bioreactor cultures of *M. alcaliphilum* 20Z^R grown in methanol, with or without copper were analyzed for organic acids by high-performance liquid chromatography (HPLC) with the Agilent 1100 Series HPLC system with Agilent 1100

isocratic pump and variable UV absorbance detector. The organic acids were separated at 25°C using ion exclusion column (Rezex ROA-Organic Acid H+ (8%) LC column; 300 mm length x 7.8 mm internal diameter) using sulfuric acid (0.005 N) in the mobile phase at a flow rate of 0.5 mL/min and a run time of 30 minutes. The injection volumes for samples used 10 µL with detection wavelength of 210 nm. Organic acid standards of formate, acetate, citrate, lactate, and succinate at 1 mM, 10 mM and 100 mM were used to create a linear equation for concentration from peak area for each standard to determine concentration in unknown samples.

Electron microscopy

Following protocols from Hayat (1981) & Collins and Kalyuzhnaya (2018), cell samples from bioreactors are mixed 1:1 (v:v) with 2% glutaraldehyde in 0.1 M cacodylate buffer for 1 hr on ice for primary fixation and washed in 0.1M cacodylate buffer afterwards twice. The cells are then resuspended in the same buffer and secondarily fixed in 1% osmium tetroxide in 0.1M cacodylate buffer for 1 hr on ice before washing cells three times in dH_2O. Fixed cells are then embedded in 1% (w/v) agarose solution in dH_2O before dehydration in a graded ethanol series (1 hr in 35% - 95% (v/v) ethanol, and three times in 100% ethanol. Samples are *en bloc* stained in 1% uranyl acetate in 75% ethanol before proceeding to higher ethanol percentages). Samples were infilitrated with Epon 812 in a 3-step graded Epon:acetone series before polymerizing the resin at 60°C under vacuum for 48 hours. Sections were then obtained on a diamond knife (Diatome) at 65nm section thickness and stained post-sectioning

with 1% uranyl acetate and then 40 mM lead nitrate solutions before drying and imaging at 100 keV in a Tecnai G2 transmission electron microscope.

ICM measurement

The intracytoplasmic membrane content of cells in each condition was measured from transmission electron micrographs using the Fiji/ImageJ software (Schindelin, *et al.* 2012). Each cell area was measured in nm^2 from the margin of the cell membrane, followed by any regions of the ICM within the cell. The percent of total ICM area of the total cell area was then calculated and plotted in GraphPad Prism version 8 (GraphPad Software, San Diego, California USA, www.graphpad.com).

Gas consumption measurement

To determine consumption rates of gas and changes in composition after passing through the bioreactor cultures, exhaust gas from each bioreactor was fed through Bluesens sensors to measure methane, oxygen, and carbon dioxide concentrations. The same sensors for each gas were also connected to the inflow gas tubing of each bioreactor to determine gas inflow starting composition for calculating consumption which is the change in percentage per flow rate.

To verify the Bluesens gas consumption results from the outflow of each bioreactor, 2 technical replicates of 25mL each were removed from each of 4 bioreactors from 2019 (Bioreactors 1 and 2 had no copper while bioreactors 3 and 4 had copper) and transferred to 125 mL crimp-sealed bottles. Once the culture was transferred, gas samples were removed for the baseline measurements and then they

were placed in a 30°C orbital shaker at 200 rpm. During a 3-hour period oxygen consumption was measured using a gas chromatograph at set time points 0, 1.5, and 3 hrs using 1 mL of gas from the headspace of each bottle.

2.3 Results

Growth parameters and cell performance impacts from trace elements

Continuous culture conditions were maintained in the DasBox system for 30 bioreactor runs during transitions between growth with and without copper containing P medium as well as during growth on methanol or methane as carbon substrate. The volume of each reactor vessel was maintained at 150 ml with a targeted flow rate new media at 10% (15 ml*hr^{-1}) total reactor volume (Tables 2.1). During growth in bioreactors copper increases growth rate measured by mean growth rate between conditions and is significantly higher for cultures growing on methanol with copper compared to without as measured by dilution rate (Graph 2.1).

During growth on methanol as a substrate, culture consumes consume significantly more methanol (mean 45 mmol * h^{-1}*g^{-1} CDW for copper) and oxygen when copper is in the culture medium (Graph 2.2). Cultures with copper consume 4.5 times more methanol than those without copper, this increased substrate consumption correlated with higher rates of O_2 consumption and CO_2 production as measured by BlueSens. However, cells show only modest increase in growth rates, and a portion of consumed carbon was secreted as formate (Table 2.6).

Cellular ultrastructure is remodeled in response to copper

The impact of copper on cell ultrastructure is seen in both Ca and La containing media regardless of carbon substrate provided for the cultures (Figure 2.1). Without copper cells lack the extensive intracytoplasmic membrane network typical of methanotrophs. The cell volume is largely filled by granules of 50-100 nm diameter low electron-density typical of glycogen storage granules known to be produced in *Methylotuvimicrobium sp.* (Fu, *et al.* 2019). The outer surfaces of cells in both Ca and La media also shows a dense array of surface layer proteins (discussed further in Chapter 3), which are not as prominent in conditions having Cu in the media. Additionally, extremely electron-dense granules of a large range of diameters are observed, which is typical of osmium-philic lipid stores. The phenotype of electron-dense granules in lack of copper compared to with copper is also seen in *Methylococcus capsulatus* (Bath) in which their function during growth without copper was unclear (Prior & Dalton, 1985).

The presence of copper in media results in a dramatic change of the interior cell volume from the formation of the intracytoplasmic membrane network. This is consistent for both Ca and La media and is independent of the carbon substrate cells are using. The display of surface layer proteins is also diminished for cells in these conditions indicating it may be transcriptionally repressed or regulated by the metal. The ICM network constitutes a large volume of the cell as measured by coverage of the cell cross sections when measured. An average of between 40-55% of cell area is covered by ICM membranes in conditions having copper compared to 5-10% for cells grown without copper (Graph 2.7). In some instances, it is observed that ICMs encircle existing

granules in micrographs (Figure 2.4), which presumably occurs in 3-dimensions around them as predicted by Weaver and Dugan (1975).

Gene expression and proteomics highly key impact of copper to central methane-based metabolism

Copper strongly induces key metabolic proteins crucial to methanotrophic bacteria regardless of growth substrate. These are enzymes involved in the oxidation of methane and methanol including particulate methane monooxygenase (*pmoBAC*) and the primary Ca-dependent methanol dehydrogenase and accessory proteins (*mxaFI*) as well as the oxygen carrier bacteriohemerythrin (*bhr*) (Table 2.2). At the protein level the Protein spectral counts (PSCs) for PmoBAC and MxaFI also are increased) The genes for synthesis of required cofactors for these genes, PQQ and related cytochrome c-L (*mxaG*) are also induced by copper. The lack of copper reveals increased transcription of copper-repressible genes such as *corAB* as well as the alternative La-dependent methanol dehydrogenase *xoxF*, which is repressed by copper in this condition. Enzymes of the TCA cycle are also upregulated in lack of copper (aconitate hydratase/fumarase). Growth on copper also affects several proteins involved in iron metabolism and acquisition such as heme transporters and receptors and iron siderophores. Without copper several genes potentially related to metal acquisition such as *corAB* are repressed while others such as divalent cation transporters (*feoB*, *feoA*) and small metal binding proteins (*smbP*) are significantly upregulated.

The electron transport chain is also affected by copper availability: without copper an alternative *hox*-type complex I (NADH dehydrogenase) is present as well as

cytochromes cyt_{cl}, $cyt_{c'beta}$, and cyt_{p460}. With copper a different *nqr*-type complex I is predominantly transcribed as well as increased transcription of complex IV and the associated oxygen carrier *bhr*. The amount of formate dehydrogenase detected also is impacted by the metals in culture conditions. The tungsten-dependent FDH is the only FDH detected by proteomics, with no PSCs measured for the molybdenum-dependent enzyme. Additionally copper results in higher amounts of FDH as well as methanol as substrate for growth.

Central metabolite changes and membrane synthesis precursors in response to copper

At the level of metabolites there some shift present between conditions containing copper compared to those without but suggests a very stable pool of intermediates in *M. alcaliphilum* overall. There is an increase in pyruvate, peptides and amino acid metabolites upstream from the TCA cycle is seen in the absence of copper (Table 2.3 & Table 2.4) as well as glycolysis pathway intermediates such as phosphoenolpyruvate in the absence of copper (Table 2.5). The presence of copper does however result in a significant increase in metabolites associated with membrane biogenesis: tetradecanedioate, phospho-ethanolamine, 1-palmitoleoyl-2-oleoyl-GPE (16:1/18:1), 1-stearoyl-GPG (18:0), myristoleate (14:1n5) as well as lipid synthesis precursors are increased several-fold (Tables 2.3, 2.4, 2.5).

Mixed acids are excreted during culture conditions of the bioreactor

During growth on methanol for copper and no copper conditions there is a retention peak at approximately 19 mins for conditions containing copper, but not in the

copper-free conditions (Table 2.6). This peak corresponds to formate, with concentrations between 2-4.6 mM in several samples. There is a small area peak at later retention times potentially corresponding to an additional excreted organic acid

Starvation and subcellular fractionation proteomics

Samples from starved cultures (4 days and 7 days) were tested for methanol concentrations at intervals after feeding with methane. For both cultures of both durations of starvation from methane, a spike of methanol in cell free supernatants is observed after feeding (Graph 2.4). This methanol peak occurs approximately 50 mins after resuming growth on methane but decreases as cells consume the excess methanol. Micrographs during the starved state show the presence of ICMs within cells, although there is some dilation of inter-ICM spaces and between stacks of the vesicles (Figure 2.3).

To confirm isolation of membranes, targeting ICM vesicles, aliquots of bands identified in sucrose gradient fractionation step were imaged by negative staining transmission electron microscopy (Figure 2.4). Micrographs show vesicle-like structures approximately 100 nm in diameter from the densest band of the sucrose gradient post-ultracentrifugation. Also seen are occasional cup-like structures which presumably are surface layer protein contamination.

Proteomics of fractions of starved cultures during the recovery phase while growing on methane show that most proteins of the central metabolic network are present (Table 2.7). An increase of PSCs for methanol dehydrogenase MxaFI after feeding, which correlates with the drop in methanol over time. Contamination from

central methane metabolism proteins such as pMMO are seen in multiple membrane fractions as well as cytosolic ones, indicating contamination of fractions during the workflow.

2.4 Discussion

To examine the changes that occur in cell performance beyond a sum of proteins or genes expressed, a true Hegelian synthesis of systems level biology and ultrastructure answers the call to see beyond the microbial cell as single 'black box' of reactions (Saks, Monge & Guzun, 2009). By pairing the observations of changes to cellular ultrastructure with multi-omics this study addresses the changes of cell performance that are seen in response to trace elements and substrate. Previous studies identified (Akberdin, *et al.* 2018) the impacts of metals such as lanthanum on cellular functions but integrating cellular structures in this Chapter explains the observed cellular performance changes that metals induce in *M. alcaliphilum* 20Z^R.

Gene expression and proteomics.

Growth on copper strongly induces the key metabolic proteins crucial to methanotrophic bacteria. These are the genes involved in the oxidation of methane and methanol: particulate methane monooxygenase (*pmoBAC*) and the primary Ca-dependent methanol dehydrogenase (*mxaFI*) and accessory proteins (*mxa* cluster). These constitute the hallmark entry point for aerobic methanotrophy in many genera of bacteria (Anthony, 1982). The effect of copper extends to the cofactors required for enzymes such as MxaFI: the cytochrome c_L (MxaG) as well as the prosthetic group pyrroloquinoline quinone (PQQ), which requires copper for synthesis as well

(Puehringer, *et al.* 2008). These Cu-dependent effects occurred with methanol or methane as substrate and with both Ca and La in the media, but media containing La results in a shift to the 'alternative' *xoxF* type methanol dehydrogenase (Chu & Lidstrom, 2016). This MDH also has an associated cytochrome *xoxG* which is induced as well as a formaldehyde activating enzyme 2 (*fae2*) that presumably captures additional carbon flux from formaldehyde to formate. Fae2 has been shown in methanotrophs like *M. extorquens* to function in 'archaeal-like' pathways which capture formaldehyde via the H_4MPT pathway to formate (Kalyuzynaya, *et al.* 2005). The formate dehydrogenase Fdh1AB is increased by copper as well as by methanol as substrate. The increased amount of Fdh1AB reflects the need to generate reducing power by regenerating NADH from the single-carbon compound, which is frequently encountered in engineering C_1 metabolism into strains such as *E. coli* (Bang, *et al.* 2020).

Previous proteomic surveys showed similar effects of copper on the methane metabolic system in *M. capsulatus* (Bath). Copper in culture media induced a shift in from soluble methane monooxygenase to particulate methane monooxygenase (Kao, *et al*. 2004). This copper shift in methane-oxidizing enzymes is not observed in *M. alcaliphilum*, which only possesses particulate forms of the enzyme. It was similarly seen in *M. casulatus* (Bath) that the oxygen carrier, bacteriohymerthrin (*bhr*), is induced by copper presumably to support O_2 demand by pMMO or Complex IV. It is established that Bhr contributes only to respiration and does not impact pMMO activity in *M. alcaliphilum* $20Z^R$ (Nariya & Kalyuzhnaya, 2020).

The function of the copper repressible gene *corAB* is still unknown but has been speculated to be involved in uptake of copper by some mechanism. The data here does identify its upregulation and PSCs without copper which is similar to some proteins such as MALCv_0971 (Chapter 3). Previous mutants for *corA* showed growth defects compared to wild type *M. albus* BG8 at several copper concentrations (Berson and Lidstrom, 1997). CorA had also been identified as a potential cell surface associated protein, which would position it in a hypothetical copper acquisition role in *M. alcaliphilum* 20Z^R (Shchukin, *et al.* 2011). The lack of copper may drive the acquisition of other metals through FeoBA or SmbP to compensate for necessary enzymes or represent a broad strategy for importing metal cations in *M. alcaliphilum* 20Z^R. Divalent cation transporters *feoBA* are known to import iron into *Vibrio* (Stevenson, *et al.* 2016) and small metal binding proteins (*smbP)* are shown to bind copper (Barney, *et al.* 2004). Additionally, an identified Lanthanum-switch transporter (TonB, MALCv4_0546) is upregulated in conditions without lanthanum in the media indicating its involvement in transport of the metal for *M. alcaliphilum* 20Z^R as it was identified in *M. buryatense* 5GB1C (Groom, *et al.* 2019).

Mineral availability impacts to the core makeup of the electron transport chain due to the availability of copper for *M. alcaliphilum* 20Z^R. Without copper, alternative *hox*-type complex I (NADH dehydrogenase) and cytochromes cyt_{cI}, $cyt_{c'beta}$, and cyt_{p460} are transcribed. A switch between the suite of c-type cytochromes was also detected by thin-layer chromatography of proteins isolated from *M. capsulatus* (Bath) which occurs in response to copper (Karlsen, *et al.* 2008). A different *nqr*-type Complex I predominate in transcripts and PSCs with copper, which is known to be a Na^+ translocating Complex

identified in marine organisms and some pathogens (Steuber, *et al.* 2014). The entire *nqr*-type Complex I is present in the *M. alcaliphilum* genome (*nqrABDDF*) and includes the known sodium channel subunit NqrB. The terminal O_2-dependent oxidases of the respiratory chain, cytochrome caa_3 and cytochrome ba_3 oxidase, are understandably induced in expression and PSCs due to copper, which is involved in O_2 reduction (Kaila and Wikstroem, 2021). The higher levels of Complex IV in copper conditions supports the observed increased oxygen consumption by cultures in this condition (Graph 2.2) and the hypothetical oxygen carrier for the ETC and pMMO *bhr* is increased as well. Oxygen consumption would be expected to increase as observed during growth on methane due to the activity of particulate methane oxygenase which is oxygen- (and copper-) dependent, so increased presence of Bhr may prevent competition between terminal oxidases and pMMO for O_2.

Metabolite shifts indicate membrane-synthesis due to copper

At the level of metabolites there is very little shift present between conditions containing copper compared to those without. This suggests a very stable pool of intermediates in *M. alcaliphilum* overall. There is an increase in pyruvate, peptides and amino acid metabolites upstream from the TCA cycle indicating a possible need to generate reducing power through the TCA cycle or a larger pool of costly to synthesis amino acids, as well as glycolysis pathway (PEP) in the absence of copper. Enhanced production of metabolites such as pyruvate and stocks which feed into acetyl-CoA pools are a key bottleneck in metabolic engineering for production of biofuels (Clomburg and Gonzalez, 2010). Metabolomic results such as these based on culture conditions and

trace minerals may represent a non-genetic mechanism in overcoming such bottlenecks at large scale.

The presence of copper does however result in a significant increase in metabolites associated with membrane biogenesis: tetradecanedioate (C14), phospho-ethanolamine, 1-palmitoleoyl-2-oleoyl-GPE (16:1/18:1), 1-stearoyl-GPG (18:0), myristoleate (14:1n5) as well as other lipids are increased several-fold which coincides with the large structural changes. Studies on fatty acid composition for Type I & Type II methanotrophs such as *M. capsulatus* (Sessions, *et al.* 2002) and *M. trichosporium* (Weaver, *et al*. 1975) indicates that phosphoethanolamine based C_{14}, C_{16} (16:1 & 16:0) and C_{18} (18:1) fatty acids are typical (Makula, R.A. 1978). As mentioned for the precursors of lipid biosynthesis, strains such as *M. alcaliphilum* $20Z^{R}$ would be ideally positioned as 'cell factories' for lipid biosynthesis with minimal genetic manipulations required and several culture-dependent enhancements to yield compared to species with do not natively produce ICMs such as *E. coli* (Lee, *et al.* 2011).

Cell Performance during culture conditions

The cellular performance seen during culture conditions are largely explained by the presence of copper in the media. During continuous culture cells grown in the presence of copper display several hallmarks of rapid growth such as a high dilution rate for bioreactors which is required to maintain a constant optical density. These actively growing cells consume more substrate either methanol or methane, as well as oxygen. This phenotype in continuous culture varies from batch cultures in the same conditions revealing a phenotype that may be indicative of trends seen and other model

systems. The impacts of growth conditions have been shown to have effects on cell performances in other closely related strains such as *Methylotuvimicrobium buryatense* 5GB1. Cells grow to a much higher density (CDW) simply by increasing agitation of during culturing, but this caused a tradeoff between cell composition – at lower agitation (500 RPM) cells have more membranes (lipid %) and less glycogen, which was opposite trend at higher agitation (Fei, *et al*. 2018). During culturing of *M. alcaliphilum* the agitation rate, and thus gas exchange was not varied (500 RPM) but in combination with trace mineral may create new metabolic states overall.

Agitation rates introduce gases such as methane to cultures but crucially oxygen as well, which can have downstream effects on metabolism and thus cell performance. *M. alcaliphilum* has been shown to produce excreted organic acids during O_2-limited conditions such as formate, acetate, succinate, and lactate (Kalyuzhnaya, *et al.* 2013). The cost of this excretion compromises biomass production for cells but represents one of the few means of generating energy in the low-O_2 conditions through the PP_i branch of the EMP (Embden–Meyerhof–Parnas) pathway of glycolysis. This culture-dependent phenotype does not account for the secretion of organic acids during adequate oxygenation of cultures as measured in Table 2.6. Such an observation has two preliminary explanations at this time: cells are experiencing sub-optimal oxygenation in the culture conditions despite vigorous agitation or cells are entering a state known as overflow metabolism.

Inadequate oxygenation could be a result of the capacity of cells to burn through available oxygen too quickly in the given volume of the reactor, or at gas flow rates provided. In copper conditions, we see increased consumption of oxygen compared to

without copper but at increased cell density the available oxygen is insufficient for the metabolic load of the reactor. At the level of individual cell O_2-limitation is experienced resulting in secreted acids like formate. The alternative, overflow metabolism, occurs in unicellular and multicellular life and is observed as an ineffective metabolism of substrate into incompletely oxidized waste state. In *E. coli* rapidly growing cells will begin to excrete organic acids like acetate while growing on other substrates, and eventually consume the acetate once other substrates are consumed (Wolfe 2005).

This phenomenon has been refined into two potential explanations that could be addressed in *M. alcaliphilum* 20Z^R due to its unique structural changes because of growth state. Overflow metabolism may be due to the compromise between space within the cell in terms of volume related to the available surface area of the cell membrane which houses respiratory machinery and other import/export proteins (Szenk, *et al.* 2017). As they grow larger, the decrease in surface area:volume ratio results in increased requirement for complexes of the respiratory chain in the cell membrane until a limit is reached. At this limit of membrane crowding by proteins, cells must rely on fermentation to increase ATP demand. *M. alcaliphilum* has the benefit of membrane rich states and a minimal membrane state due to copper in which to test this available ‘real-estate’ hypotheses. The ICMs may also produce another kind of ‘real-estate’ demand beyond the 2-dimensional plane of the membrane, because they occupy and potentially sequester areas of cell volume required for cytosolic enzymes. Cells also create glycogen storage granules, even during conditions which promote ICMs in the cell. These two areas indicate the metabolic costs of occupying space in the cell, between membranes or storage granules of glycogen are not equal. This reasoning

explains the higher substrate consumption, but weaker cell growth performance of the glycogen synthesis mutant strain AP18 of *M. buryatense* 5GB1 (Fei, *et al.* 2018).

An additional explanation for overflow metabolism is based on the biosynthetic costs of enzymes in fermentation and respiration are not equal, thus under conditions of substrate limitation the energetically cheaper pathway will be used for efficiency (Basan, *et al.* 2015). In the case of *E. coli* this explains acetate excretion with plentiful oxygenation as the result of rapid growth during abundant substrate conditions, compared to respiration which is favorable at lower growth rates or reduced carbon availability. For *M. alcaliphilum* there exists two possible routes for breakdown of the sugar formed by condensation of formaldehyde and ribulose-monophosphate in the ribulose-monophosphate pathway (RuMP) preceding glycolysis: the Entner-Doudoroff (ED) and the Embden-Meyerhof-Parnas (EMP). As shown by Kalyuzhnaya*, et al.* (2013) the EMP results in higher efficiency in generating ATP and NADH for cells, but why maintain enzymes in the ED pathway? In *M. buryatense* 5GB1 elements of the ED pathway were essential for growth on methane likely due to reducing power generated by NADPH in the pathway or regulating accumulation of pathway products (He, *et al.* 2021). Maintenance of both pathways may be tied to the energetic costs of the enzymes in them (ED < EMP) or there exists a thermodynamic chokepoint affecting the two pathways unequally. A possible bottleneck is the pentose phosphate pathway (PPP), which is required for regeneration of ribulose 5-phosphate for C1-unit assimilation. The PPP connects EMP and several other key steps of metabolism in *M. alcaliphilum* such as the TCA cycle and the ED pathway (Stincone, *et al.* 2016). The breakdown of storage granules of glycogen upon starvation or during active growth may favor one

pathway over another route, as glucose dehydrogenase (GDH) and gluconate kinase (GntK) connect glucose into gluconate-6P which can enter the ED pathway (Rozova, *et al.* 2021).

The allotment of proteome resources between the various catabolic and anabolic reaction downstream of methane oxidation and carbon fixation into ribulose-monophosphate explain the observation of excreted formate as overflow metabolism. Further modeling will have to synthesize the wealth of multi-omics data paired with the extensive structural information to determine if the 'real estate' or biosynthesis cost hypotheses for are valid in explaining overflow metabolism in *M. alcaliphilum*.

Structural changes

The structural impact of copper seen in *M. alcaliphilum* $20Z^R$ resulted in changes to the appearance of the surface layer protein as well as increased membrane content internally due to the intracytoplasmic network. The apparent regulation of the surface layer protein was similarly seen in *Methylomonas albus* BG8 which displayed a more prominent surface layer in conditions lacking copper compared to media with the metal (Collins, Buchholz & Remsen, 1991). For *M. albus* BG8 copper induced ICM formation that was concomitant with increased methane oxidation rates due to higher activity of methane monooxygenase which was detected to be increased in abundance by SDS-PAGE. The transition from granules to intracytoplasmic membranes within the cell volume was observed to be induced by substrate in *Methylosinus trichosporium* OB3b (Brannan and Higgins, 1981) and in *Methylococcus capsulatus* (Texas) (Hyder, *et al.*, 1979), however these studies did not examine trace minerals. In *M. trichosporium* OB3b

membranes are predominant in cells under high CH_4:O_2 batch culture conditions compared to high O_2:CH_4 ratios. These membranes are diminished to singly layered structures during continuous culture and cells begin to accumulate large poly-β-hydroxybutyrate. For *M. capsulatus* (Texas) methanol grown cells featured electron-lucent inclusions and little to no ICMs compared to cultures grown on methane. This is not observed in *M. alcaliphilum* 20Z^R, instead cells respond to copper instead of substrate availability in both batch and continuous cultures. The formation of intracytoplasmic glycogen granules appears to be important for normal growth in *M. alcaliphilum* 20Z^R as deletion of glucokinase inhibits growth and mutations of sucrose-based glycogenesis does not prevent formation of glycogen granules (Mustakhimov, *et al.* 2016).

Transitions between structural states was postulated to occur in response to copper in media for the Type II methanotroph *Methanomonas margaritae*. By transitioning copper-grown cells to media without copper a remodeling of the internal membrane network was observed for cell-membrane parallel ICMs (Takeda and Tanaka, 1980). The membranes degenerate from tightly stacked bands at the cell membrane with copper into dilated vesicles distributed throughout the cell without copper in the media. The synthesis of particulate enzymes such as pMMO (or another unidentified protein) may be sufficient for generating the formation of ICMs; in *E. coli* overexpression of a major membrane protein the F(1)F(o) ATP synthase causes the formation of intracytoplasmic membranes (Arechaga, *et al.* 2000). Ultimately the ‘gatekeeper’ protein of ICM formation remains unknown.

Supernatants of bioreactor cultures contain excreted acids

Cultures grown with copper on methanol, but not without copper excrete formate into the culture media during adequate aeration. This excretion occurs importantly with sufficient oxygen and during a state when much of the cell volume is occupied by membranes. The excretion of mixed acids during states like these are characteristics of overflow metabolism, discussed further below. *M. alcaliphilum* 20Z^{R} has previously been shown to excrete organic acids such as formate and acetate because of the lack of tungsten in the media during batch methane culture (Akberdin, *et al.* 2018). Formate concentration (2.4 mM) measurements in that study are approximately the concentrations as HPLC measurements here (Table 2.4), for conditions containing tungsten as well. The supernatant of *M. buryatense* 5GB1 grown in batch cultures showed an accumulation of mixed acids, particularly formate, when grown on methanol compared to methane (Fu, *et al.* 2019) indicating that this common feature of the genus may not be due to oxygen availability entirely. The excretion of formate is consistent with the phenotype of overflow metabolism but the exact cellular mechanism responsible will require additional computational modeling which accounts for the structural changes as well as metabolic networks of the *M. alcaliphilum*.

Starvation from methane

The dynamics of transitions between states of starvation from and active growth on methane show that the active growing metabolic network is dynamic to substrate availability. The excretion of methanol into the media after feeding indicates an incomplete methane assimilation pathway, primarily a lack of periplasmic methanol

dehydrogenase (MDH) which oxidized the methanol produced from methane by pMMO. Strains of *M. trichosporium* OB3b have been engineered to similarly accumulate this methanol in the media by controlled expression of a XoxF-type MDH over the typical MxaF-type (Ito, *et al.* 2021). In the absence of methane, the starved cells demonstrate some of the hallmarks of 'substrate free growth' seen in Type II methanotrophs by Takeda and Tanaka (1980) in which vesicle-like structures replace the organized ICM network. The proteomics taken from the starved to transition state reveals that fractions are heavily contaminated by the key enzyme of methane oxidation (pMMO). Particulate methane monooxygenase was detected in all fractions, indicating ineffective separation of unique ICM-based vesicles. A study on membrane fractions from *M. capsulatus* detected methane oxidation activity in multiple fractions during ultracentrifugation pull-downs, so distribution of particulate methane monooxygenase may be throughout the cell in ICMs as well as cytoplasmic membranes (Ribbons and Michalover, 1970). This excreted methanol also indicates a different source of electrons for the reactivation of methane oxidation by pMMO than was hypothesized. Methane is oxidized without a direct coupling of methanol oxidation by MDH, a mechanism proposed previously (Culpepper and Rosenzweig, 2014). It indicates a complex energetic network in *M. alcaliphilum* is involved in the very initial stage of aerobic methane oxidation, which is independent from the direct coupling model prediction.

As shown in this study structural changes are critical for explaining the cell performance outputs which change in response to trace metals such as copper in media for *M. alcaliphilum* 20Z^R. These changes are captured by multi-omics at a global level

but contextualized by the changes at the cellular level when structural changes are compared between metal conditions in media. Synthesis of cellular structural changes with systems level -omics will lead to more complete models for methanotrophs as we refine metabolic models. The phenotype of overflow metabolism is also one which would not be predicted from these analyses. While metabolomics would indicate excretion of fermentation products it is not something which would be recognized by proteomics or transcriptomics and structural analysis also provides an explanation for overflow metabolism by analysis of the cell but is equally unable to predict the phenotype by itself. Linking data from multi-omics, structural measurements and metabolic models will require future computational modeling to explore the unexpected overflow phenotype in *M. aculiphilum* $20Z^R$.

2.5 References

Akberdin, I.R., Thompson, M., Hamilton, R., Desai, N., Alexander, D., Henard, C.A., Guarnieri, M.T., Kalyuzhnaya, M.G. (2018) Methane utilization in Methylomicrobium alcaliphilum 20Z^R: a systems approach. Scientific Reports **8:** 2512 doi.org/10.1038/s41598-018-20574-z.

Akberdin, I.R., Collins, D.A., Hamilton, R., Oshchepkov, D.Y., Shukla, A.K., Nicora, C.D., Nakayasu, E.S., Adkins, J.N., Kalyuzhnaya, M.G. (2018) Rare earth elements alter redox balance in *Methylomicrobium alcaliphilum* 20Z^R. Frontiers in Microbiology **9**:2735. doi: 10.3389/fmicb.2018.02735.

Altenburg, B.C., Suit, J.C. (1970). Relationship between deoxyribonucleic acid and intracytoplasmic membranes in *Echerischia coli* $O111_{a1}$. Journal of Bacteriology **103**(1):227-237.

Almas, E., Kovacs, B., Vicsek, T., Oltvai, Z.N., Barabasi, A.L. (2004). Global organization of metabolic fluxes in the bacterium *Escherichia coli*. Nature **427**: 839-843.

Anthony C. The Biochemistry of Methylotrophs. London: Academic; 1982

Antoine, R., Rivera-Millot, A., Roy, G., Jacob-Dubuisson, F. (2019). Relationships between copper-related proteomes and lifestyles in beta Proteobacteria. Frontiers in Microbiology. doi.org/10.3389/fmicb.2019.02217.

Arechaga, I., Miroux, B., Karrasch, S., Huijbregts, R., de Kruijff, B., Runswick, M.J., Walker, J.E. (2000). Characterisation of new intracellular membranes in Escherichia coli accompanying large scale over-production of the b subunit of F(1)F(o) ATP synthase. FEBS Letters **482**(3):215-9. doi: 10.1016/s0014-5793(00)02054-8.

Bang, J., Hwang, C.H., Ahn, J.H., Lee, J.A, Lee, S.Y. (2020). *Escherichia coli* is engineerd to grow on CO_2 and formic acid. Nature Microbiology. doi.org/10.1038/s41564-020-00793-9.

Barney, B.M., LoBrutto, R., Francisco, W.A. (2004). Characterization of a small metal binding protein from *Nitrosomonas europaea*. Biochemistry **43**(35):11206-13. doi: 10.1021/bi049318k.

Basan, M., Hui, S., Okano, H., Zhang, Z., Shen, Y., Williamson, J.R., Hwa, T. (2015). Overflow metabolism in *Escherichia coli* results from efficient proteome allocation. Nature **528**:99-106 doi:10.1038/nature15765.

Beal, E.J., House, C.H., Orphan, V.J. (2009). Manganese- and iron-dependent marine methane oxidation. Science **325**:184-187.

Berson, O., Lidstrom, M.E. (1997). Cloning and characterization of *corA*, a gene encoding a copper-repressible polypeptide in the type I methanotroph, *Methylomicrobium albus* BG8. FEMS Microbiology Letters **148**:169-174.

Brannan, S.J., Higgins, I.J. (1981). The effect of growth conditions on intracytoplasmic membranes and methane mono-oxygenase activities in *Methylosinus trichosporium* OB3b. Journal of General Microbiology **125**:63-72.

Chu, F., Lidstrom, M.E. (2016). XoxF acts as the predominant methanol dehydrogenase in the type I methanotroph *Methylomicrobium buryatense*. Journal of Bacteriology **198**(8). DOI: https://doi.org/10.1128/JB.00959-15

Collins, M.L.P., Buchholz, L.A., Remsen, C.C. (1991). Effect of copper on *Methylomonas albus* BG8. Applied and Environmental Microbiology **57**(4):1261-1264.

Clomburg, J.M., Gonzalez, R. (2010). Biofuel production in *Eschericia coli*: the role of metabolic engineering and synthetic biology. Applied Microbiology and Biotechnology **86**:419-434.

Culpepper, M.A., Rosenzweig, A.C. (2014). Structure and protein–protein interactions of methanol dehydrogenase from *Methylococcus capsulatus* (Bath). Biochemistry **53:**6211–6219. doi: 10.1021/bi500850j

Davie, S.L., Whittenbury, R. (1970). Fine structure of methane and other hydrocarbon-utilizing bacteria. Journal of General Microbiology **61**:227-232.

De Boer, W.E., Hazeu, W. (1972). Observations on the fine structure of a methane-oxidizing bacterium. Antonie van Leeuwenhoek **38**: 33-47.

Diaz, J., Vazuez, A. (2018). A physical model of cell metabolism. Scientific Reports **8**:8349. doi.org/10.1038/s41598-018-26724-7.

Fei, Q., Puri, A.W., Smith, H., Dowe, N., Pienkos, P.T. (2018). Enhanced biological fixation of methane for microbial lipid production by recombinant *Methylomicrobium buryatense*. Biotechnlogy for Biofuels **11**:129. doi.org/10.1186/s13068-018-1128-6.

Fu Y, He L, Reeve J, Beck DAC, Lidstrom ME. 2019. Core metabolism shifts during growth on methanol versus methane in the methanotroph Methylomicrobium buryatense 5GB1. mBio 10:e00406-19. https://doi.org/10.1128/mBio.00406-19.

Groom, J.D., Ford, S.M., Peseky, M.W., Lidstrom, M.E. (2019). A mutagenic screen identifies a TonB-dependent receptor required for the lanthanide metal switch in the type I methanotroph *Methylotuvimicrobium buryatense* 5GB1C. Journal of Bacteriology **201**(15): e00120-19.

Kao, W.C., Chen, Y.R., Yi, E.C., Lee, H., Tian, Q., Wu, K.M., Tsai, S.F., Yu, S.S.F., Chen, Y.J., Aebersold, R., Chan, S.I. (2004) Quantitative proteomic analysis of metabolic regulation by copper ions in *Methylococcus capsulatus* (Bath). Journal of Biological Chemistry **279**(49):51554-51560.

Hayat, M. A. (1981). Fixation for electron microscopy. Academic Press.

Hyder, S.L., Meyers, A., and Cayer, M.L. (1979) Membrane modulation in a methylotrophic bacterium *Methylococcus capsulatus* (Texas) as a function of growth substrate. Tissue & Cell **11**(4):597-610.

He, L., Groom, J.D., Lidstrom, M.E. (2021). The Entner-Doudoroff pathway is an essential metabolic route for *Methylotuvimicrobium buryatense* 5GB1C. Applied and Environmental Microbiology **87**(3):e02481-20.

Henard, C.A., Smith, H.K, Guarnieri, M.T. (2017). Phosphoketolase overexpression increases biomass and lipid yield from methane in an obligate methanotrophic biocatalyst. Metabolic Engineering **41**:152-158.

Hibi, Y., Asai, K., Arafuka, H., Hamajima, M. Ito H., Yoshimori K., Ishikawa M., Hori K., Kamachi, T. (2021) Switching between methanol accumulation and cell growth by expression control of methanol dehydrogenase in *Methylosinus trichosporium* OB3b mutant. Frontiers in Microbiology 12:639266. doi: 10.3389/fmicb.2021.639266

Karlsen, O.A., Lillehaug, J.R., Jensen, H.B. (2008). The presence of multiple c-type cytochromes at the surface of the methanotrophic bacterium *Methylococcus capsulatus* (Bath) is regulated by copper. Molecular Microbiology **70**(1):15-26.

Kalyuzhnaya, M. G., Korotkova, N., Crowther, G., Marx, C. J., Lidstrom, M. E., & Chistoserdova, L. (2005). Analysis of gene islands involved in methanopterin-linked C1 transfer reactions reveals new functions and provides evolutionary insights. Journal of bacteriology, 187(13), 4607–4614. https://doi.org/10.1128/JB.187.13.4607-4614.2005

Kalyuzhnaya, M.G., Yang, S., Rozova, O.N., Smalley, N.E., Clubb, J., Lamb, A., Nagana Gowda, G.A., Raftery, D., Fu, Y., Bringel, F., Vuilleumier, S., Beck, D.A.C., Trotsenko, Y.A., Khmelenina, V.N., Lidstrom, M.E. (2013). Highly efficient methane biocatalysis revealed in a methanotrophic bacterium. Nature Communications **4**:2785.

Lee, S., Jeon, E., Jung, Y., Lee, J. (2012). Heterologous co-expression of *accA*, *fabD*, and thioesterase genes for improving long-chain fatty acid production in *Pseudomonas aeruginosa* and *Escherichia coli*. Applied Biochmistry and Biotechnology **167**:24-38.

Prior, S.D., Dalton, H. (1985). The effect of copper ions on membrane content and methane monooxygenase activity in methanol-grown cells of *Methylococcus capsulatus* (Bath). Journal of General Microbiology **131**:155-163.

Mangos TJ, Haas MJ. 1996. Enzymatic determination of methanol with alcohol oxidase, peroxidase, and the chromogen 2,2‘-azinobis(3-ethylbenzthiazoline-6-sulfonic acid) and its application to the determination of the methyl ester content of pectins. J Agric Food Chem 44:2977–2981.

Makula, R.A. (1978). Phospholipid composition of methane-utilizing bacteria. Journal of Bacteriology **134**(3):771-777.

Mustakhimov, I.L., Rozova, O.N., Solntseva, N.P., Khmelenina, V.N., Reshetnikov, A.S., Trotsenko, Y.A. (2016). The properties and potential metabolic role of glucokinase in halotolerant obligate methanotroph *Methylomicrobium alcaliphilum* 20Z. Antonie Van Leeuwenhoek **110**(3):375-386. doi: 10.1007/s10482-016-0809-z.

Nariya, S., Kalyuzhnaya, M.G. (2020). Hemerythrins enhance aerobic respiration in Methylomicrobium alcaliphilum 20Z^{R}, a methane-consuming bacterium, FEMS Microbiology Letters **367(**2): fnaa003, https://doi.org/10.1093/femsle/fnaa003

Parca, L., Beck, M., Bork, P., Ori, A. (2018) Quantifying compartment-associated variations of protein abundance in proteomics data. Molecular Systems Biology **14**: e8131. DOI: 10.15252/msb.20178131

Pol, A., Barends, T.R.M., Dietl, A., Khadem, A.F., Eygensteyn, J., Jetten, M.S.M., Op den Camp, H.J.M. (2013). Rare earth metals are essential for methanotrophic life in volcanic mudpots. Environmental Microbiology doi:10.1111/1462-2920.12249.

Puehringer, S., Metlitzky, M., Schwarzenbacher, R. (2008). The pyrroloquinoline quinone biosynthesis pathway revisited: A structural approach. BMC Biochemistry **9**:8 https://doi.org/10.1186/1471-2091-9-8

Ray, S., Kassan, A., Busija, A.R., Rangamani, P., Patel, H.H. (2016). The plasma membrane as a capacitor for energy and metabolism. American Journal of Physiology Cell Physiology **310**(3): C181–C192. doi:10.1152/ajpcell.00087.2015: 10.1152/ajpcell.00087.2015

Ribbons, D.W., Michalover, J.L. (1970) Methane oxidation by cell-free extracts of *Methylococcus capsulatus*. FEBS Letters **11(1):**41-44.

Rozova, O.N., Ekimova, G.A., Molochkov, N.V., Reshetnikov, A.S., Khmelenina, V.N., Mustakhimov, I.I. (2021). Enzymes of an alternative pathway of glucose metabolism in an obligate methanotroph. Scientific Reports **11**:8795.

Saks, V., Monge, C., Guzun, R. (2009). Philosophical basis and some historical aspects of systems biology: From Hegel to Noble – Applications for bioenergetic research.

Sanadi, D.R. (1965). Energy-linked reactions in the mitochondria. Annual Review of Biochemistry **34**:21-48.

Schindelin, J., Arganda-Carreras, I., Frise, E., Kaynig, V., Longair, M., Pietzsch, T., Cardona, A. (2012). Fiji: an open-source platform for biological-image analysis. Nature Methods, 9(7), 676–682. doi:10.1038/nmeth.2019

Shuchukin, V. N., Khmelenina, V. N., Eshinimayev, B. Ts., Suzina, N. E., Trotsenko, Yu. A. (2011) Primary characterization of dominant cell surface proteins of halotolerant methanotroph *Methylomicrobium alcaliphilum* 20Z. Microbiology, 2011, Vol. 80, No. 5, pp.608–618

Semrau, J.D., DiSpirito, A.A., Gu, W., Yoon, S. (2018). Metals and methanotrophy. Applied and Environmental Microbiology **84**(6): e02289-17. doi: 10.1128/AEM.02289-17

Semrau J.D., Jagadevan S., DiSpirito A.A., Khalifa A., Scanlan J., Bergman B.H., Freemeier B.C., Baral B.S., Bandow N.L., Vorobev A., Haft D.H., Vuilleumier S., Murrell J.C. (2013). Methanobactin and MmoD work in concert to act as the 'copper-switch' in methanotrophs. Environmental Microbiology **15**(11):3077-86. doi: 10.1111/1462-2920.12150.

Sessions, A.L., Jahnke, L.L., Schimmelmann, A., Hayes, J.M. (2002). Hydrogen isotope fractionation in lipids of the methane-oxidizing bacterium *Methylococcus capsulatus.* Geochimica et Cosmochimica Acta **66(**22):3955–3969.

Smith, U., Ribbons, D.W. (1970) Fine Structure of *Methanomonas methanooxidans*. Arch. Mikrobiology **74**:116-122.

Stanley, S.H., Prior, S.D., Leak, D.J., Dalton, H. (1983). Copper stress underlies the fundamental change in intracellular location of the methane mono-oxygenase in methane-oxidizing organisms: studies in batch and continuous cultures. Biotechnology Letters **5**(7):487-492.

Stevenson B., Wyckoff E.E., Payne S.M. (2016). *Vibrio cholerae* FeoA, FeoB, and FeoC interact to form a complex. Journal of Bacteriology **198**(7):1160-70. doi: 10.1128/JB.00930-15.

Stincone, A., Prigione, A., Cramer, T., Wamelink, M.M.C., Campbell, K., Cheung, E., Olin-Sandoval, V., Gruening, N.M., Krueger, A., Alam, M.T., Keller, M.A., Breitenbach, M., Brindle, K.M., Rabinowitz, J.D., Ralser, M. (2016). The return of metabolism: biochemistry and physiology of the pentose phosphate pathway. Biological Reviews Cambridge Philosophical Society **90**(3):927-963. doi.org/10.1111/brv.12140.

Suzina, N.E., Chetina, E.V., Trotsenko, Y.A., Fikhte, B.A. (1985). Peculiarities of the supramolecular organization of intracytoplasmic membranes in methanotrophs. FEMS Microbiology Letters **30**:111-114.

Szenk, M., Dill, K.A., de Graff, A.M.R. (2017). Why do fast-growing bacteria enter overflow metabolism? Testing the membrane real-estate hypothesis. Cell Systems **5**(2):95-104 doi.org/10.1016/j.cels.2017.06.005

Takeda, K., Tanaka, K. (1980). Ultrastucture of intracytoplasmic membranes of *Methanomonas margaritae* cells grown under different conditions. Antonie van Leeuwenhoek **46**:15-25.

van Niftrik, L., Jetten, M.S. (2012). Anaerobic ammonium-oxidizing bacteria: unique microorganisms with exceptional properties. Microbiology and Molecular Biology Reviews **76**(3): 585–596. https://doi.org/10.1128/MMBR.05025-11

Varga, A.R., Staehelin, L.A. (2021). Spatial differentiation in photosynthetic and non-photosynthetic membranes of *Rhodopseudomonas palustris*. Journal of Bacteriology **154**(3). DOI: https://doi.org/10.1128/jb.154.3.1414-1430.1983

Villada, J.C., Duran, M.F., Lim, C.K., Stein, L.Y., Lee, P.K.H. (2021) Integrative genome-scale metabolic modeling reveals versatile metabolic strategies for methane utilization in *Methylomicrobium album* BG8. BioRxiv doi.org/10.1101/2021.03.21.436352.

Vita, N., Platsaki, S., Basle, A., Allen, S.J., Paterson, N.G., Crombie, A.T., Murrell, J.C. (2015). Nature **525**:140-143. doi:10.1038/nature14854

Weaver T.L., Dugan, P.R. (1975). Ultrastructure of *Methylosinus trichosporium* as revealed by freeze etching. Journal of Bacteriology **121**(2):704-710.

Weaver, T.L., Patrick, M.A., Dugan, P.R. (1975). Whole-cell and membrane lipids of the methylotrophic bacterium *Methylosinus trichosporium*. Journal of Bacteriology **124**(2):602-605.

Wolfe, A.J. (2005). The acetate switch. Microbiology and Molecular Biology Reviews **69**(1):12-50. doi: 10.1128/MMBR.69.1.12-50.2005.

Xu, W., Barrientos, T., Andrews, N.C. (2013). Iron and copper in mitochondrial diseases.Cell Metabolism **17**. doi.org/10.1016/j.cmet.2013.02.004.

Zhuang, K., Vemuri, G.N., Mahadevan, R. (2011). Economics of membrane occupancy and respiro-fermentation. Molecular Systems Biology **7**(1):500. doi:10.1038/msb.2011.34.

Table 2.1: Summary of conditions maintained during Bioreactor runs of multiple experiments

Variable	2018						2019		2020	
Media / Substrate	Ca (-)Cu CH_3OH	Ca (+)Cu CH_3OH	Ca (+)Cu CH_4	La (-)Cu CH_3OH	La (+)Cu CH_3OH	La (+)Cu CH_4	Ca (-)Cu CH_3OH	Ca (+)Cu CH_3OH	Ca (-)Cu CH_3OH	Ca (+)Cu CH_3OH
Temperature (°C)	30	30	30	30	30	30	30	30	30	30
Gas Flow (slh)	0.1	0.2	0.5	0.1	0.1	0.1	0.3	0.3	0.5	0.5
Agitation (RPM)	500	500	500	500	500	500	500	500	500	500
Volume (mL)	150	150	150	150	150	150	150	150	150	150
Mean flow rate ($mL*hr^{-1}$)	15.5	15.5	15.5	9	10.5	11	7	15.5	9.5	15.75
Replicates (n)	2	2	2	2	2	2	4	4	3	3

Data collected with Richard Hamilton.

Graph 2.1: Growth rates of bioreactor cultures with or without copper on methanol.

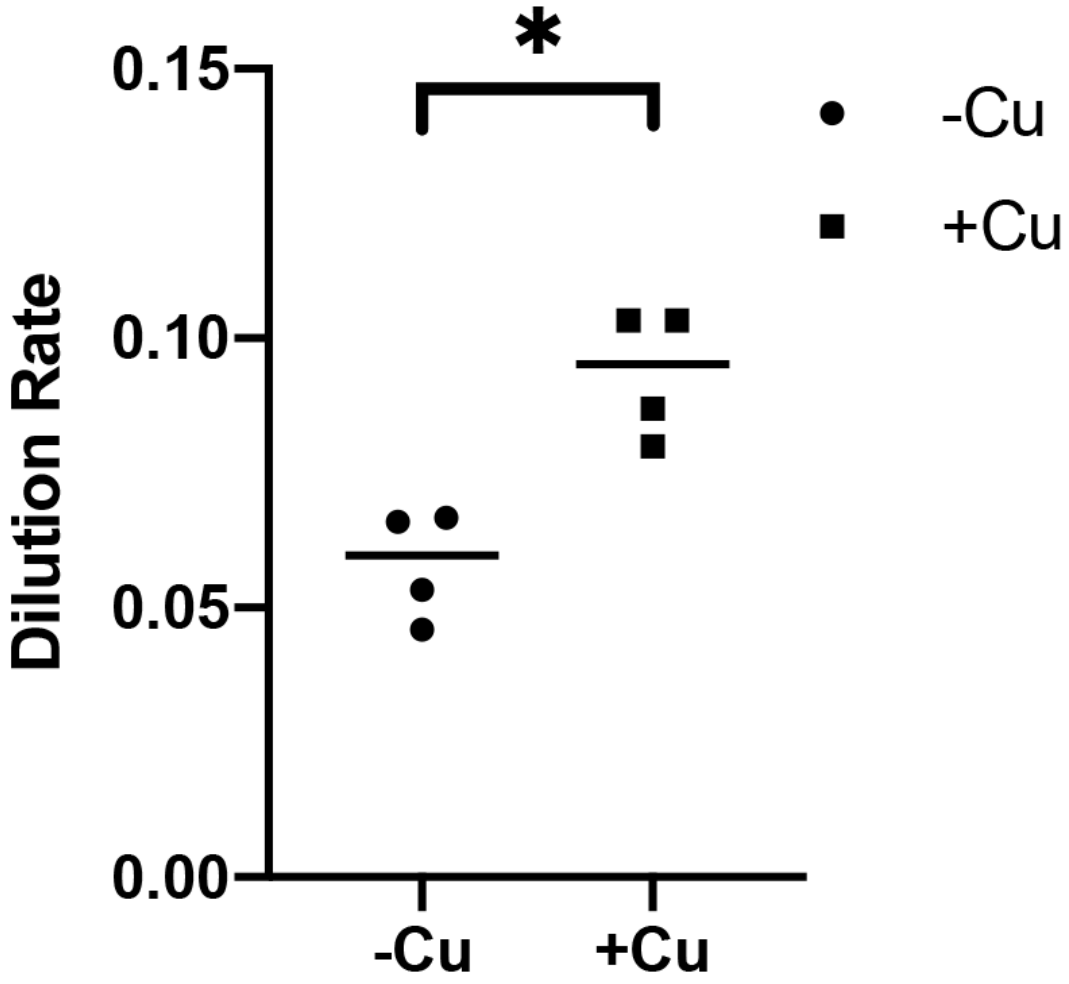

Data collected with Richard Hamilton.

Graph 2.2: Oxygen and methanol consumption rates for bioreactor cultures.

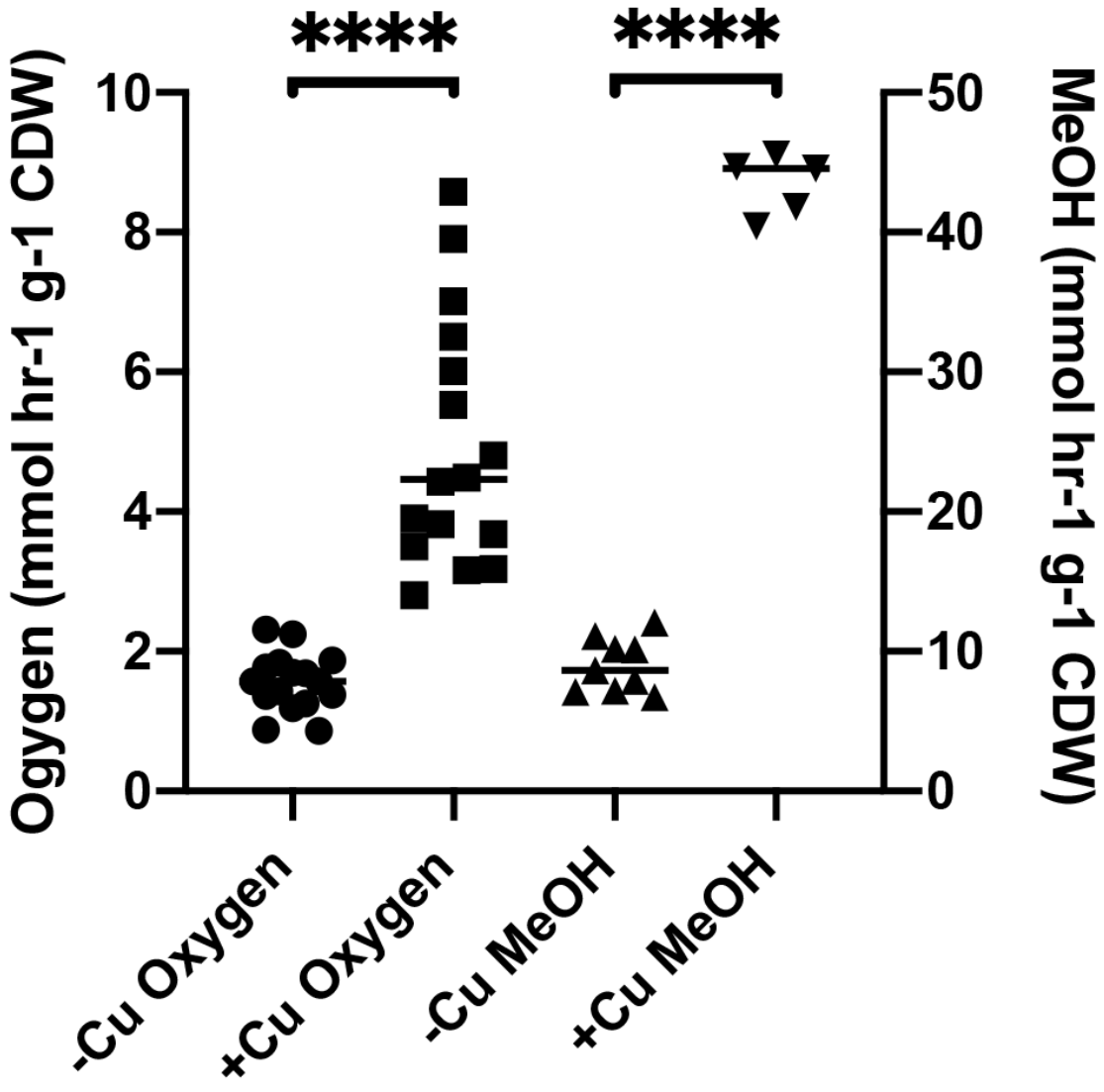

Data collected with Richard Hamilton.

Table 2.2: Transcriptome and proteome changes of major metabolic functions in bioreactor conditions.

				log2FoldChange>0	> in Ca-NoCu-CH3OH		> in La-noCu-CH3OH		> in La-NoCu-CH3OH		> in La-CH4		Ca PSCs			La PSCs			
				log2FoldChange<0	> in Ca-CH4		> in La-CH4		> in Ca-NoCu-CH3OH		> in Ca-CH4								
Gene ID	Protein ID	Gene Name	Protein Name		log2FC	p-value	log2FC	p-value	log2FC	p-value	log2FC	p-value	Ca noCu PSC Total	Ca wCu PSC Total	Ca Cu CH4 PSC Total	La noCu PSC Total	La wCu PSC Total	La Cu CH4 PSC Total	PSC
Methane oxidation																			
MEALZ_0514	CCE22212	pmoC	methane monooxygenase subunit C		-2.37	3.43E-107	-1.78	3.81E-08	0.30	5.23E-01	-0.28	8.13E-02	38	148	50	57	168	88	1000
MEALZ_0515	CCE22213	pmoA	methane monooxygenase subunit A		-3.47	9.60E-208	-3.31	6.99E-36	-0.29	3.92E-01	-0.44	1.36E-02	11	87	43	17	81	44	100
MEALZ_0516	CCE22214	pmoB	methane monooxygenase subunit B		-3.51	1.50E-143	-2.40	1.82E-12	0.55	2.37E-01	-0.54	2.81E-03	1133	3159	893	1167	3208	1139	10
Methanol oxidation (Ca)																			1
MEALZ_3438	CCE25101	mxaL	MxaL protein		-3.21	8.79E-02	-2.47	2.89E-12	-3.44	1.29E-01	-4.18	4.45E-126	40	4	11	0	0	0	0
MEALZ_3439	CCE25102	mxaK	MxaK protein		-3.18	9.25E-02	-1.80	2.71E-04	-3.54	1.22E-01	-4.95	1.43E-152	28	8	7	0	0	0	
MEALZ_3440	CCE25103	mxaC	MxaC protein		-2.99	1.44E-01	-1.24	9.45E-03	-3.85	1.15E-01	-5.62	1.69E-212	39	3	6	0	0	0	
MEALZ_3442	CCE25105	mxaS	MxaS protein		-2.36	2.92E-01	-1.27	2.94E-02	-5.15	4.66E-02	-6.27	1.45E-230	21	3	9	0	0	0	
MEALZ_3444	CCE25107	mxaR	protein MxaR		-2.38	3.12E-01	-0.61	2.40E-01	-5.57	3.76E-02	-7.35	0.00E+00	124	44	34	0	1	0	
MEALZ_3445	CCE25108	mxaI	methanol dehydrogenase, small subunit		-2.71	2.85E-01	0.16	8.10E-01	-5.42	6.34E-02	-8.27	0.00E+00	176	35	16	0	0	0	
MEALZ_3446	CCE25109	mxaG	cytochrome c-L		-2.82	2.93E-01	-0.59	2.77E-01	-6.59	3.08E-02	-8.81	0.00E+00	156	50	22	1	1	0	
MEALZ_3447	CCE25110	mxaJ	protein MxaJ involved in regulation of methanol oxidation		-2.55	3.59E-01	-0.89	7.10E-02	-6.75	3.05E-02	-8.39	2.33E-90	61	48	26	0	0	0	
MEALZ_3448	CCE25111	mxaF	methanol dehydrogenase, large subunit		-2.69	3.49E-01	-0.50	2.64E-01	-7.72	1.67E-02	-9.91	0.00E+00	1262	294	182	16	11	2	
Methanol oxidation (La)																			
MEALZ_3497	CCE25159	xoxF	dehydrogenase xoxF		3.24	2.75E-69	-0.92	4.88E-03	-0.39	4.09E-01	3.78	3.68E-232	338	899	123	918	1125	266	
MEALZ_3498	CCE25160	xoxJ1	MxaJ-like protein		0.17	3.29E-01	-0.12	7.87E-01	-0.50	1.60E-01	-0.20	3.59E-01	78	94	17	91	83	14	
MEALZ_2642	CCE24317	xoxG4	cytochrome X (putative)		-0.77	2.48E-05	2.13	1.42E-06	2.43	5.89E-06	-0.45	2.99E-03	68	95	11	72	68	9	
Formaldehyde oxidation																			
MEALZ_2428	CCE24109	fae	formaldehyde-activating enzyme		-1.07	3.25E-21	0.18	6.87E-01	0.89	2.45E-02	-0.34	1.62E-02	1006	1218	307	1335	1160	313	
MEALZ_1456	CCE23144	fae	formaldehyde activating protein		-0.38	1.08E-02	-0.21	5.77E-01	-0.31	3.65E-01	-0.47	6.23E-03	74	99	27	76	76	24	
MEALZ_0850	CCE22544	fae2	formaldehyde-activating enzyme		-0.94	2.43E-07	0.06	9.06E-01	5.24	6.73E-85	4.25	2.98E-20	17	22	5	40	33	11	
MEALZ_0272	CCE21972	SQRDL	sulfide:quinone oxidoreductase, mitochondrial		1.86	8.41E-31	0.18	7.30E-01	-1.43	4.93E-04	0.26	3.71E-01	5	5	3	1	5	2	
Formate oxidation																			
MEALZ_1882	CCE23568	fdh1A	Tungsten-containing NAD-dependent formate dehydrogenase, alpha subunit		0.31	1.24E-02	0.07	8.78E-01	-0.43	2.07E-01	-0.17	3.29E-01	311	293	61	365	233	72	
MEALZ_1883	CCE23569	fdh1B	Tungsten-containing NAD-dependent formate dehydrogenase, beta subunit		0.21	1.41E-01	-0.31	5.00E-01	-0.68	1.21E-01	-0.15	4.14E-01	142	144	30	167	96	29	
MEALZ_0215	CCE21915	fdsD	NAD-linked formate dehydrogenase, molybdenum containing, delta subunit		0.18	5.88E-01	0.29	5.37E-01	0.27	5.32E-01	0.16	7.35E-01	0	0	0	0	0	0	
MEALZ_0216	CCE21916	fdsC	NAD-linked formate dehydrogenase, molybdenum containing, accessory protein		-0.93	3.41E-01	-2.80	7.99E-06	-0.06	9.65E-01	1.81	5.71E-03	0	0	0	0	0	0	
MEALZ_0217	CCE21917	fdsA	formate dehydrogenase subunit alpha		-0.53	5.47E-01	-2.28	3.03E-05	0.27	7.91E-01	2.02	2.97E-04	0	0	0	0	0	0	

Table 2.2: Transcriptome and proteome changes of major metabolic functions in bioreactor conditions, continued.

				log2FoldChange>0	> in Ca-NoCu-CH3OH		> in La-noCu-CH3OH		> in La-NoCu-CH3OH		> in La-CH4		Ca PSCs			La PSCs			
				log2FoldChange<0	> in Ca-CH4		> in La-CH4		> in Ca-noCu-CH3OH		> in Ca-CH4								
Gene ID	Protein ID	Gene Name	Protein Name		log2FC	p-value	log2FC	p-value	log2FC	p-value	log2FC	p-value	Ca noCu PSC Total	Ca wCu PSC Total	Ca Cu CH4 PSC Total	La noCu PSC Total	La wCu PSC Total	La Cu CH4 PSC Total	PSC
ETS																			
Complex I																			1000
MEALZ_2228	CCE23914	nqrF	Na(+)-translocating NADH-quinone reductase subunit F		-0.76	2.64E-08	-0.31	3.77E-01	0.10	8.21E-01	-0.34	2.99E-02	119	120	38	152	145	43	100
MEALZ_2230	CCE23916	nqrD	Na(+)-translocating NADH-quinone reductase subunit D		-0.83	9.01E-10	-0.71	2.04E-02	-0.26	4.74E-01	-0.37	1.74E-02	21	24	8	27	26	8	1
MEALZ_2231	CCE23917	nqrC	Na(+)-translocating NADH-quinone reductase subunit C		-1.04	1.47E-14	-1.01	7.25E-04	-0.21	6.01E-01	-0.23	1.63E-01	176	183	48	194	173	54	0
MEALZ_2232	CCE23918	nqrB	Na(+)-translocating NADH-quinone reductase subunit B		-0.64	2.24E-06	-0.41	3.12E-01	-0.33	4.59E-01	-0.55	2.69E-04	50	54	14	71	65	18	
MEALZ_2233	CCE23919	nqrA	Na(+)-translocating NADH-quinone reductase subunit A		-0.78	2.60E-10	-0.92	2.34E-02	-0.57	2.42E-01	-0.42	2.46E-03	146	177	46	200	229	61	
MEALZ_2234	CCE23920	nadA	quinolinate synthase A		-0.63	5.85E-07	0.60	1.12E-01	0.73	6.27E-02	-0.49	1.31E-03	31	31	9	33	31	10	
MEALZ_1304	CCE22993	hoxH	NAD-reducing hydrogenase hoxS subunit beta		1.66	2.39E-42	0.60	9.58E-02	-0.99	6.78E-03	0.08	7.14E-01	208	235	57	271	229	66	
MEALZ_1306	CCE22995	-	NADH:ubiquinone oxidoreductase, subunit G, iron-sulfur binding		1.31	3.83E-21	0.55	1.00E-01	-0.59	7.59E-02	0.18	3.92E-01	78	92	20	87	47	21	
MEALZ_1307	CCE22996	hoxF	NAD-reducing hydrogenase hoxS subunit alpha		1.95	6.38E-63	0.94	5.24E-03	-0.98	8.83E-03	0.04	8.51E-01	83	90	20	96	69	22	
MEALZ_1287	CCE22976	ndh	NADH dehydrogenase		-0.16	3.77E-01	-0.78	1.90E-02	-0.84	1.80E-02	-0.21	3.37E-01	14	19	4	17	25	8	
Complex II																			
MEALZ_2679	CCE24354	sdhB	succinate dehydrogenase		0.86	4.21E-09	0.39	3.35E-01	-0.33	4.47E-01	0.15	5.15E-01	26	19	2	30	18	5	
MEALZ_2680	CCE24355	sdhA	succinate dehydrogenase		1.05	2.42E-13	0.29	5.57E-01	-0.68	1.50E-01	0.09	7.26E-01	58	62	21	104	65	19	
Complex III																			
MEALZ_0632	CCE22327	petC	cytochrome c1		-0.15	3.81E-01	0.07	8.77E-01	0.05	9.12E-01	-0.16	4.84E-01	106	103	33	121	91	32	
MEALZ_0633	CCE22328	petB	cytochrome b		0.13	3.48E-01	-0.32	3.91E-01	-0.80	1.97E-02	-0.33	3.70E-02	29	32	14	18	30	19	
MEALZ_0634	CCE22329	petA	Ubiquinol-cytochrome c reductase iron-sulfur subunit (RISP)		-0.31	3.53E-02	-0.77	3.13E-02	-0.72	6.57E-02	-0.24	1.95E-01	82	117	25	116	105	34	
Complex IV - cytochrome caa3 oxidase																			
MEALZ_2312	CCE23993	-	cytochrome C oxidase polypeptide III		-1.84	2.08E-47	-1.21	9.97E-05	0.09	8.55E-01	-0.53	2.52E-04	2	10	2	7	10	2	
MEALZ_2313	CCE23994	ctaG	cytochrome C oxidase assembly protein CtaG		-1.54	9.31E-20	-1.61	5.99E-09	-0.25	5.01E-01	-0.17	4.73E-01	3	0	2	2	6	4	
MEALZ_2314	CCE23995	ctaD	cytochrome c oxidase subunit 1 (cytochrome aa3 subunit 1)		-0.89	8.99E-15	-1.10	3.02E-04	-0.77	2.85E-02	-0.55	5.43E-05	7	23	3	5	21	7	
MEALZ_2315	CCE23996	ctaC	cytochrome C oxidase subunit II		-1.89	6.80E-53	-1.86	6.04E-12	-0.42	2.40E-01	-0.43	2.90E-03	44	126	42	61	145	50	
MEALZ_2316	CCE23997	bhr	Bacteriohemerythrin		-2.06	4.42E-13	-1.39	1.95E-03	1.02	7.52E-02	0.36	2.64E-01	35	410	81	20	146	84	
Complex IV - cytochrome ba3 oxidase																			
MEALZ_1292	CCE22981	cbaD	cytochrome c oxidase, CbaD subunit		-0.58	1.50E-01	-1.21	5.21E-02	-0.98	1.02E-01	-0.34	5.73E-01	0	0	1	0	0	0	
MEALZ_1293	CCE22982	-	cytochrome C oxidase subunit II		-1.38	1.32E-16	-1.22	6.12E-05	-0.02	9.67E-01	-0.17	5.00E-01	0	7	2	0	7	2	
MEALZ_1294	CCE22983	-	cytochrome C oxidase subunit I		-1.23	1.19E-12	-0.46	1.88E-01	0.09	8.44E-01	-0.67	5.62E-04	0	0	0	0	0	0	

Table 2.2: Transcriptome and proteome changes of major metabolic functions in bioreactor conditions, continued.

				log2FoldChange>0	> in Ca-NoCu-CH3OH		> in La-noCu-CH3OH		> in La-NoCu-CH3OH		> in La-CH4		Ca PSCs			La PSCs			
				log2FoldChange<0	> in Ca-CH4		> in La-CH4		> in Ca-noCu-CH3OH		> in Ca-CH4								
Gene ID	Protein ID	Gene Name	Protein Name		log2FC	p-value	log2FC	p-value	log2FC	p-value	log2FC	p-value	Ca noCu PSC Total	Ca wCu PSC Total	Ca Cu CH4 PSC Total	La noCu PSC Total	La wCu PSC Total	La Cu CH4 PSC Total	
Cytochromes																			PSC
MEALZ_1724	CCE23411	bfr	cytochrome B557.5		-2.68	4.77E-67	-2.65	1.07E-24	0.49	1.53E-01	0.47	8.09E-03	0	0	0	0	0	0	1000
MEALZ_1725	CCE23412	bfd	bacterioferritin-associated ferredoxin Bfd		-4.30	1.93E-104	-2.61	4.24E-13	1.58	1.77E-03	-0.10	7.04E-01	0	0	0	0	0	0	100
MEALZ_0938	CCE22632	petJ	cytochrome C6		-0.96	1.33E-06	1.06	2.27E-02	1.33	1.55E-02	-0.67	3.14E-04	74	193	41	82	110	48	10
MEALZ_0390	CCE22090	-	cytochrome c class I		-0.75	3.10E-08	-0.42	2.44E-01	0.21	5.98E-01	-0.11	6.18E-01	12	14	1	4	3	0	1
MEALZ_0602	CCE22297	-	cytochrome b561		-0.56	5.40E-03	-0.49	1.85E-01	-0.03	9.44E-01	-0.09	7.89E-01	2	0	0	0	0	0	0
MEALZ_0918	CCE22612	cyp	cytochrome P460		0.45	3.69E-03	-0.45	2.17E-01	-0.77	2.79E-02	0.14	5.50E-01	7	18	1	9	10	5	
MEALZ_0702	CCE22397	cytS	cytochrome c'-beta		1.24	6.48E-13	0.89	2.25E-02	0.04	9.44E-01	0.40	2.72E-02	83	81	8	93	32	7	
MEALZ_1120	CCE22811	-	cytochrome c class I		0.43	8.10E-03	-0.36	2.97E-01	-0.63	6.02E-02	0.18	4.05E-01	0	0	0	0	0	0	
MEALZ_1295	CCE22984	-	cytochrome c family protein		-1.12	1.18E-10	-0.80	3.34E-02	0.39	3.89E-01	0.09	7.48E-01	2	0	1	1	3	0	
MEALZ_3827	CCE25482	-	cytochrome-c peroxidase		1.36	8.24E-22	0.09	8.66E-01	-1.09	1.03E-02	0.20	3.95E-01	71	57	17	85	44	19	
ATP synthesis																			
MEALZ_0329	CCE22029	atpB	ATP synthase F0, A chain		-1.14	1.51E-18	-0.73	2.25E-02	-0.08	8.60E-01	-0.48	1.00E-03	1	1	0	1	0	1	
MEALZ_0330	CCE22030	atpE	ATP synthase subunit c		-1.19	9.34E-13	-0.82	5.36E-03	-0.10	8.29E-01	-0.45	4.28E-03	0	0	1	1	0	0	
MEALZ_0331	CCE22031	atpF	ATP synthase F0 subunit B		-0.79	2.08E-10	-0.63	4.25E-02	-0.13	7.54E-01	-0.28	7.29E-02	222	196	55	238	213	55	
MEALZ_0332	CCE22032	atpH	ATP synthase subunit delta		-0.20	1.26E-01	-0.47	2.74E-01	-0.55	2.24E-01	-0.27	6.92E-02	59	56	18	71	57	18	
MEALZ_0333	CCE22033	atpA	ATP synthase subunit alpha (ATP synthase F1 sector subunit alpha)		0.06	7.34E-01	0.28	5.51E-01	-0.57	2.14E-01	-0.78	1.74E-08	304	303	66	348	317	78	
MEALZ_0334	CCE22034	atpG	ATP synthase gamma chain (ATP synthase F1 sector gamma subunit)		-0.40	3.37E-03	-0.47	1.65E-01	-0.14	7.14E-01	-0.07	7.74E-01	83	80	31	88	83	25	
MEALZ_0335	CCE22035	atpD	ATP synthase F1 subunit beta		-0.43	1.34E-03	0.12	7.57E-01	-0.13	7.47E-01	-0.67	2.51E-07	683	706	169	906	801	187	
MEALZ_0336	CCE22036	atpC	ATP synthase F1 subunit epsilon		-0.76	2.17E-09	0.34	3.61E-01	0.43	2.30E-01	-0.65	9.46E-07	3	0	0	1	1	2	
MEALZ_3735	CCE25391	atpD	ATP synthase subunit beta 2		0.75	1.35E-08	0.62	6.32E-02	-0.39	2.66E-01	-0.24	2.34E-01	8	14	2	11	13	3	
MEALZ_3741	CCE25397	-	ATP synthase subunit b 2 (fragment)		0.41	5.99E-03	0.56	9.57E-02	0.00	9.98E-01	-0.14	5.67E-01	17	18	7	24	25	8	
MEALZ_3742	CCE25398	atpA	ATP synthase subunit alpha 2		0.89	2.44E-07	0.87	3.44E-03	-0.17	6.59E-01	-0.14	6.27E-01	2	1	0	1	5	0	

Table 2.2: Transcriptome and proteome changes of major metabolic functions in bioreactor conditions, continued.

				log2FoldChange>0	> in Ca-NoCu-CH3OH		> in La-noCu-CH3OH		> in La-NoCu-CH3OH		> in La-CH4		Ca PSCs			La PSCs			
				log2FoldChange<0	> in Ca-CH4		> in La-CH4		> in Ca-noCu-CH3OH		> in Ca-CH4								
Gene ID	Protein ID	Gene Name	Protein Name		log2FC	p-value	log2FC	p-value	log2FC	p-value	log2FC	p-value	Ca noCu PSC Total	Ca wCu PSC Total	Ca Cu CH4 PSC Total	La noCu PSC Total	La wCu PSC Total	La Cu CH4 PSC Total	PSC
Central Metabolism																			
RuMP/PPP																			1000
MEALZ_1912	CCE23598	hpsi2	Hexulose-6-phosphate synthase and isomerase		0.05	7.50E-01	0.06	8.97E-01	-0.21	5.57E-01	-0.21	2.23E-01	172	215	53	196	194	61	100
MEALZ_3948	CCE25604	tal	transaldolase		0.34	1.08E-02	0.20	6.07E-01	-0.36	3.09E-01	-0.21	1.98E-01	1648	2057	345	2027	1859	427	10
MEALZ_3951	CCE25607	tkt	transketolase		0.61	1.25E-06	0.01	9.88E-01	-1.15	2.50E-02	-0.54	4.16E-04	1272	1348	363	1551	1303	417	1
MEALZ_3952	CCE25608	hpi1	3-hexulose-6-phosphate isomerase		0.10	4.49E-01	0.56	7.42E-02	-0.24	4.97E-01	-0.69	6.34E-08	201	186	42	228	136	55	0
MEALZ_3953	CCE25609	hps1	3-hexulose-6-phosphate synthase		0.26	3.91E-02	0.60	4.82E-02	-0.46	1.54E-01	-0.78	1.91E-10	437	467	122	633	477	172	
EMP																			
MEALZ_3947	CCE25603	fbaA	fructose-bisphosphate aldolase		0.37	2.58E-03	0.06	8.78E-01	-0.58	6.17E-02	-0.27	7.52E-02	751	883	144	907	849	150	
MEALZ_3079	CCE24745	gap	glyceraldehyde 3-phosphate dehydrogenase		0.47	3.50E-03	-0.81	5.01E-02	-1.23	8.07E-03	0.06	7.89E-01	308	376	67	478	424	111	
MEALZ_3080	CCE24746	pykA	pyruvate kinase II		0.28	4.87E-02	0.29	4.37E-01	-0.42	2.30E-01	-0.42	6.10E-03	403	401	84	446	369	108	
MEALZ_3549	CCE25207	pgk	phosphoglycerate kinase		0.61	1.43E-06	-0.02	9.69E-01	-0.85	2.33E-02	-0.20	2.60E-01	250	249	61	277	259	63	
EDD																			
MEALZ_0104	CCE21808	pgi	glucose-6-phosphate isomerase		0.10	5.42E-01	-0.67	8.80E-02	-0.81	5.50E-02	-0.04	8.81E-01	92	101	19	128	113	26	
MEALZ_1362	CCE23051	eda	2-dehydro-3-deoxyphosphooctonate aldolase		0.33	1.87E-02	0.13	8.04E-01	-0.69	1.16E-01	-0.48	4.93E-03	27	45	8	41	47	9	
MEALZ_1363	CCE23052	edd	6-phosphogluconate dehydratase		0.34	8.27E-03	-0.42	3.61E-01	-0.97	3.11E-02	-0.20	2.49E-01	139	163	28	193	161	43	
MEALZ_1699	CCE23386	gdhI	glucose 1-dehydrogenase 1		0.17	4.99E-01	-0.68	5.02E-02	-0.15	7.37E-01	0.70	2.47E-03	8	6	0	12	10	1	
TCA																			
MEALZ_0310	CCE22010	acnA	aconitate hydratase		2.00	2.09E-48	1.41	2.40E-07	-0.55	9.77E-02	0.05	8.35E-01	121	109	24	128	98	34	
MEALZ_1360	CCE23049	gltA	Citrate synthase 2		0.93	1.86E-14	0.26	4.92E-01	-0.81	1.55E-02	-0.13	5.13E-01	128	102	29	133	102	40	
MEALZ_1576	CCE23263	gabD	succinate-semialdehyde dehydrogenase		-0.23	1.97E-01	-0.22	5.94E-01	-0.21	6.03E-01	-0.21	3.73E-01	35	61	7	59	34	13	
MEALZ_1578	CCE23265	odhL	dihydrolipoyl dehydrogenase		0.79	5.51E-09	0.42	2.09E-01	-0.37	2.63E-01	0.02	9.52E-01	71	71	13	78	73	20	
MEALZ_1579	CCE23266	sucB	2-oxoglutarate dehydrogenase E2		0.60	3.82E-06	0.21	5.79E-01	-0.42	2.21E-01	-0.02	9.42E-01	77	73	15	90	79	25	
MEALZ_1580	CCE23267	sucA	2-oxoglutarate dehydrogenase E1		0.81	8.36E-12	0.02	9.64E-01	-0.86	2.44E-02	-0.06	7.68E-01	39	57	18	88	68	21	
MEALZ_3024	CCE24690	gltA	citrate synthase		0.23	1.31E-01	-0.08	8.68E-01	-0.46	2.40E-01	-0.14	5.42E-01	26	38	9	30	27	13	
MEALZ_3025	CCE24691	acnB	Aconitate hydratase 2		0.56	2.18E-05	0.34	4.65E-01	-0.67	1.47E-01	-0.44	3.62E-03	278	285	59	322	268	75	
MEALZ_3026	CCE24692	icd	Isocitrate dehydrogenase, NAD-dependent		0.23	1.22E-01	0.35	3.35E-01	-0.29	4.50E-01	-0.41	6.90E-03	93	85	13	171	93	18	
MEALZ_3290	CCE24955	sucD	succinyl-CoA ligase subunit alpha		0.94	8.82E-13	0.18	6.93E-01	-0.79	3.50E-02	-0.02	9.39E-01	36	44	9	62	46	13	
MEALZ_3291	CCE24956	succ	succinyl-CoA synthetase, beta subunit		0.63	1.77E-05	-0.41	3.02E-01	-0.91	1.92E-02	0.14	5.10E-01	82	61	24	101	78	24	
MEALZ_3844	CCE25499	icd	NADP-dependent isocitrate dehydrogenase		0.93	2.14E-13	0.25	5.44E-01	-0.74	4.43E-02	-0.05	8.27E-01	119	146	35	156	114	39	

Table 2.2: Transcriptome and proteome changes of major metabolic functions in bioreactor conditions, continued.

				log2FoldChange>0	> in Ca-NoCu-CH3OH		> in La-noCu-CH3OH		> in La-NoCu-CH3OH		> in La-CH4		Ca PSCs			La PSCs			
				log2FoldChange<0	> in Ca-CH4		> in La-CH4		> in Ca-noCu-CH3OH		> in Ca-CH4								
Gene ID	Protein ID	Gene Name	Protein Name		log2FC	p-value	log2FC	p-value	log2FC	p-value	log2FC	p-value	Ca noCu PSC Total	Ca wCu PSC Total	Ca Cu CH4 PSC Total	La noCu PSC Total	La wCu PSC Total	La Cu CH4 PSC Total	PSC
Central Metabolism																			
Serine Cycle and H4folate																			1000
MEALZ_3215	CCE24880	mtkB	malate thiokinase, small subunit		-0.60	4.38E-06	-0.34	4.42E-01	-0.25	5.92E-01	-0.51	2.33E-03	50	33	8	65	53	13	100
MEALZ_3216	CCE24881	mtkA	malate thiokinase, large subunit		-0.56	1.39E-05	-0.55	1.75E-01	-0.35	4.50E-01	-0.35	3.41E-02	72	98	25	111	108	20	10
MEALZ_3217	CCE24882	mclA1	malyl-CoA lyase		-0.86	7.91E-12	-0.67	5.38E-02	-0.25	5.46E-01	-0.43	7.66E-03	139	144	31	161	151	40	1
MEALZ_3218	CCE24883	sgaA	serine-glyoxylate aminotransferase		0.13	3.80E-01	-0.59	2.59E-01	-1.16	3.64E-02	-0.43	6.61E-03	403	431	66	472	418	85	0
MEALZ_3219	CCE24884	hpr2	2-hydroxyacid dehydrogenase NAD-binding		0.34	3.52E-02	-0.06	9.20E-01	-0.61	1.65E-01	-0.20	3.94E-01	56	43	12	56	51	15	
MEALZ_3220	CCE24885	mdh	malate dehydrogenase		-0.42	8.83E-04	-0.24	5.50E-01	-0.14	7.58E-01	-0.31	5.07E-02	69	79	8	61	87	22	
MEALZ_3221	CCE24886	mtdA	methylenetetrahydromethanopterin dehydrogenase; methylenetetrahydrofolate dehydrogenase		-0.10	6.38E-01	-0.21	6.76E-01	-0.53	2.53E-01	-0.41	6.41E-02	39	37	11	54	34	13	
MEALZ_3222	CCE24887	gck2	glycerate 2-kinase		0.11	5.74E-01	0.36	3.62E-01	-0.03	9.46E-01	-0.27	2.58E-01	8	2	1	13	9	3	
MEALZ_3223	CCE24888	glyA	serine hydroxymethyltransferase		0.33	1.79E-02	-0.40	3.72E-01	-1.00	2.33E-02	-0.26	1.32E-01	66	117	40	74	106	41	
MEALZ_3224	CCE24889	ftfL	formate-tetrahydrofolate ligase		0.49	1.06E-04	0.36	4.00E-01	-0.71	8.39E-02	-0.57	1.38E-04	45	51	15	76	50	17	
Fatty acid metabolism																			
MEALZ_0452	CCE22151	fadE	acyl-coenzyme A dehydrogenase		2.23	8.28E-17	1.06	7.59E-03	-0.30	4.71E-01	0.89	4.72E-02	1	1	0	4	0	1	
MEALZ_0453	CCE22152	-	3-hydroxyacyl-CoA dehydrogenase		3.18	8.39E-48	0.66	1.22E-01	-0.98	3.06E-03	1.58	5.17E-06	11	9	2	17	5	4	
MEALZ_0454	CCE22153	fadA	3-ketoacyl-CoA thiolase		3.33	3.66E-31	0.50	3.26E-01	-1.35	1.14E-04	1.49	2.89E-03	5	5	2	3	0	9	
MEALZ_2523	CCE24201	shc	squalene--hopene cyclase		0.77	9.52E-03	-1.16	5.95E-04	-0.23	6.07E-01	1.71	2.40E-11	1	0	0	0	0	0	
MEALZ_3955	CCE25611	dhaK	dihydroxyacetone kinase		1.22	7.91E-17	0.01	9.88E-01	-1.32	3.19E-06	-0.10	7.32E-01	68	68	10	42	41	17	
MEALZ_3956	CCE25612	dhaL	dihydroxyacetone phosphatase		0.28	6.37E-02	0.23	6.69E-01	1.73	9.96E-05	1.79	3.18E-31	49	39	9	48	27	15	
Coenzyme PQQ																			
MEALZ_0595	CCE22290	pqqE	coenzyme PQQ synthesis protein E		-0.33	4.11E-02	0.40	2.68E-01	0.24	5.07E-01	-0.48	1.68E-02	23	16	3	32	17	4	
MEALZ_0596	CCE22291	pqqD	coenzyme PQQ synthesis protein D		-0.52	4.83E-02	-0.92	2.53E-02	-0.64	1.53E-01	-0.23	5.46E-01	2	7	0	0	6	0	
MEALZ_0598	CCE22293	pqqC	pyrroloquinoline-quinone synthase		-0.50	1.28E-03	0.03	9.62E-01	-0.23	6.24E-01	-0.74	1.68E-05	25	16	10	27	9	8	
MEALZ_0599	CCE22294	pqqB	coenzyme PQQ synthesis protein B		-0.39	8.74E-03	-0.73	1.76E-01	-0.82	1.66E-01	-0.48	7.22E-03	34	34	10	43	39	11	
MEALZ_0600	CCE22295	pqqA	coenzyme PQQ synthesis protein A		-4.03	1.36E-05	-3.26	1.55E-17	1.17	6.57E-02	0.42	7.56E-01	0	0	0	0	0	0	

Table 2.2: Transcriptome and proteome changes of major metabolic functions in bioreactor conditions, continued.

				log2FoldChange>0	> in Ca-NoCu-CH3OH		> in La-noCu-CH3OH		> in La-NoCu-CH3OH		> in La-CH4		Ca PSCs			La PSCs			
				log2FoldChange<0	> in Ca-CH4		> in La-CH4		> in Ca-noCu-CH3OH		> in Ca-CH4								
Gene ID	Protein ID	Gene Name	Protein Name		log2FC	p-value	log2FC	p-value	log2FC	p-value	log2FC	p-value	Ca noCu PSC Total	Ca wCu PSC Total	Ca Cu CH4 PSC Total	La noCu PSC Total	La wCu PSC Total	La Cu CH4 PSC Total	
Copper acquistion																			PSC
MEALZ_0172	CCE21873	copA	copper-exporting P-type ATPase A		1.32	4.98E-25	1.41	4.40E-07	-0.36	3.15E-01	-0.44	5.49E-03	92	108	17	109	52	17	1000
MEALZ_1324	CCE23013	-	copper resistance D domain-containing protein		0.24	2.02E-01	0.89	4.58E-03	0.14	7.35E-01	-0.49	1.71E-02	18	10	4	26	13	5	100
MEALZ_1325	CCE23014	-	copper resistance protein CopC		0.06	8.80E-01	0.99	1.12E-02	0.57	1.72E-01	-0.35	4.48E-01	19	11	4	23	12	5	10
MEALZ_1645	CCE23332	copA	copper-exporting P-type ATPase A		0.58	1.24E-05	0.01	9.76E-01	-0.59	8.50E-02	-0.02	9.43E-01	61	61	14	83	54	18	1
MEALZ_2278	CCE23960	-	copper-exporting ATPase		0.96	6.02E-09	0.69	3.36E-02	-0.33	3.44E-01	-0.05	8.82E-01	62	57	21	77	37	19	0
MEALZ_2831	CCE24497	corA	copper-repressible polypeptide		4.54	2.07E-172	5.33	1.85E-82	-0.86	7.37E-03	-1.63	7.68E-05	684	544	77	1012	408	110	
MEALZ_2832	CCE24498	corB	CorB		4.24	2.34E-217	4.94	1.01E-54	-0.98	2.27E-02	-1.66	9.08E-26	294	298	45	349	169	37	
Iron acquisition																			
MEALZ_0546	CCE22244	-	TonB-dependent receptor		-4.26	0.00E+00	-4.69	8.23E-56	-0.49	2.63E-01	-0.04	8.28E-01	63	311	111	53	618	112	
MEALZ_2489	CCE24167	feoB	ferrous iron transport protein B		-4.16	1.78E-109	-3.75	7.63E-53	0.41	3.47E-01	0.01	9.57E-01	11	25	4	5	54	8	
MEALZ_2490	CCE24168	feoA	ferrous iron transport protein A		-4.37	1.14E-10	-3.50	4.00E-36	0.54	4.10E-01	-0.31	1.58E-01	0	1	0	0	7	0	
MEALZ_3766	CCE25422	hmuT	heme ABC transporter substrate-binding protein		-4.75	4.27E-260	-5.16	1.05E-86	-0.25	5.84E-01	0.18	2.96E-01	3	32	20	3	69	18	
MEALZ_3767	CCE25423	hugZ	heme oxygenase		-4.58	1.97E-218	-5.76	4.76E-104	-0.62	1.24E-01	0.57	9.88E-05	6	9	2	0	46	5	
MEALZ_3971	CCE25627	-	ferric siderophore transport system, C-terminal periplasmic binding protein TonB		-2.41	5.29E-46	-1.98	6.73E-13	0.39	3.23E-01	-0.03	9.06E-01	0	1	2	0	5	0	
MEALZ_3973	CCE25629	-	ferric siderophore transport system, biopolymer transport protein ExbB		-2.84	5.54E-55	-2.16	8.69E-14	0.86	3.47E-02	0.19	3.74E-01	0	0	0	1	1	0	

Table 2.3: Metabolites from growth on Methanol without Copper vs Methane with Copper.

Red and green shaded cells indicate p≤0.05 (red indicates mean values significantly higher for that comparison; green values significantly lower). Light red and light green shaded cells indicate 0.05<p<0.10 (Light red indicates mean values trend higher for that comparison; light green values trend lower). Data collected with Metabolon.

Comp ID	Super Pathway	Sub Pathway	Biochemical Name	MeOH w/o Cu vs CH4 w/ Cu
38276	Amino Acid	Branched Chain Amino Acids (pyruvate derived)	2,3-dihydroxyisovalerate	4.83
34398	Peptide	Dipeptide	glycylleucine	2.7
573	Nucleotide	Pyrimidine metabolism	cytosine	4.82
46148	Carbohydrate	Amino sugar and nucleotide sugar	UDP-N-acetylglucosamine/galactosamine	4.2
1437	Carbohydrate	TCA cycle	succinate	4.03
48990	Carbohydrate	Glycolysis	pyruvate	2.85
53	Amino Acid	Glutamate family (alpha-ketoglutarate derived)	glutamine	2.38
63357	Lipids	Fatty acid, hydroxy	2-hydroxysebacate	1.99
32352	Nucleotide	Purine metabolism	guanine	1.76
1125	Amino Acid	Branched Chain Amino Acids (OAA derived)	isoleucine	1.73
18362	Lipids	Fatty acid, Dicarboxylate	azelate (C9-DC)	1.59
46225	Amino Acid	Glutamate family (alpha-ketoglutarate derived)	pyroglutamine*	0.45
37499	Secondary metabolism	Benzenoids	p-toluic acid	0.42
27503	Lipids	Fatty acid, hydroxy	3-hydroxypalmitate	0.37
32418	Lipids	Free fatty acid	myristoleate (14:1n5)	0.29
40730	Amino Acid	Glutamate family (alpha-ketoglutarate derived)	imidazole propionate	0.24
22176	Amino Acid	Serine family (phosphoglycerate derived)	cysteine s-sulfate	0.23
1572	Carbohydrate	Photorespiration	glycerate	0.22
48152	Carbohydrate	Glycolysis	glucose	0.74
62069	Lipids	Fatty acid, hydroxy	3-hydroxyadipate*	0.27
62278	Amino Acid	Glutamate family (alpha-ketoglutarate derived)	histidine betaine (hercynine)*	0.1
34437	Lipids	Lyso-phospholipids	1-stearoyl-GPG (18:0)	0.1
35159	Amino Acid	Glutathione metabolism	cysteine-glutathione disulfide	0.09
1604	Nucleotide	Purine metabolism	urate	0.04
57565	Nucleotide	Pyrimidine metabolism	hydroxymethylpyrimidine	0.01

Table 2.4: Metabolites from growth on Methanol and Copper vs Methane and Copper.

Red and green shaded cells indicate p≤0.05 (red indicates mean values significantly higher for that comparison; green values significantly lower). Light red and light green shaded cells indicate 0.05<p<0.10 (Light red indicates mean values trend higher for that comparison; light green values trend lower). Data collected with Metabolon.

Comp ID	Super Pathway	Sub Pathway	Biochemical Name	MeOH w/ Cu vs CH_4 w/ Cu
53	Amino Acid	Glutamate family (alpha-ketoglutarate derived)	**glutamine**	**4**
34398	Peptide	Dipeptide	**glycylleucine**	**2.32**
52469	Lipids	Phospholipids	**1-palmitoleoyl-2-oleoyl-GPE (16:1/18:1)***	**2.13**
42382	Amino Acid	Aspartate family (OAA derived)	**S-adenosylhomocysteine (SAH)**	**2.03**
18374	Amino Acid	Aspartate family (OAA derived)	**methionine sulfoxide**	**1.62**
60	Amino Acid	Branched Chain Amino Acids (pyruvate derived)	**leucine**	**1.53**
33487	Amino Acid	Glutamate family (alpha-ketoglutarate derived)	**glutamate, gamma-methyl ester**	**9.05**
573	Nucleotide	Pyrimidine metabolism	**cytosine**	**7.64**
38276	Amino Acid	Branched Chain Amino Acids (pyruvate derived)	**2,3-dihydroxyisovalerate**	**6.31**
15676	Amino Acid	Branched Chain Amino Acids (pyruvate derived)	**3-methyl-2-oxovalerate**	**2.82**
2829	Amino Acid	Aspartate family (OAA derived)	**N-formylmethionine**	**2.71**
485	Amino Acid	Amines and polyamines	**spermidine**	**2.37**
32489	Lipids	Free fatty acid	**caproate (6:0)**	**2.23**
21127	Lipids	Glycerolipids - Monoacyl	**1-palmitoylglycerol (16:0)**	**2.19**
34428	Lipids	Lyso-phospholipids	**1-palmitoyl-GPA (16:0)**	**2.12**
35669	Lipids	Fatty acid, Dicarboxylate	**tetradecanedioate (C14-DC)**	**1.99**
63357	Lipids	Fatty acid, hydroxy	**2-hydroxysebacate**	**1.58**
1125	Amino Acid	Branched Chain Amino Acids (OAA derived)	**isoleucine**	**1.52**
5345	Nucleotide	Pyrimidine metabolism	**uridine 5'-diphosphate (UDP)**	**1.51**
1302	Amino Acid	Aspartate family (OAA derived)	**methionine**	**1.27**
1645	Lipids	Free fatty acid	**laurate (12:0)**	**0.74**
37499	Secondary metabolism	Benzenoids	**p-toluic acid**	**0.74**
62069	Lipids	Fatty acid, hydroxy	**3-hydroxyadipate***	**0.43**
62918	Lipids	Fatty acid, Dicarboxylate	**tetradecadienedioate (C14:2-DC)***	**0.32**

Table 2.5: Metabolites from growth on Methanol without Copper vs Methanol with copper.

Red and green shaded cells indicate p≤0.05 (red indicates mean values significantly higher for that comparison; green values significantly lower). Light red and light green shaded cells indicate 0.05<p<0.10 (Light red indicates mean values trend higher for that comparison; light green values trend lower). Data collected with Metabolon.

Comp ID	Super Pathway	Sub Pathway	Biochemical Name	MeOH w/o Cu vs. MeOH w/ Cu
597	Carbohydrate	Glycolysis	**phosphoenolpyruvate (PEP)**	**2.31**
555	Nucleotide	Purine metabolism	**adenosine**	**0.77**
53	Amino Acid	Glutamate family (alpha-ketoglutarate derived)	**glutamine**	**0.59**
32492	Lipids	Free fatty acid	**caprylate (8:0)**	**0.5**
18335	Amino Acid	Aromatic amino acid metabolism (PEP derived)	**quinate**	**0.48**
1505	Nucleotide	Pyrimidine metabolism	**orotate**	**0.4**
1600	Lipids	Phospholipid Metabolism	**phosphoethanolamine**	**0.38**
15676	Amino Acid	Branched Chain Amino Acids (pyruvate derived)	**3-methyl-2-oxovalerate**	**0.35**
52469	Lipids	Phospholipids	**1-palmitoleoyl-2-oleoyl-GPE (16:1/18:1)***	**0.32**
40010	Peptide	Dipeptide	**leucylalanine**	**0.26**
41374	Peptide	Dipeptide	**phenylalanylalanine**	**0.21**
22176	Amino Acid	Serine family (phosphoglycerate derived)	**cysteine s-sulfate**	**0.17**
57565	Nucleotide	Pyrimidine metabolism	**hydroxymethylpyrimidine**	**0.04**
33471	Cofactors, Prosthetic Groups, Electron Carriers	Nicotinate and nicotinamide metabolism	**nicotinate ribonucleoside**	**0.49**
35669	Lipids	Fatty acid, Dicarboxylate	**tetradecanedioate (C14-DC)**	**0.44**
63061	Cofactors, Prosthetic Groups, Electron Carriers	CoA metabolism	**pantoate**	**0.29**
40730	Amino Acid	Glutamate family (alpha-ketoglutarate derived)	**imidazole propionate**	**0.21**
35159	Amino Acid	Glutathione metabolism	**cysteine-glutathione disulfide**	**0.1**

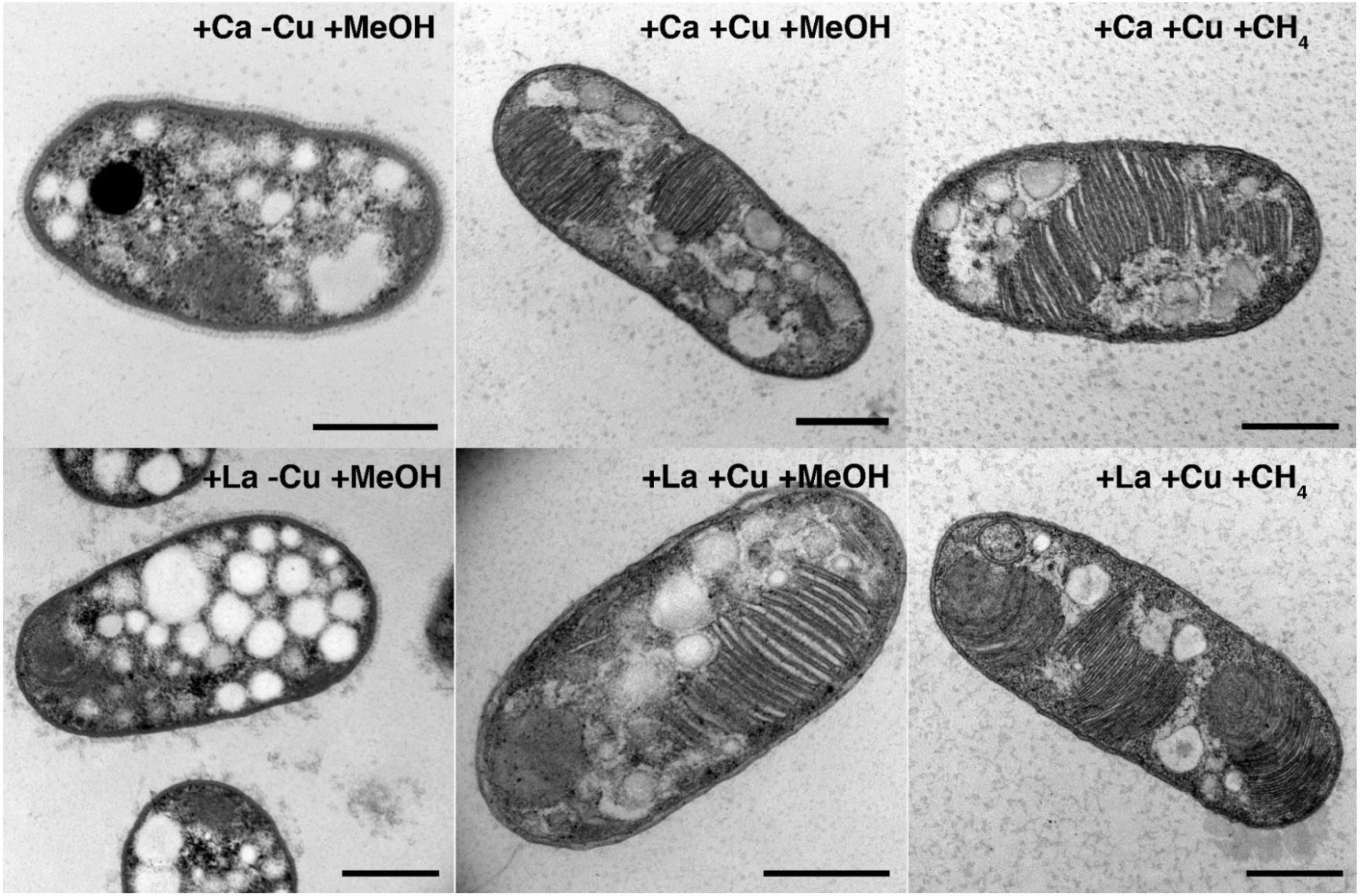

Figure 2.1: Thin section micrographs of cultures in response to metals and substrate. 500 nm scalebars.

Graph 2.3: Intracytoplasmic membrane coverage area in cell micrographs

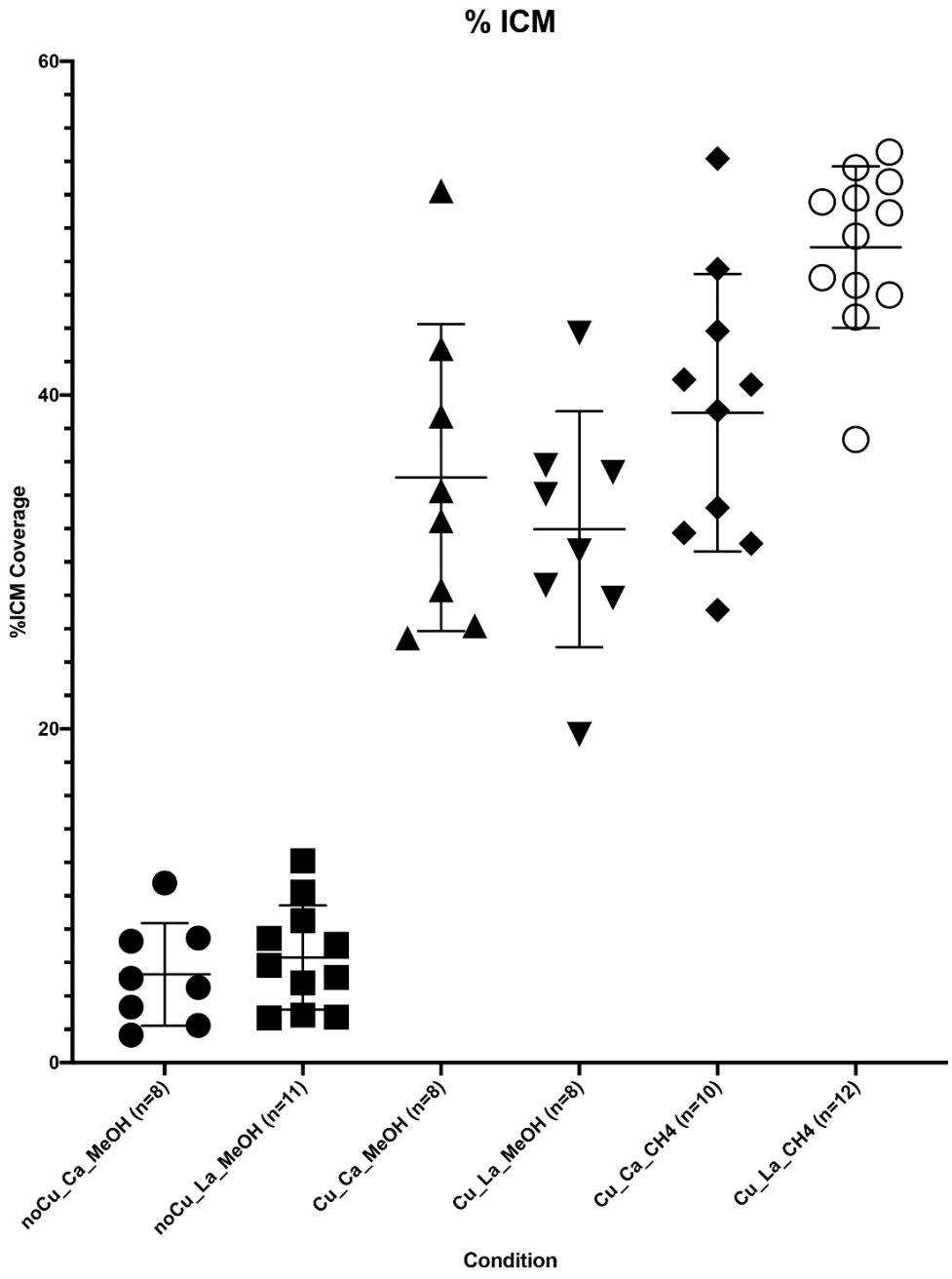

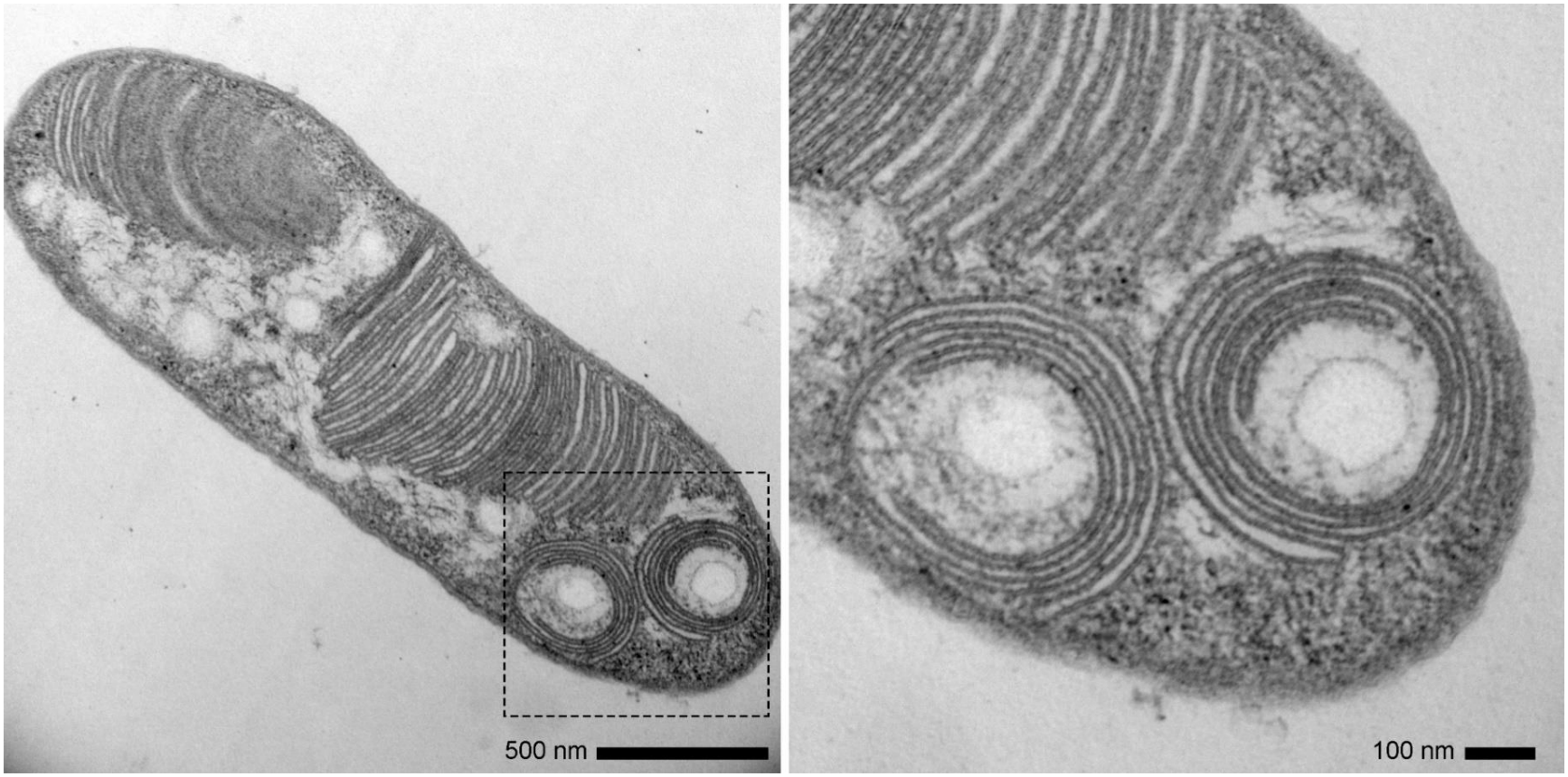

Figure 2.2: Thin section micrograph of granules surrounded by ICMs

Graph 2.4: Formate concentrations from 2020 Bioreactor cultures by HPLC.

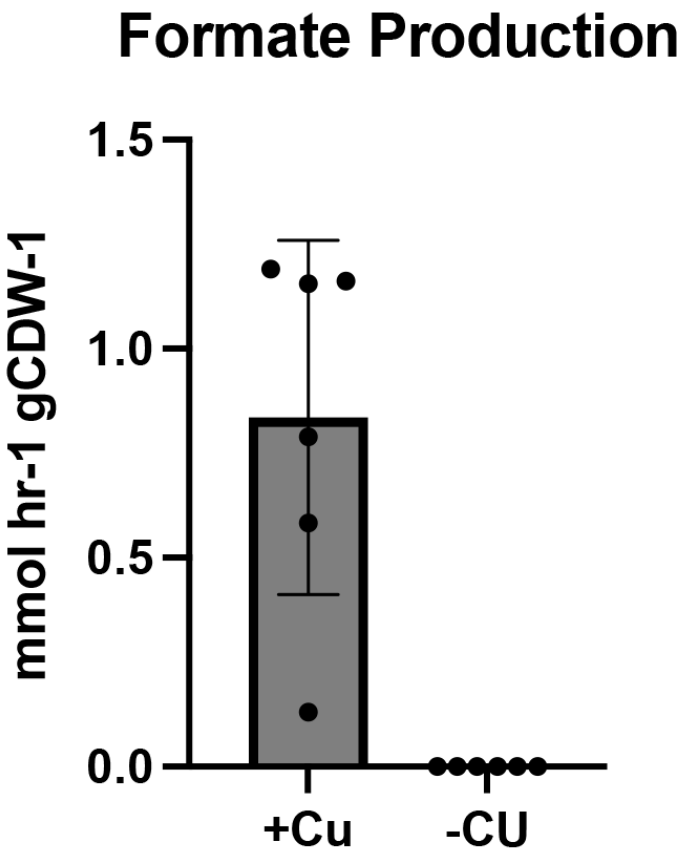

Data collected with Richard Hamilton and Dennis Krutkin.

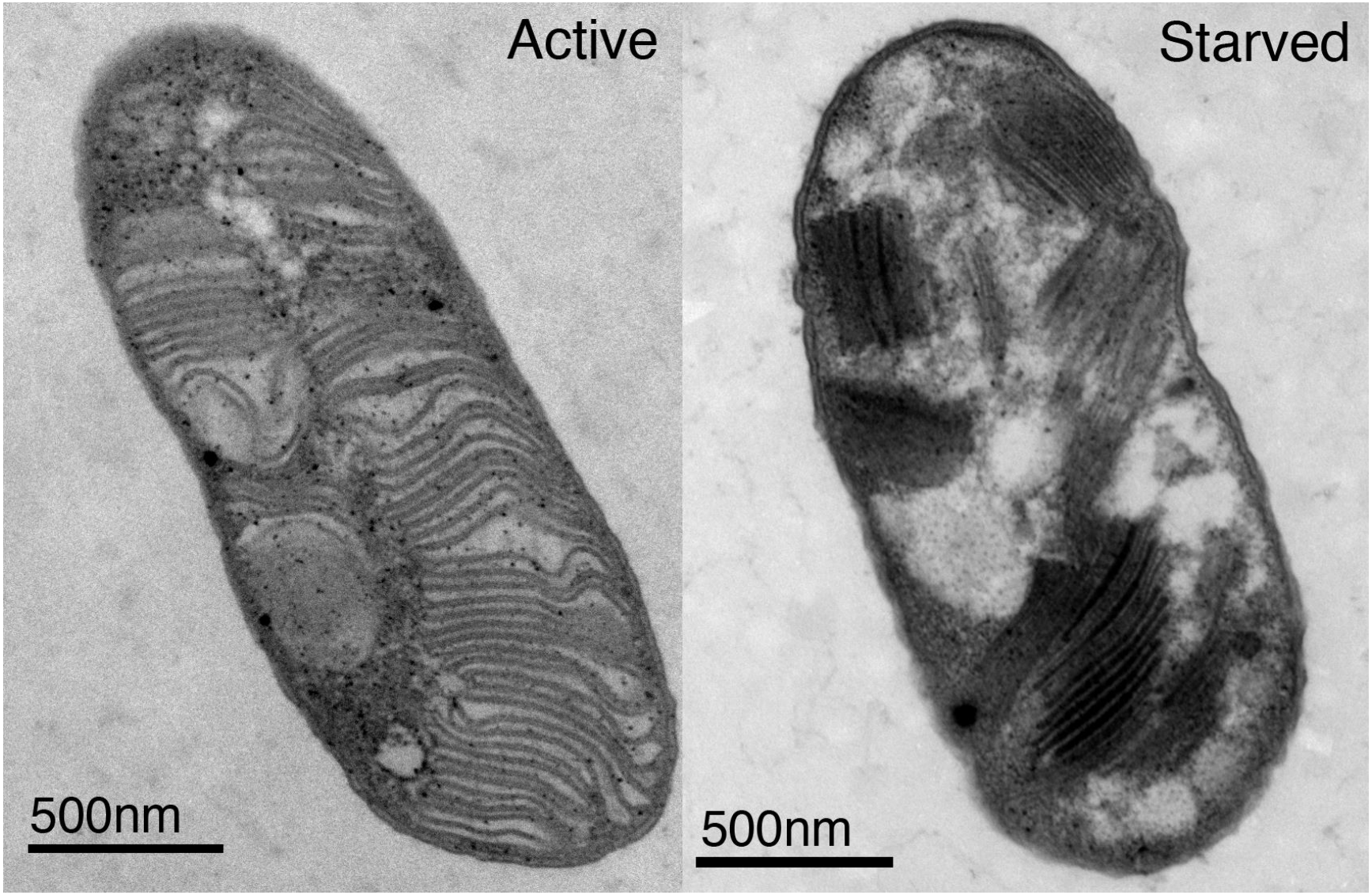

Figure 2.3: Thin section micrographs of actively growing vs starved cultures of *M. alcaliphilum* 20Z^{R}.

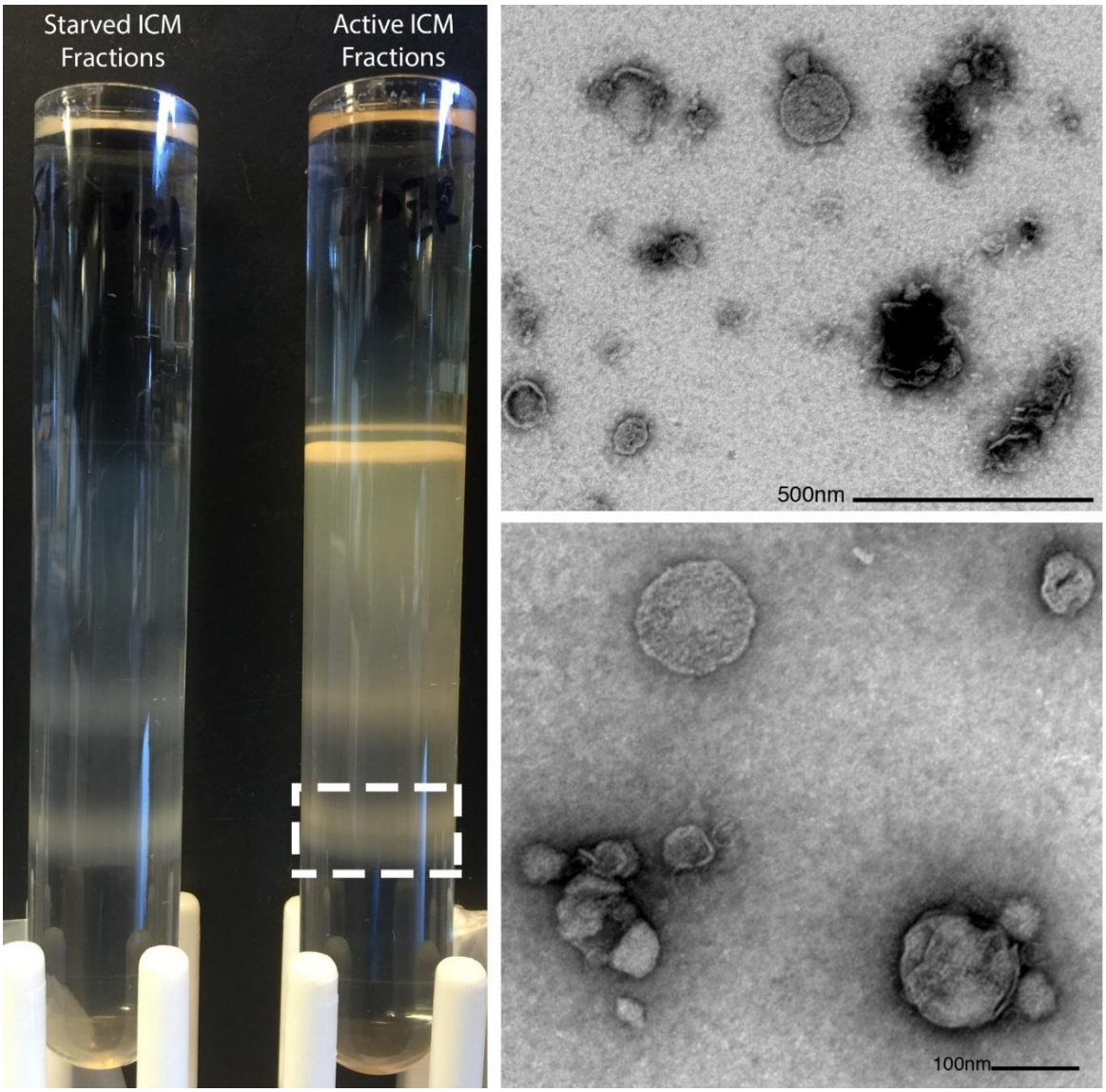

Figure 2.4: Subcellular fractions of active and starved cultures and representative negatively stained micrographs

Table 2.6: Proteome of central metabolism proteins during recovery from starvation.

Gene ID	Gene Name	Protein Name	Calcium 0.5 hr post CH_4	Calcium 1 hr post CH_4	Calcium 2 hr post CH_4	Calcium 4 hr post CH_4	Calcium 6 hr post CH_4	Calcium 23 hr post CH_4	Calcium 48 hr post CH_4
Methane oxidation									
MEALZ_0514	pmoC	methane monooxygenase subunit C	46	48	39	55	49	35	50
MEALZ_0515	pmoA	methane monooxygenase subunit A	27	36	29	29	27	18	43
MEALZ_0516	pmoB	methane monooxygenase subunit B	837	793	767	794	882	650	893
Methanol oxidation (Ca)									
MEALZ_3445	mxaI	methanol dehydrogenase, small subunit	16	9	12	14	20	21	16
MEALZ_3446	mxaG	cytochrome c-L	22	24	16	28	23	22	22
MEALZ_3447	mxaJ	protein MxaJ involved in regulation of methanol oxidation	30	33	29	40	35	26	26
MEALZ_3448	mxaF	methanol dehydrogenase, large subunit	108	136	136	144	142	172	182
Methanol oxidation (La)									
MEALZ_3497	xoxF	dehydrogenase xoxF	171	168	167	173	165	135	123
MEALZ_3498	xoxJ1	MxaJ-like protein	16	15	17	24	20	12	17
MEALZ_2642	xoxG4	cytochrome X (putative)	11	11	13	12	15	21	11
Formaldehyde oxidation									
MEALZ_2428	fae	formaldehyde-activating enzyme	318	271	264	260	311	170	307
MEALZ_1456	fae	formaldehyde activating protein	23	27	25	21	21	16	27
MEALZ_0850	fae2	formaldehyde-activating enzyme	9	6	7	3	7	8	5

Graph 2.5: Methanol excretion by starved cultures after CH_4 feeding.

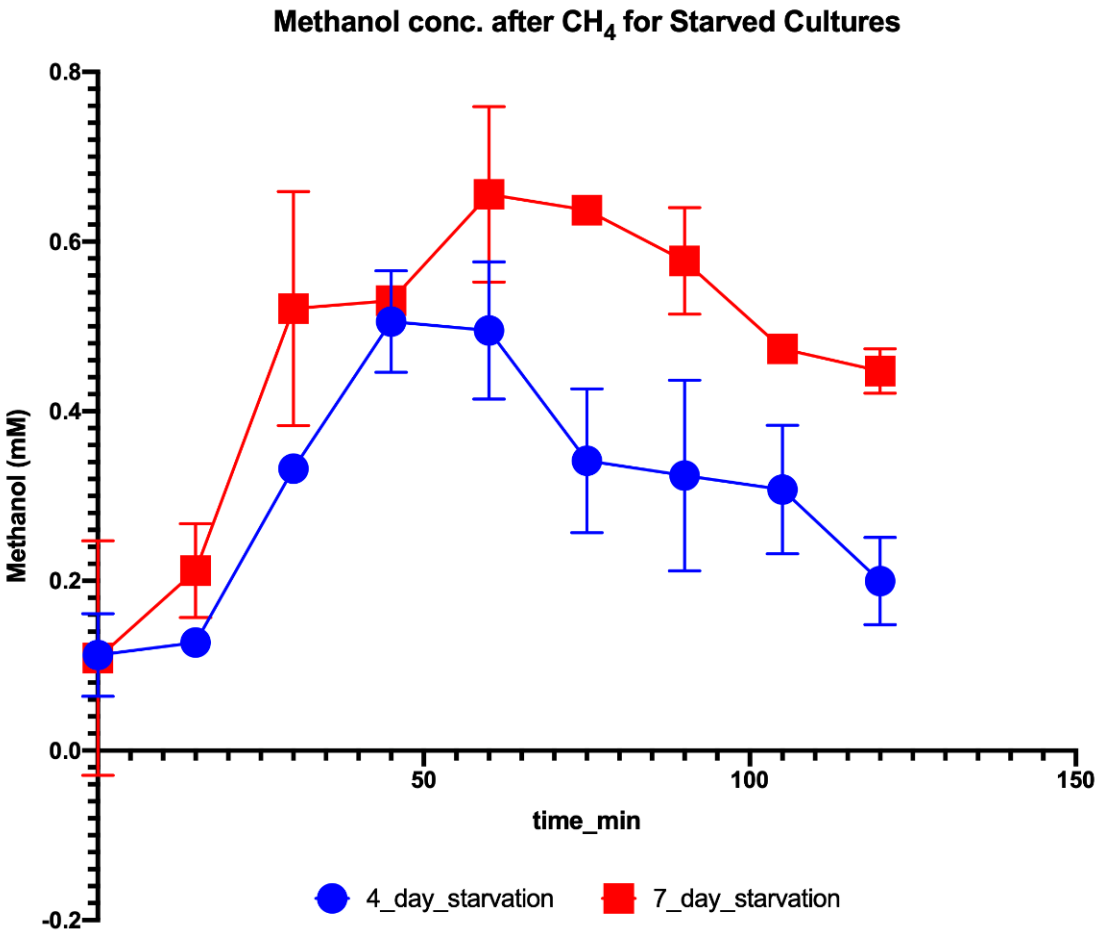

Chapter 2, in part is currently being prepared for submission for publication of the material by Collins, D., Hamilton, R., Krutkin, D.D., Kalyuzhnaya, M.G. (2021) as "Copper availability controls cell structure, cell energetics and MxaF/XoxF expression in *Methylotuvimirobium alcaliphilum* 20Z^{R}, a model methanotroph possessing only particulate methane-monooxygenase". The dissertation author is the primary investigator and author of this material.

CHAPTER 3

Identification of genetic elements of Surface Layer Protein (SLP) in *Methylotuvimicrobium alcaliphilum* 20Z^{R}

Abstract

Several genera of aerobic methanotrophic bacteria express extracellular surface layer protein (SLP) structures arrayed outside of their outer membranes. The SLP have no known functions and the genes responsible have not yet been identified. Two proteins MALCv4_0971 (2181 aa, 227 kDa) and MALCv4_0972 (30 kDa) were found to be highly expressed in previous global proteomics studies (Chapter 2). Deletions of the larger MALCv4_0971 protein resulted in a loss of surface layer proteins displayed on the cell surface as does deletion of the smaller MALCv4_0972 protein. Green fluorescent protein (sfGFP) translational fusions to the large MALCv4_0971 show differential localization based on the termini fused with GFP. The TEM studies indicate that the SLP-C_{ter}-sfGFP mutants accumulate protein granules inside, suggesting the deficiency in secretion pathways. The deletion of a proximally encoded Type 1 Secretion System (T1SS, MALCv4_0964, MALCv4_0965, MALCv4_0966) resulted in a loss of surface layer protein display, and cytoplasmic protein inclusions. Growth performance of the strains show growth defects at higher salinity and growth impacts in trace element limitation compared to wildtype SLP cultures, indicating possible functions of the SLP for *M. alcaliphilum* in trace element acquisition. Growth defects were also observed at higher salinity (6%), but not high methanol, indicating impacts from metals solubility rather than cell wall integrity are improved by the SLP. These results identify

the genetic inventory essential for SLP assembly and export but require definitive functional assessment for the SLP in the future.

3.1 Introduction

In contrast to Euryarchaeota and Crenarchaeota which display surface layer protein (SLP) as the main cell wall element nearly ubiquitously, the exterior ultrastructure of Gram-positive and Gram-negative bacteria rarely display a protein shell (Rodrigues-Oliveira, *et al*. 2017). Furthermore, the role of SLPs may be as varied as the diverse bacteria species they are found in potentially functioning as a nanomolecular sieve (Sara & Sleytr 1987), a molecular pattern display system in mucosa (do Carmo, *et al.* 2018), and potentially for metal ion binding and acquisition (Beveridge 1979, Tarlovsky, *et al.* 2010).

Methanotrophic bacteria are widespread in the ecosystem and are capable of growth on methane as their sole source of carbon and energy (Anthony 1982). Methanotrophs play an essential role in restricted methane flux from various environments, including those with extreme pH, temperatures and/or salinity. Several strains of gammaproteobacterial methanotrophs were identified as having surface layer proteins (Collins, et al., 1991; Khmelenina et al., 2013). While the presence of SLP is not unique to extremophilic methanotrophs, it has been noted that the protein envelop are more readily detected on surface of bacteria isolated from saline or alkaline environment (Kalyuzhnaya, *et al.* 2001). Initial structural characterizations of the cell surfaces of the *Methylomicrobium* genus shows SLPs to be widespread and consistently having hexagonally symmetric (p6) monolayers (Khmelenina, *et al.* 2010).

The function of these structures is of interest in methanotrophs from extreme environments and have the potential for biotechnology applications. In this study the genetic elements responsible for the SLP is found in *M. alcaliphilum* 20Z^R as well as the

nature of export to the cell surface. The factors determining the expression and leveraging a protein export system in an industrial methanotrophic bacterium are important steps in future microbial cell factories.

Based on data from previous -omics studies I hypothesize that a protein of unknown function (MALCv4_0971) constitutes the surface layer protein in *M. alcaliphilum* $20Z^R$ and will examine this possibility through mutagenesis and phenotyping of mutants generated to determine the function of this cell feature.

3.2 Methods

Cultivation

Cultures were routinely grown in P media with or without 1.2 $g*L^{-1}$ $CuSO_4$ x 5 H_2O for conditions lacking copper (Chapter 1; Collins & Kalyuzhnaya 2018; Akberdin, *et al.* 2018). For growth condition comparisons of SLP mutants each strain was pre cultured in the basal media before obtaining each culture's optical density at 600 nm (Jenway). Cultures of each strain were then sub-cultured to the same starting OD into the test media in triplicate and incubated at 30°C in an orbital shaker at 200 RPM in bottles containing methane gas (1%-20% of the headspace) or methanol (0.02%-5% v/v). Growth curves were obtained over the given time course by removing a small volume of culture through the septum and OD measured. For trace element sensitivity cultures were grown in media lacking the specified trace element in virgin plastic culture vessels to limit trace element contamination.

Identification of SLP locus

Published previously in Akberdin et al 2018, wildtype *M. alcaliphilum* bioreactor samples were collected in media containing calcium or lanthanum growing on methane or methanol as substrate for proteomic analysis by liquid chromatography-tandem mass spectrometry (LC- MS/MS) at Pacific Northwest National Laboratory. For transcriptome analysis RNA from pelleted cells was extracted with RNeasy kit (Qiagen) and treated with PureLink DNase I (Thermo Fisher Scientific) before sequencing on an Illumina HiSeq2500 by IGM Genomics Center, University of California, San Diego. The Fastq files were trimmed and aligned to the annotated *M. alcaliphilum* 20Z^R genome. The potential SLP locus was determined by abundance of protein spectral counts and FPKMs for non-metabolic genes having no identified function or annotation in the reference genome. Percent PSC was calculated from the PSCs detected for a given protein of the total PSCs detected per condition.

Mutagenesis of SLP locus

Using high-fidelity PCR, the upstream and downstream homology region flanks 600 bp from the target gene (MALCv4_0971: 1102328-1108873, 6546 bp. MALCv4_0972: 1109021-1109893, 873 bp. MALCv4_0964, MALCv4_0965, MALCv4_0966: 1091340-1095915, 4575 bp) is amplified with primers including 20 bp homology to the cloning site of the vector pCM433. The PCR products for upstream flank, downstream flank, and vector pCM433 is then agarose gel purified, and fragments assembled using the gene assembly protocol of HiFi DNA Assembly Master Mix (NEBiolabs). The resulting plasmid is validated by sequencing and cloned into the host methanotroph strain by conjugation. Biparental mating via conjugation is performed

by preparing a lawn of the methanotrophic recipient culture and donor *E. coli* S17-1 *λpir* (Simon, *et al.* 1984) containing the plasmid construct and mixing the donor and recipient on mating media (0.1% NaCl P medium supplemented with 10% LB media, pH 7). The two strains are evenly mixed on the mating media and incubated at 30°C with methane to support growth of both parent species for 2 days.

Following the genetic manipulations by conjugation protocol (Chapter 1, Collins & Kalyuzhnaya, 2018) kanamycin resistant colonies are obtained after conjugation before counter-selection by levansucrase (*sacB*). Sucrose-resistant colonies are then patch plated onto fresh media with and without a selective antibiotic to identify clones which are sucrose-resistant, and kanamycin-sensitive for genotyping by PCR for the desired deletion and sequenced to confirm the mutation. Strains generated in this study are listed in Table 3.2.

Electron microscopy

Liquid samples of strain cultures are mixed by inversion 1:1 with 4% glutaraldehyde in 0.2 M cacodylate buffer for 1 hr on ice for primary fixation and washed in cold 0.1 M cacodylate buffer afterwards twice. The cells are resuspended in the same buffer and secondarily fixed by mixing 1:1 with 1% osmium tetroxide in 0.1 M cacodylate buffer for 1 hr on ice before washing cells three times in dH_2O. Fixed cells are then immobilized in 1% (w/v) agarose solution in dH_2O before dehydration in a graded ethanol series (1+ hrs in 35% - 95% (v/v) ethanol, and three times in 100% ethanol. Samples are *en bloc* stained in 1% uranyl acetate in 75% ethanol before proceeding to higher ethanol percentages). Samples are then infiltrated with Epon 812 in a 3-step graded Epon:acetone series before polymerizing the resin at 60°C under vacuum for 48

hrs. Sections are then obtained on a diamond knife (Diatome) at 65nm section thickness and stained post-sectioning with 1% uranyl acetate and then 40 mM lead nitrate solutions before imaging at 120 keV in a Tecnai G2 transmission electron microscope. For negatively stained samples, whole cells are seated on glow-discharged Formvar coated copper mesh grids before negative staining with 1% uranyl acetate and dried before imaging. For SEM images, fixed cells were seated on 1 µm nanopore membranes (Millipore) by filtration before dehydration in an ethanol series followed by CO_2 critical point drying. Dehydrated cell sample was then mounted on an aluminum stub and sputter coated with 6 nm of platinum measured by FTM (film thickness monitor). The conductive sample was then imaged for secondary electron emissions at low accelerating voltage (5-10 keV) and short working distance (5 mm) on the Quanta FEG platform.

Fluorescence microscopy

A 1% agarose solution in $P_{3\%}$ media is pipetted into a welled microscope slide and covered with another slide, which is removed after hardening. If stained, cells are incubated with 0.5–1 µg/mL Fm4-64 (Invitrogen) along with 0.5–1 µg/mL of DAPI (Invitrogen) for 1 hour at 30°C. Cells are seated by pipetting 5–10 µL of cells onto the agarose and allowing to stand for 10 min before applying a coverslip to the agarose pad. Cells and imaged with a Zeiss fluorescence microscope under immersion oil at each emission/exciting wavelength (Fm4-64: 515 nm excitation, 640nm emission; DAPI: 341nm excitation, 452nm emission; GFP: 488nm excitation, 510 nm emission) and overlayed with phase contrast image for localization of GFP translational fusion proteins.

3.3 Results

Putative SLP locus is highly expressed and represented in proteome in several growth conditions.

Previously published multi-omics by Akberdin, *et al.* (2018) identified a locus of unknown function encoding a hypothetical protein which was highly expressed by FPKM (fragments per kilobase of transcript per million) in conditions containing calcium or lanthanum with copper on methane as a substrate, as well as with calcium or lanthanum without copper on methanol as a substrate. Notably a 2-fold change in PSC (protein spectral count) detection of the larger hypothetical protein MALCv4_0971 in media without copper for calcium-containing media, but not in lanthanum-containing media (Table 1). Proteomics of these conditions also shows an increase in detection for the SLP in absence of copper in growth media of these conditions.

Absence of copper in growth media affects density of SLP in cells

Reflecting the change in protein spectral counts for the putative SLP locus in response to copper in the media, thin sections show a change in cell surface phenotype in response to copper as well (Figure 3.1). Grown without copper, cells have a dense array of cup-like structures extending approximately 20 nm from the outer membrane. These SLP structural arrays are not as readily apparent in media containing copper, although are still detected in transcriptome and total protein mass spectrometry. Scanning electron microscopy of wt *M. alcaliphilum* 20Z^R shows that the surface layer

protein is still present on the exterior of the cell in these same copper containing conditions (Figure 3.2).

Mutant phenotypes indicate elements of SLP expression and potential transport mechanism

Negatively stained whole cells grown in copper containing media show the typical SLP arrangement in a hexagonal lattice in wildtype cells, having a cup diameter approaching 10 nm (Figure 3.3). This feature is seen across the cell surface in the wild type cells but is lost in mutants for MALCv4_0971, MALCv4_0972 and the T1SS cluster. These mutants display no SLP lattice on their surfaces instead have the phenotype of a bare envelope of the outer membrane. The deletion of the upstream T1SS locus from MALCv4_0971 and MALCv4_0972 indicate a possible role in the translocation of the SLP complex to the outer membrane.

To further evaluate the phenotype of mutants for the SLP locus, thin sections of each strain grown without copper in the growth media and fixed before imaging by TEM. Wildtype cells as demonstrated show a dense array of SLP across the cell surface (Figure 3.4). Deletions of the larger gene MALCv4_0971 results in the loss of the SLP on the cell as well as additionally distinct cellular inclusions from the Wt. Approximately 150 nm diameter electron-lucencies are observed with a distinctly more electron dense 20 nm margin surrounding them, which is not seen in Wt cells. This phenotype seen for mutants of the smaller gene MALCv4_0972 show inclusions like Wt cells and a large amount of material is seen surrounding cells. This material is difficult to resolve through thin sectioning (SLP size c. 20 nm, thin sections are 65 nm), but picks up staining during

TEM sample processing like proteins in solution. Deletion of the T1SS locus upstream of MALCv4_0971 and MALCv4_0972 causes a loss in the SLP phenotype again. A new type of inclusion is seen in this mutant, with higher electron density than those seen in ΔMALCv4_0971, ΔMALCv4_0972 and Wt granules.

The dependence of the SLP export on T1SS is further demonstrated by translational fusions with heterologous proteins in which GFP or Lipase (Lip1) was cloned in-frame with the MALCv4_0971 c-terminus. Localization of GFP is seen to be in terminal cellular polar inclusions distinct from DNA containing regions stained with DAPI and apart from intracytoplasmic membranes stained with lipophilic Fm4-64 (Figure 3.5). Electron micrographs of a similar in-frame translational fusion of a commercially relevant enzyme Lipase with MALCv4_0971 similarly forms polar inclusion bodies. Together with deletion of the T1SS locus these translational fusions indicate that occlusion of the c-terminus by a heterologous peptide sequence prevents the typical recognition of exported substrates by T1SS.

Growth performance impacts of SLP mutations on M. alcaliphilum 20Z^{R}

To evaluate the possible function of the surface layer protein growth experiments were performed in several conditions across culturing parameters encountered for *M. alcaliphilum*. Growth of Wt SLP and *ΔMALCv4_0971* and *ΔMALCv4_0972* was compared at 6% and 8% NaCl in P media (Graph 3.1). A growth defect is observed after the lag phase for higher salt concentrations which is not observed in Wt cultures for both ΔMALCv4_0971 and ΔMALCv4_0972. This defect is increased at 8%.

Additional tests on cell performance for SLP mutants in multiple conditions

Comparing the role of SLP mutants against Wt SLP cells in media without trace metals copper or tungsten shows a growth defect for all cells in the trace mineral solution media lacking copper and tungsten (Graph 3.2). In the presence of trace minerals in the media the phenotype is only seen in ΔMALCv4_0971 and ΔT1SS mutants. In media with higher concentrations of methanol (5%) compared to lower amounts of methanol (0.2%), a slight growth defect is seen in ΔMALCv4_0972 compared to other strains, but all strains show a reduced growth rate (Graph 3.3).

3.4 Discussion

The surface layer protein in *M. alcalphilum* $20Z^R$ was identified early as a major ultrastructural feature and recent studies identify it through multi-omics as well (Table 3.1). The expression data shows that copper is important in regulating its expression when comparing conditions having copper (Ca/CH_4 & La/CH_4) to those without (Ca/CH_3OH &La/CH_3OH). This is seen directly in micrographs of the cell surface in conditions with and without copper which changes the density of SLP on the cell surface (Figure 3.1). The presence of the SLP in copper containing conditions is also confirmed in SEM of wt *M. alcaliphilum* (Figure 3.2) despite the lower expression appearance by TEM. Expression of the previously reported copper repressible peptide CorAB, which had been localized to the cell surface also responds similarly to copper (Shuchukin, *et al.* 2011).

The deletion of *MALCv4_0971* & *MALCv4_0972* results in a consistent phenotype of the cell surface, losing a commonly seen hexagonal symmetry (p6) (Sleytr & Messner, 1988) of the SLP. This indicates that both the large subunit MALCv4_0971

and the small subunit MALCv4_0972 are required for display of the SLP on the cell. Additionally, deletion of the small subunit results in observations of free protein-like structures around cells (Figure 3.4, Δ0972) indicating a possible anchoring function for MALCv4_0972 if free SLP (MALCv4_0971) is secreted without attachment to the cell.

The structures of Type 1 secretion systems from Gram-negative bacteria have been determined largely from pathogenic bacteria, consisting of an ABC cytosolic domain, a transmembrane channel, and outer membrane pore (Morgan*, et al*. 2017). These ATP-dependent transporters export cytosolic proteins, without a periplasmic intermediate transport step based on c-terminal recognition sequences. Evidence of this mechanism as the transport step for *M. alcaliphilum* SLP comes from deletion of the T1SS locus (Figures 3.3 & 3.4) as well as occlusion of any putative c-terminal recognition sequence by translational fusions with heterologous proteins such as GFP (Figure 3.5).

The halophilic species *M. alcaliphilum* grows across a range of sodium chloride concentrations in nature beyond the standard culturing condition of 3% NaCl. A lack of SLP beyond the outer membrane of cells indicates a potential role in osmoprotection during changes in ambient salt conditions. This may be a protectant to cellular integrity during cell division which has been observed to be lost in some strains once they lose their SLP (Rothfuss, *et al.* 2006). The growth defect seen in *Δslp* strains may reflect this lost cellular integrity compared to the lack of defect in Wt *slp*. An additional explanation is that reduced solubility of trace metal elements as NaCl concentrations increase limits growth through impaired transport or acquisition without a functional SLP. The tests of additional routine culture parameters (Graphs 3.2, 3.3) including trace elements and

methane limitation show no definitive role in the SLP for acquiring metals or substrate acquisition. There is a growth phenotype associated with ΔMALCv4_0971 and ΔT1SS with trace element deficiency when compared to wt and ΔMALCv4_072. This may result from impaired acquisition of metals mediated by the large protein subunit of the SLP. The higher concentrations of methanol in the media show that the envelope stress associated in that condition do not affect mutants equally as the envelope stress associated with higher NaCl concentrations.

Characterization of Copper-suppressed genes in *Methylotuvimicrobium* suggested that SLP may function along with *corAB* in acting as siderophores for free copper ions (Shchukin, *et al.* 2011). Copper demand is high in methanotrophs due to methane monoxygenases active sites containing the metal ion (Ro, *et al.* 2019) and several strains without SLPs secrete a low-weight peptide for copper chelation methanobactin (Semrau, *et al*, 2020).

This identification of MALCv4_0971 as the large protein subunit of the SLP, MALCv4_0972 as the smaller anchoring subunit of the SLP, and a T1SS (MALCv4_0964, MALCv4_0965, MALCv4_0966) dependent transport mechanism has the potential for downstream biotechnology applications. By harnessing the expression of heterologous protein to a constitutive export system the realization of microbial ‘cell factories’ powered by waste gases such as methane can result in cost effective production of next generation protein materials.

3.5 References

Anthony, C. The Biochemistry of Methylotrophs. London: Academic; 1982

Beveridge, T. J. 1979. Surface arrays on the cell wall of Sporosarcina ureae. J. Bacteriol. 139:1039-1048.

Collins ML, Buchholz LA, Remsen CC. Effect of Copper on Methylomonas albus BG8. Appl Environ Microbiol. 1991;57(4):1261-1264. doi:10.1128/aem.57.4.1261-1264.1991

do Carmo, F.L.R., Rabah, H., De Oliveira Carvalho, R.D., Gaucher, F., Cordeiro, B.F., da Silva, S.H., Le Loir, Y., Azevedo, V., Jan, G. (2018). Extractable Bacterial Surface Proteins in Probiotic–Host Interaction. Frontiers in Microbiology **9**:645. doi: 10.3389/fmicb.2018.00645

Kalyuzhnaya, M.G., Khmelenina, V.N., Eshinimaev, B.Ts.,Suzina, N.E., Nikitin, D., Solonin, A., Lin, J.L.,McDonald, I.R., Murrell, J.C., and Trotsenko, Yu.A., (2001). Taxonomic Characterization of New Alkaliphilic and Alkalitolerant Methanotrophs from Soda Lakes of the Southeastern Transbaikal Region and Description of *Methylomicrobium buryatense sp. nov*., Systematics and Applied Microbiology **24(**2):166–176.

Khmelenina, V.N., Shchukin, V.N., Reshetnikov, A.S., Mustakhimov, I.I., Suzina, N.E., Eshinimaev, B.Ts., Trotsenko, Yu.A. (2010). Structural and Functional Features of Methanotrophs from Hypersaline and Alkaline Lakes. Microbiology **79(**4):472–482.

Khmelenina VN, Suzina NE, Trotsenko IuA. [Surface layers of methanotrophic bacteria]. Mikrobiologiia. 2013 Sep-Oct;82(5):515-27. Russian. PMID: 25509389.

Morgan, J.W.L., Acheson, J.F., Zimmer, J. (2017). Structure of a Type-1 Secretion System ABC Transporter. Structure **25**:522–529. dx.doi.org/10.1016/j.str.2017.01.010

Rodrigues-Oliveira, T., Belmok, A., Vasconcellos, D., Schuster, B., Kyaw, C.M. (2017). Archaeal S-Layers: Overview and Current State of the Art. Frontiers in Microbiology **8**:2597. doi: 10.3389/fmicb.2017.02597

Rothfuss, H., Lara, J.C., Schmid, A.K., Lidstrom, M.E. (2006). Involvement of the S-layer proteins Hpi and SlpA in the maintenance of cell envelope integrity in *Deinococcus radiodurans* R1. Microbiology **152**:2779–2787.

Sara, M., Sleytr, U.B. (1987). Molecular sieving through S layers of *Bacillus stearothermophilus* strains. Journal of Bacteriology. **169**:4092–4098.

Shuchukin, V. N., Khmelenina, V. N., Eshinimayev, B. Ts., Suzina, N. E., Trotsenko, Yu. A. (2011) Primary characterization of dominant cell surface proteins of

halotolerant methanotroph *Methylomicrobium alcaliphilum* 20Z. Microbiology, 2011, Vol. 80, No. 5, pp. 608–618.

Simon, R., Priefer, U., & Puhler, A. (1984). A broad host range mobilization system for in vivo genetic engineering: Transposon mutagenesis in Gram-negative bacteria. Biotechnology, 1, 784–791.

Semrau, J.D., DiSpirito, A.A., Obulisamy, P.K., Kang-Yun, C.S. (2020). Methanobactin from methanotrophs: genetics, structure, function and potential applications. FEMS Microbiology Letters **367**(5):fnaa045, https://doi.org/10.1093/femsle/fnaa045.

Ro, S.Y., Schachner, L.F., Koo, C.W., Purohit, R., Remis, J.P., Kenney, G.E., Liauw, B.W., Thomas, P.M., Patrie, S.M., Kelleher, N.L., Rosenzweig, A.C. (2019). Native top-down mass spectrometry provides insights into the copper centers of membrane-bound methane monooxygenase. Nature Communications **10**:2675 doi.org/10.1038/s41467-019-10590-6.

Sleytr, U.B., Messner, P. (1988). Crystalline surface layers in procaryotes. Journal of Bacteriology **170**:2891–2897.

Tarlovsky, Y., Fabian, M., Solomaha, E., Honsa, E., Olson, J.S., Maresso, A.W. (2010). A *Bacillus anthracis* S-layer homology protein that binds heme and mediates heme delivery to IsdC. Journal of Bacteriology **192**:3503–3511.

Trotsenko, Y.A., Doronina, N.V., Khmelenina, V.N. (2005). Biotechnological potential of aerobic methylotrophic bacteria: a review of current state and future prospects. Applied Biochemistry and Microbiology **41:**433–441.

Table 3.1: Proteomic and Transcriptomic Summary of Putative SLP Locus.

FPKMs = fragments per kilobase of transcript per million, PSCs = protein spectral counts.

FPKMs					
Gene ID	**Description**	**Ca/Cu/CH4**	**Ca/CH_3OH**	**La/Cu/CH_4**	**La/CH_3OH**
MALCv4_0971	hypothetical protein	11528.71	18145.99	10210.57	10823.45
MALCv4_0972	hypothetical protein	4807.21	7866.09	4633.32	4254.57
MALCv4_0514	pmoC	65473.28	13436.63	64428.12	20490.05
MALCv4_0515	pmoA	57201.13	5452.10	50262.83	5524.97
MALCv4_0516	pmoB	53103.78	4947.19	43556.31	8997.39
MALCv4_3445	mxaI	12616.14	2042.30	48.55	59.19
MALCv4_3448	mxaF	13570.19	2219.58	17.09	13.06
MALCv4_2831	corA	1260.26	30910.93	483.09	21088.43
MALCv4_2832	corB	272.098	5437.06	101.98	3381.19
Gene ID	**Description**	**Ca/Cu/CH_4 Total**	**Ca/CH_3OH Total**	**La/Cu/CH_4 Total**	**La/CH_3OH Total**
MALCv4_0971	hypothetical protein	4321	10592	5215	11015
MALCv4_0972	hypothetical protein	30	214	98	227
MALCv4_0971	hypothetical protein	0.0839	0.0899	0.0762	0.0785
MALCv4_0972	hypothetical protein	0.00058	0.00182	0.00143	0.00162

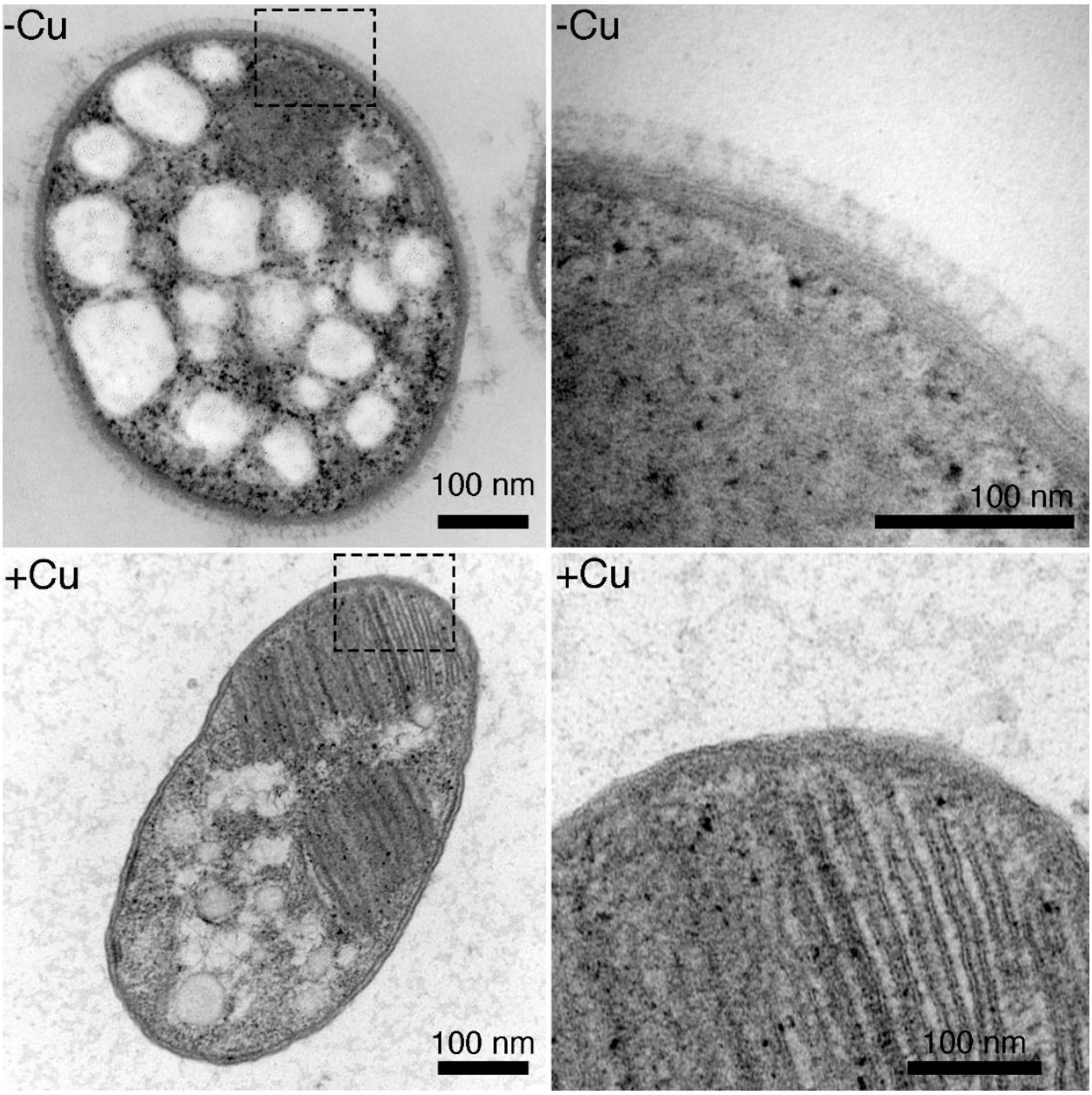

Figure 3.1: SLP density on cell surface is dependent on copper availability in media.

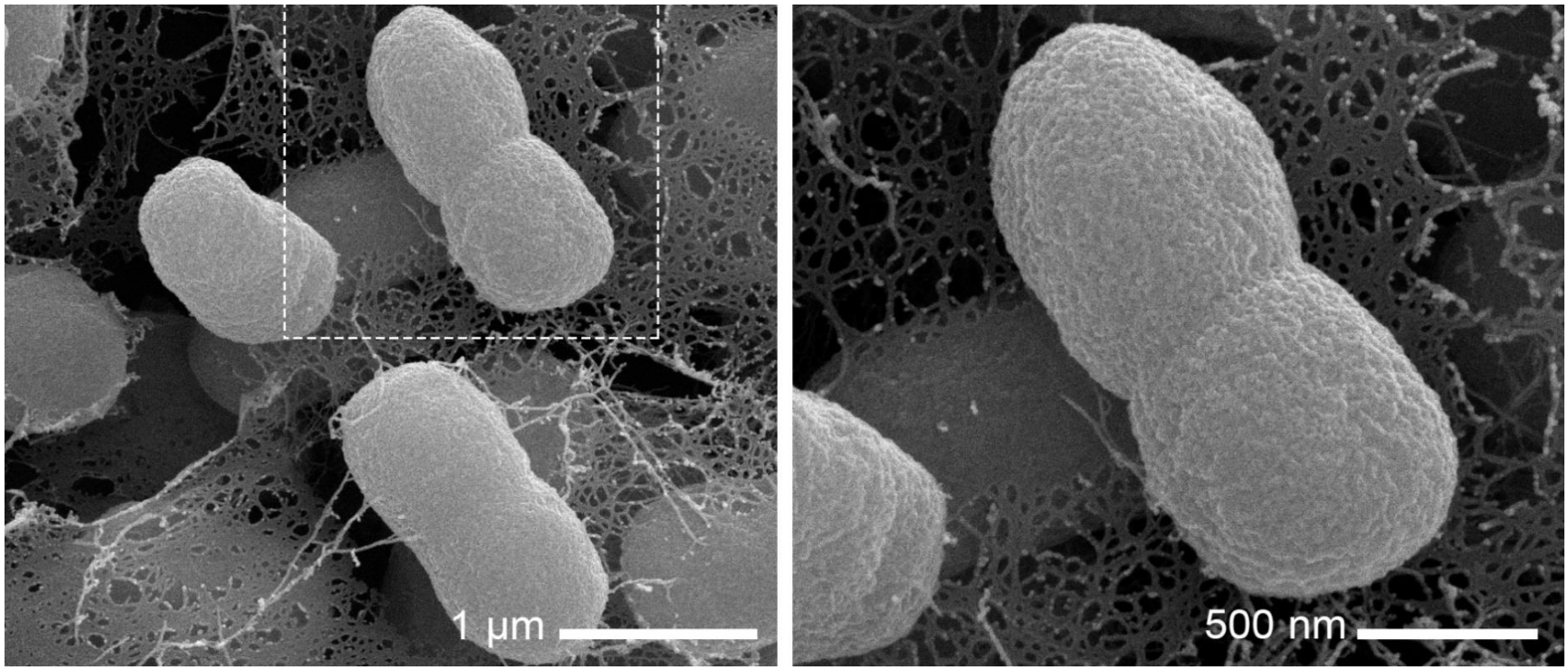

Figure 3.2: Scanning electron micrographs of *M. alcaliphilum* in standard conditions shows SLP.

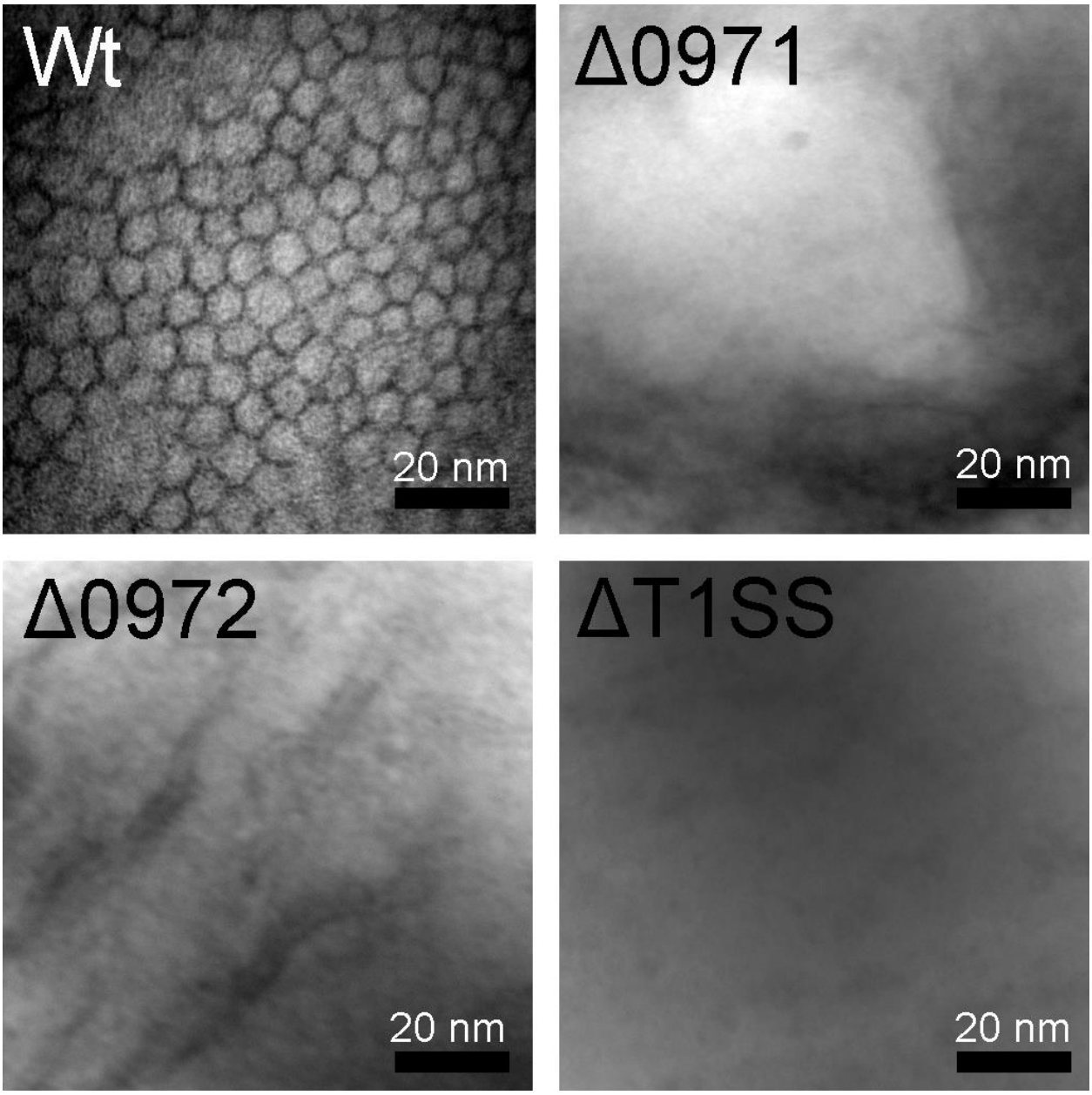

Figure 3.3: Negative stained whole cells surface phenotype shows loss of SLP in ΔMALCv4_0971, ΔMALCv4_0971 and ΔT1SS.

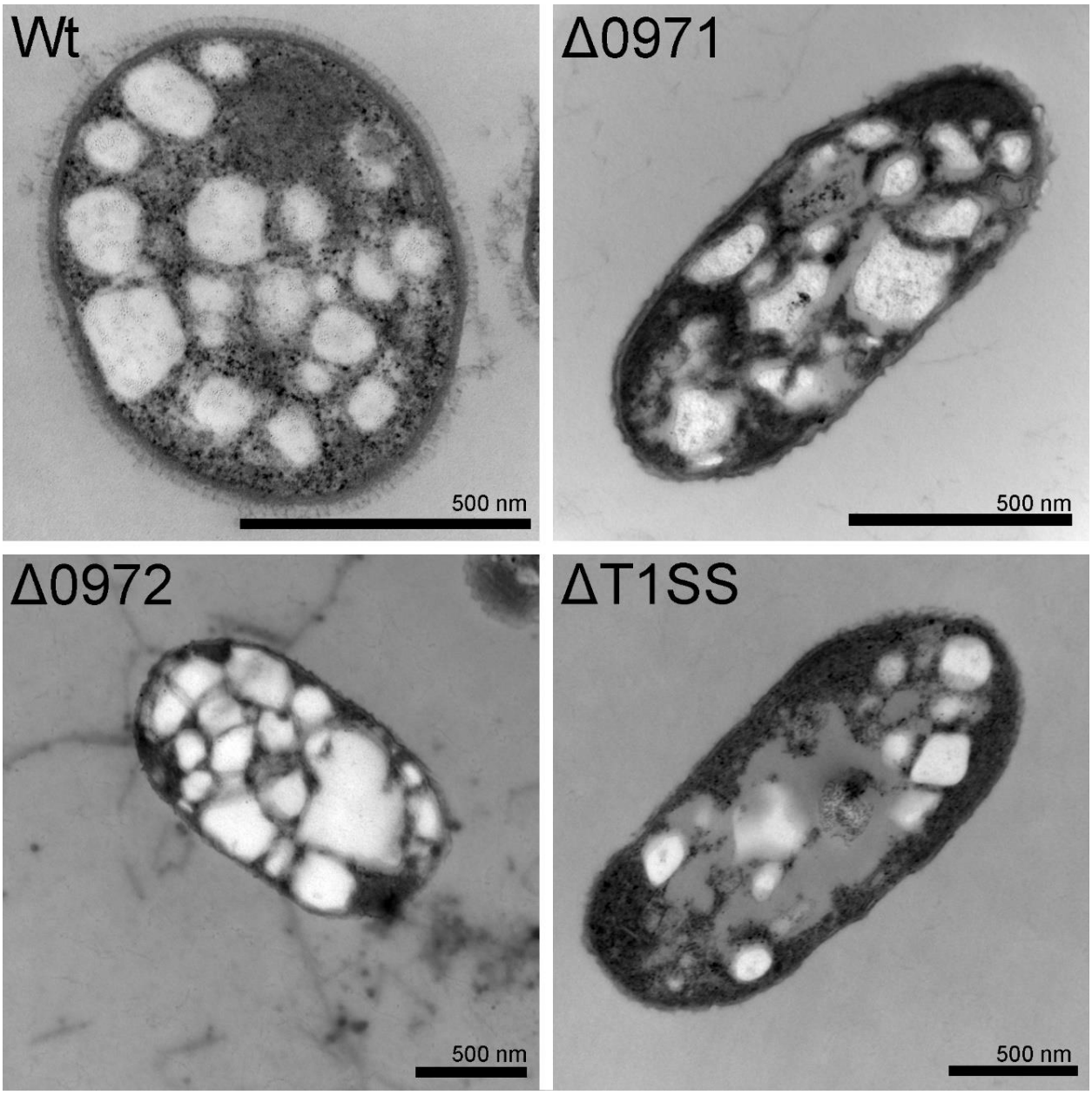

Figure 3.4: Thin sections of mutants shows a loss of SLP in ΔMALCv4_0971, ΔMALCv4_0971 and ΔT1SS.

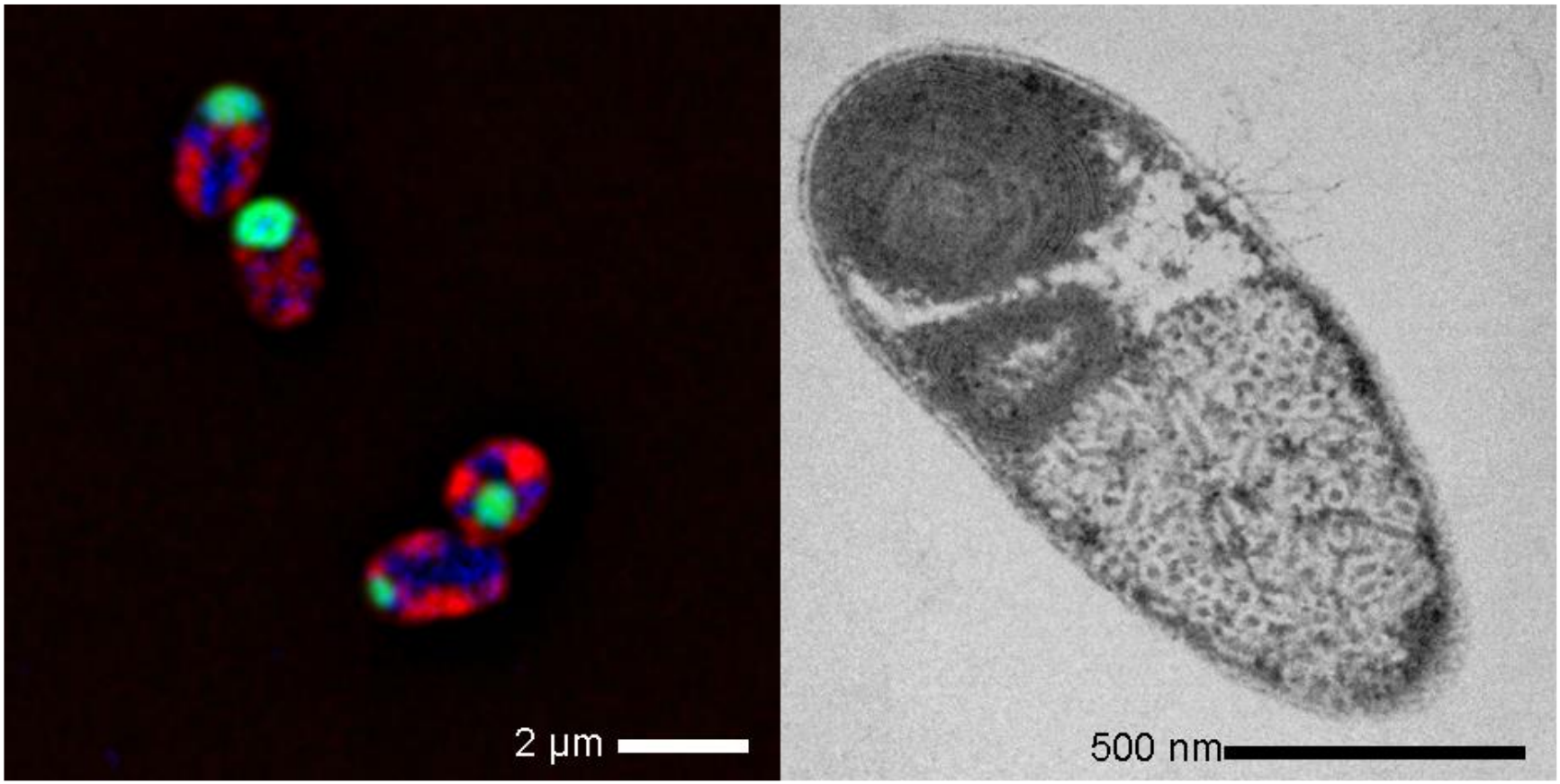

Figure 3.5: C-terminal fusions with MALCv4_0971 localize as inclusion bodies.

Graph 3.1: Growth Curves for SLP mutants at increasing salt concentrations.

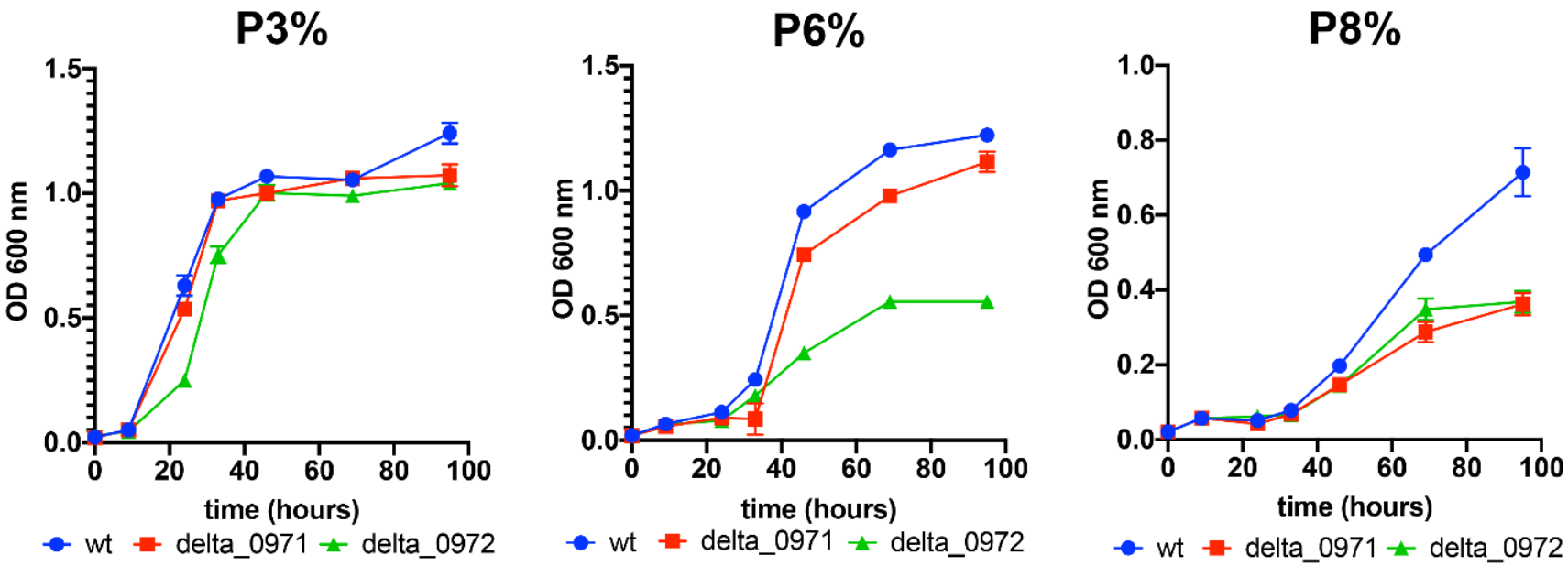

Graph 3.2: Growth without Cu or W for SLP mutants

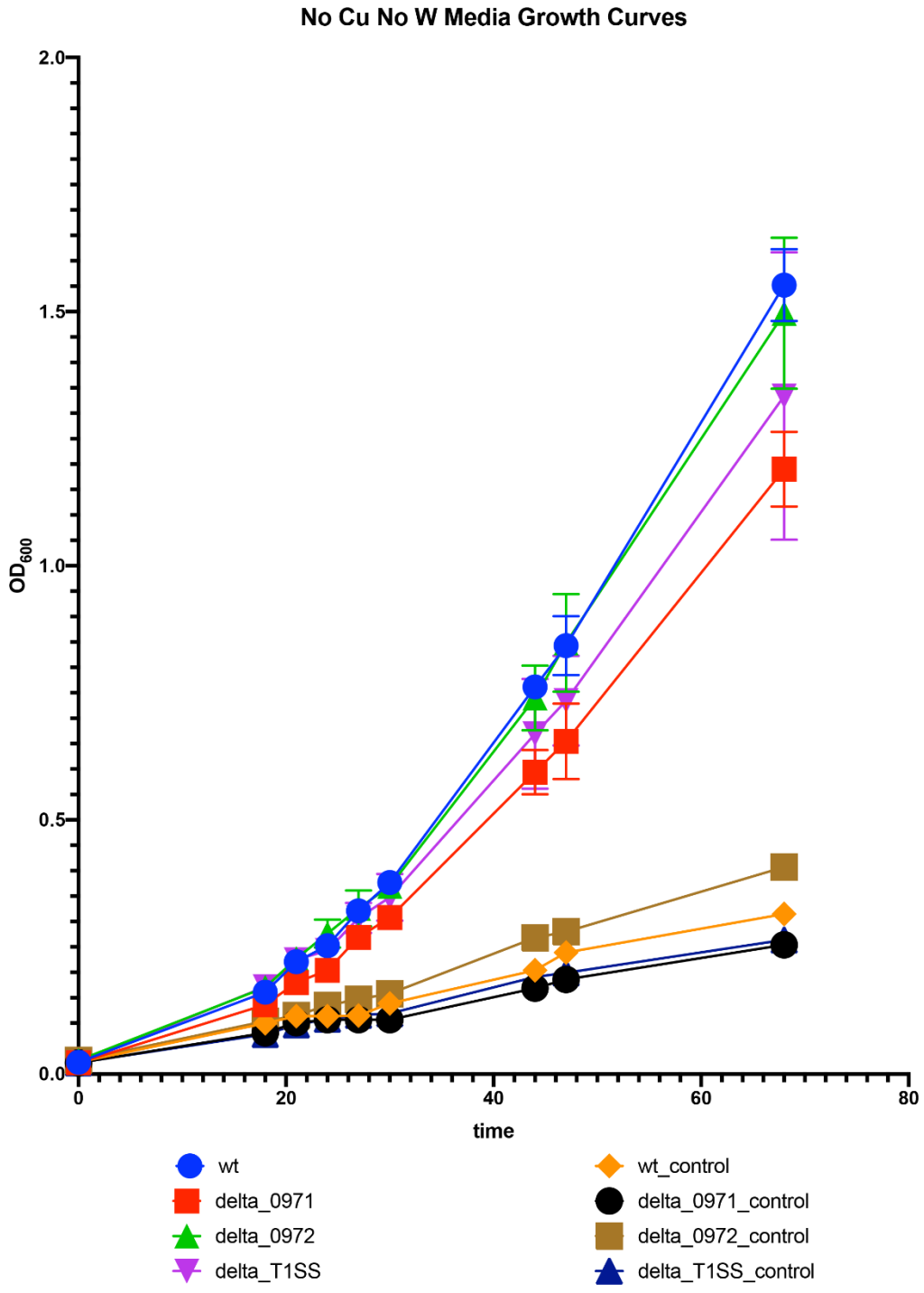

Data collected by Arturo Vazquez. Control normal p3%

Graph 3.3: Growth in varying Methanol concentrations for SLP mutants.

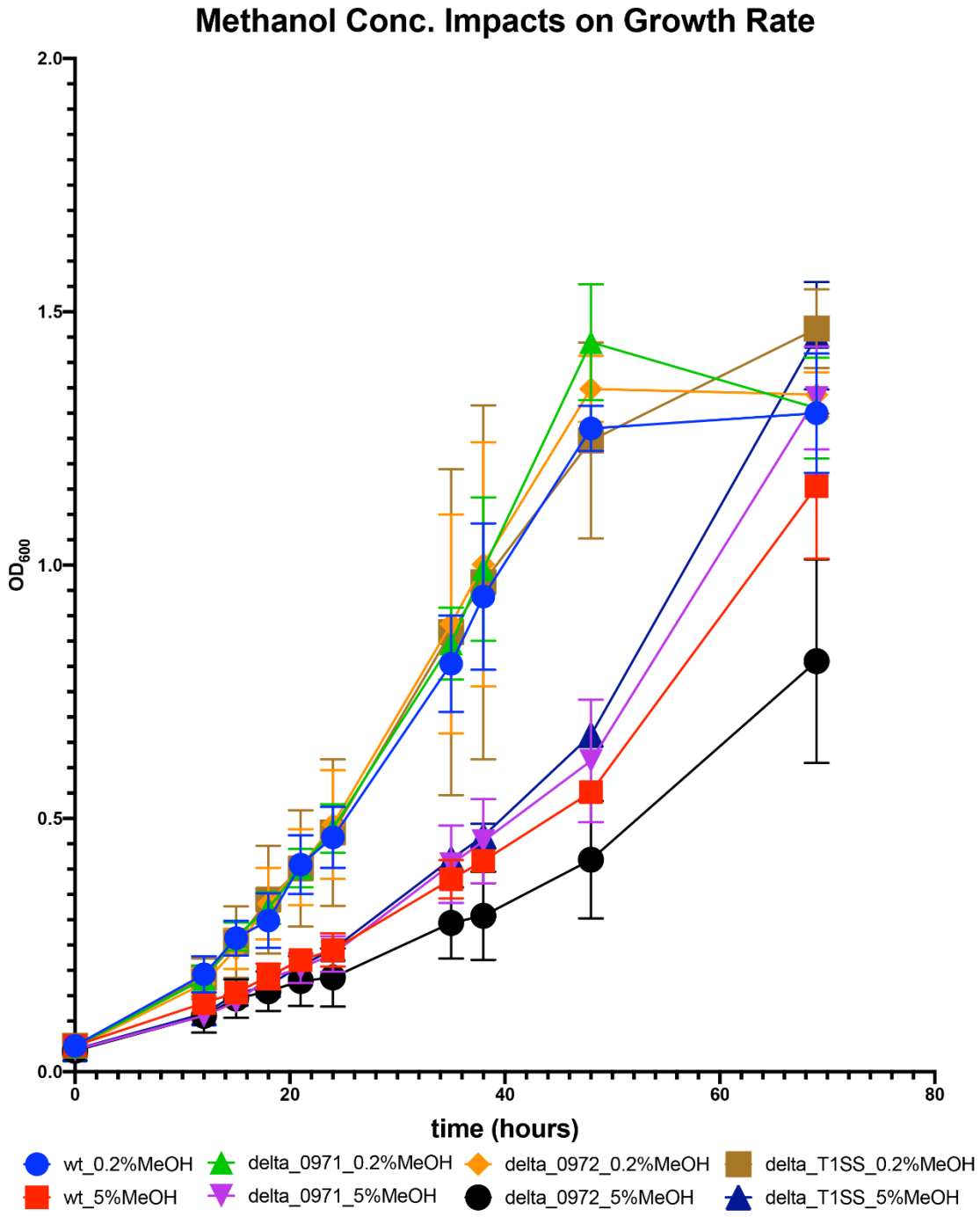

Data collected by Arturo Vazquez. Inoculum 0.2% meoh

Table 3.2: SLP strains generated

Strain	Description	Ref.
M. alcaliphilum 20Z^R	wildtype	Kalyuzhnaya, et al. 2001
20z^R *ΔMALCv4_0971*	Large SLP knockout	This study
20z^R *ΔMALCv4_0972*	Small SLP knockout	This study
20z^R *ΔMALCv4_0964 ΔMALCv4_0965 ΔMALCv4_0966*	Type 1 Secretion System knock out	This study
20z^R *MALCv4_0971::L1*	SLP large protein c-terminal Lipase (Lip1) fusion	O. Demidenko (unpublished)
20z^R *MALCv4_0971::GFP*	SLP large protein c-terminal GFP fusion	This study

Chapter 3, in full, contains material and data that will be submitted as “Genetic elements of surface layer protein” in Molecular Microbiology (2021) by Collins, D., Vazquez, A.V., Kalyuzhnaya, M. The dissertation author is the primary investigator and author of this material.

CHAPTER 4

Identification of a novel chemotaxis system in *M. alcaliphilum* 20Z^{R}

Abstract

In motile bacteria movement towards an attractant or away from a repellent constitutes the chemotaxis system in its simplest form. This phenotype involves the interplay of multiple signal transduction proteins downstream of sensing structures which modulate flagellar activity using effector proteins. Simple diffusible molecules in solution are easily tested for bacteria to test their attractive properties, but this is complicated by autotrophic bacteria which solely rely on gaseous substrates. In this study a method of measuring chemotaxis for methanotrophic bacteria was devised and a methane-tactic phenotype have identified in *Methylotuvimicrobium alcaliphilum* 20Z^{R}. this led to identification of multiple chemotaxis gene clusters with many potential targets for methane sensing. Structural studies identify one candidate MALCv4_2872 with unusual membrane topology and mutagenesis confirmed its role in oxygen sensing over methane. This leaves many potential future candidates for widespread mutagenesis to identify the methane sensing pathway in *M. alcaliphilum* 20Z^{R}.

4.1 Introduction

The observation of bacterial chemotaxis is the sum of coordination between signal transduction and affecter output which results in the movement of motile bacteria in a net direction (Baker, *et al.* 2002). This movement does not occur in a single directional vector, however, is the accumulation of movement in small bursts towards a net direction (Watari & Larson, 2010). This migration takes place through runs and tumbles during periods of which the flagella or flagellum moves in one direction (runs) and then reverses directions (tumbles). By controlling the direction the flagella rotate a bacterium can also spend their time in one area that is favorable or continuing to move in a direction.

The phenotype of movement towards stimuli results from the multiple sensors in bacteria for the many compounds in the environment they might encounter (Wadhams & Armitage, 2004). Between sensor proteins and the flagellum there is a complex signal transduction cascade with multiple steps between sensing of a compound to the change of flagellar rotation. At the beginning of the signal transduction cascade seen in Figure 4.1 are transmembrane methyl accepting chemotaxis proteins (MCP) which contain multiple functional domains such as the periplasmic sensor domain and importantly cytoplasmic histidine residues which are the target of kinases. The CheA histidine kinase, begins a phosphorylation cascade which results in the phosphorylation of a terminal protein CheY; the phosphorylated form of which ultimately affects flagellar rotation (Falke, *et al.* 2010). Signal and output are multiple intermediate proteins such as CheB and CheZ which can affect the sensitivity of the system and eventually act to

turn off the signal by acting as a methyl esterases and a phosphatase respectively (Wuichet & Zhulin, 2010).

The earliest attempt to measure bacterial chemotaxis involved attractants in capillary tubes which were placed into suspensions of bacteria. Using this method motile bacteria were seen to move towards these capillary tubes and even enter it by Pfeffer (1884). Nearly a century later attempts at more quantitative measurements of chemotaxis were created and similarly use capillary tubes of attractants but with improvements in controlling other factors of bacterial motility (Adler 1973). An example of this capillary based chemotaxis measurement system is reproduced in Figure 4.1 from Adler (1973). Other plate-based methods of assaying the taxis use semi-soft agar which facilitates the motility of a strain to compounds or even conditions such as osmolarity (Li, *et al.* 1988).

The benefit of these previous studies is they have measured chemotaxis in heterotrophs like *E. coli* towards typically small molecules which can diffuse through a semisoft medium. This principle was adapted as a method of purifying methanotrophs, which would require the cells be able to migrate, from a mixed culture towards methane and generate an axenic culture in the process (Danilova, *et al.* 2016). This method highlights the potential of examining methane-based chemotaxis in a model system such as *M. alcaliphilum* 20Z^R and eventually the mechanism of methane sensing for methanotrophs.

4.2 Method

Culturing *M. alcaliphilum* 20Z^{R}

As described previously (Chapter 2) *M. alcaliphilum* 20Z^{R} was routinely cultured in P3% media for liquid cultures with supplemented phosphate and carbonate solutions and 20% headspace methane. For solid cultures 1.5% Bactoagar is added, and during selection 100 µg/mL kanamycin sulfate was supplied. Semisoft agar was created by adding 0.3% w/v Bactoagar to P3% for chemotaxis assays.

CryoEM identification

Tomograms of vitrified cells were obtained by electron cryotomography as described (Ortega, *et al.* 2020) a FEI TITAN Krios 300 keV field emission gun microscope with lens aberration correction through Gatan energy filters and on “K2 summit” counting electron detector camera with a cumulative electron dose was 160 e^{-}/Å2 or less.

Chemotactic cluster discovery and Proteome analysis

The sequenced and annotated genome of *M. alcaliphilum* was searched for chemotactic genes and putative MCP receptors. These clusters were then grouped based on their Flagellar-type architectures (Ortega, *et al.* 2020). Additionally, the dataset for starved culture proteome of *M. alcaliphilum* (Chapter 2) was examined for genes of these clusters to highlight any changes in response to starvation and feeding for potential methane sensing results. Z-score transformations of PSCs for identified chemotaxis proteins were created from fractions of actively CH_4-growing, CH_4-starved, and CH_4 starvation recovered cultures.

Chemotaxis assay

Synthesizing methods described by Adler (1973) and Danilova, *et al.* (2016) test 15 mL test tubes were filled with 3 mL of semisoft P3% agar (0.3% agar) containing 0.2% 2,3,5-triphenyltetrazolium chloride (TTC) and allowed to solidify (Figure 4.31). The glass tip of a 9” Pasteur pipette was advanced along the inside of the tube to the end of the test tube before slowly adding pure methane, 50% methane, or room air until the gas displaced the semisoft agar to the opening of the test tube (Figure 4.32). The Pasteur pipette was slowly withdrawn, and the inverted tube was placed in an $OD_{600nm} \geq 1$ culture of *M. alcaliphilum* $20Z^R$ (Figure 4.33). The configuration of the assay is depicted in Figure 4.3. The semisoft agar was left in contact, submerged beneath 10 mL of culture in a 50 mL conical tube and checked for migration of cells over 48 hours (Figure 4.34). To evaluate for methane-taxis tubes were removed from cultures and the agar examined for pink color, indicating growth of bacteria which reduce the indicator TTC (Tengerdy, *et al.* 1967). This method was performed using the mutant Δ2872 as well with a slight modification of having agar at the bottom of syringe in order to control disturbing the agar after solidifying with gas in the sealed headspace of the syringe.

Mutagenesis

Based on structural predictions from Cryo EM data, a candidate MCP was targeted for initial mutagenesis. Following protocols in Chapter 1, putative MCP MALCv4_2872 was deleted by two step single-crossover through the selection/counterselection plasmid pCM433kan by biparental mating. Primers used: to amplify pCM433, AGATCTAGACGTCAGGTGGCAC and

GAGCTCACTAGAGGATCCAGCCGA; to amplify UP genomic region, AAAGTGCCACCTGACGTCTAGATCTATTTGCCTATTGTCCGCATG and CGTCATAGGGTCTGTTTAAGGTTGTAAGGTTTCCCCGTAAACTG; to amplify DOWN genomic region, CAGTTTACGGGGAAACCTTACAACCTTAAACAGACCCTATGACG and GGTCGGCTGGATCCTCTAGTGAGCTCGATGCATCGACTTCCAGTG. PCR products were gel purified and combined in Gibson assembly. The resulting plasmid was transformed into *E. coli* S17-1 and mated with wt *M. alcaliphilum*. Kanamycin-sensitive, sucrose-resistant clones were isolated and confirmed for deletion of MALCv4_2872 by PCR genotyping.

4.3 Results

Electron cryotomography shows dual chemotactic sensor arrays

Electron cryotomography of wild type cells grown with copper and the presence of methane show several structural features in common with traditional TEM such as surface layer proteins and the intracytoplasmic membrane network (Chapter 2, 3). Additionally, it reveals the presence of finer protein structures including two chemotactic sensor arrays located at the flagellar pole of the cell, marked by arrows in in Figure 4.4. These arrays demonstrate a typical architecture based on width from the cellular membrane for F6 and F7 type chemotactic sensor arrays (Ortega, *et al.* 2020).

Chemotaxis phenotype is present in Wt M. alcaliphilum 20Z^R

Identification of two types of chemotactic sensor arrays in wildtype *M. alcaliphilum* 20Z^R led to testing of a chemotactic phenotype towards methane. As seen

in Figure 4.5, the reduction of TTC is only seen in gas mixtures containing methane. with room air as an attractant no migration of *M. alcaliphilum* 20Z^R is seen through the semisoft agar. With gas mixtures containing methane, either 50% or 100% CH_4, migration of 20Z^R is seen near the surface of and through the semisoft agar. This indicates modification of Danilova's method for purifying methanotrophs can indeed be used to test for methane-taxis.

Multiple chemotaxis gene clusters are present in M. alcaliphilum 20Z^R.

A survey of the genome of 20Z^R shows that there are three major F-type clusters of chemotaxis genes. The two complete clusters are the F6 and F7 type like those predicted by structural data in electron cryotomography. A third incomplete F8 type is also identified. The F7 type cluster contains multiple elements of a complete signal transduction pathway: these include the canonical histidine kinase CheA (MALCv4_2870), methyl-accepting chemotaxis proteins - MCPs (MALCv4_2872), flagellar effector proteins CheY (MALCv4_2869), as well as intermediate regulatory proteins CheW (MALCv4_2871, MALCv4_2873) and CheD (MALCv4_2876).

The F6 type cluster includes its own histidine kinase CheA (MALCv4_3156) as well as flagellar effector proteins CheY (MALCv4_3158) and response regulatory proteins (MALC4_3150 & MALCv4_3157). There is no identified MCP in this cluster. The F8 cluster contains a CheA kinase (MALCv4_2941) as well as a MCP (MALCv4_2939). The three loci for these clusters are summarized in Table 4.1.

Reanalysis of starved proteome for chemotaxis genes

Analysis of the proteome from CH_4-starved, recovered, and actively growing cultures reveals that many proteins in the chemotaxis clusters change their abundances in response to conditions involving presence of methane (Table 4.2). Some regulatory proteins of the MCPs such as the CheR (MALCv4_2875) methyltransferase proteins are only detected during active feeding and are less abundant during starvation. MALCv4_3158 Two flagellar affecter proteins (CheY; MALCv4_3158) are abundant during feeding on methane after starvation recovery, while others decrease during active growth to starvation to recovery (CheY; MALCv4_2869). Some components of the flagellar motor complex also appear to change an abundance is based on feeding conditions, PomA and MotA are abundant in membrane fractions from active growth but are decreased during starvation and recovery.

Mutagenesis of MALCv4_2872 does not prevent methane-tactic phenotype

Based off the structural predictions of the MCP MALCv4_02872 from electron cryotomogram averages modeled by Ortega (2020), this protein contains an unusual topology of its sensing domains. A putative PAS domain does not reside in the periplasm but instead appears sandwiched between the cellular membranes. Mutagenesis of this F7 MCP generated a mutant Δ2872 which displayed a chemotactic phenotype like wild type. Using a modification of the assay with room air, 50% methane, and 100% methane as attractants, chemotaxis was seen to gas mixtures containing methane (Figure 4.6). This indicates the function of MALCv4_2872 may not be related to methane sensing at all despite its unusual membrane topology.

4.4 Discussion

This study indicates the importance of the synthesis of structural data with cellular function and the phenotypic screening of mutants. Chemotaxis was identified as an important phenotype in bacteria very early on and constitutes a system of data processing which enables survival of a population of cells in response to chemical stimuli (Colin, *et al.* 2019). Extrapolation of this phenomena beyond heterotrophic bacteria leads to many possibilities of technologies once the core sensing machinery is identified in methanotrophs.

The growing role of electron cryomicroscopy in bacterial cell biology is highlighted here as the discovery of the chemotactic sensor arrays in *M. alcaliphilum* led to the testable prediction of it having a role in methane sensing. By examining the classically observed phenotype of chemotaxis using the unique model system of methanotrophs identified the methane-based chemotactic phenotype. The position of the F6 and F7 sensor arrays at the polar flagellum indicates that *M. alcaliphilum* integrates multiple signals pathways and possesses means of sensing gases other than methane. Several PAS domain proteins are identified in the genome and these sensors are known to be responsible for oxygen sensing; likely integrating these signals into the same chemotaxis signal transduction pathways (Watts, *et al.* 2011). Collaboration with Watts resulted in heterologous expression system of MALCv4_2872 in *E. coli* which tumbles in the presence of oxygen indicating oxygen sensing as a role for MALCv4_2872 (unpublished). This corroborates the lack of methane sensing phenotype in the Δ2872 mutant. Only one gene was tested for prediction-based mutagenesis, mining the genome for other potential MCPs as well as those already identified in this

study presents a list of possible candidates for further experiments. The modified chemotaxis assay or potentially adapting it for quantitative analysis using microscopy will enable the testing of further mutants for a possible role in methane sensing.

The examination of the proteome from starved, actively growing, and methane recovering cells shows that there is a dynamic response in methane sensing proteins to feeding conditions. Ideally this should be followed up with transcriptomics the same conditions or over smaller time skills than the proteome was collected to further narrow down the list of potential genes responsible for methane sensing. In this data set proteins involved in the regulation of MCP sensitivity were the most susceptible to changes in feeding state. These methyltransferases and methylesterases post-translationally modify MCPs, affecting the clustering and packing of MCPs in the cell membrane (Levit & Stock, 2002). This results in increased sensitivity or decreased sensitivity to stimuli from a decrease or increase in the phosphorylation activity of the histidine kinase CheA which is associated with the cytoplasmic side of the MCP receptor. Combining this with the data from the proteome it appears that cells may be poised to sense for methane during starvation or contrarily dampen the sensitivity to methane during feeding. I predict this would correspond to the typical running or tumbling phenotype seen microscopically in motile bacteria in response to stimuli in which *M. alcaliphilum* may exhibit increased running in absence of methane or increased tumbling in the presence of methane, hallmarks of chemotaxis towards favorable stimuli.

The chemotactic phenotype identified in *M. alcaliphilum* shows that it moves towards methane the core substrate in its metabolism. Presumably oxygen is of equal

importance in combination highlights the role that PAS domain proteins play in cointegrating sensing signals. TTC provided in the assay media was reduced, seen by the pink color, which indicates metabolically active cells. It is not known if cells detected by the TTC are all migrants towards the methane or daughter generations from the initial tactic bacteria (or a combination of both). The mutant created in this study shows the same phenotype as wild type cells and response towards methane in the headspace of the chemotaxis assay and ideally is not the last mutant created and tested using the chemotaxis assay. The importance of determining methane sensors in methanotrophic bacteria extends beyond the phenotype of taxis towards the gas. Methane is an important industrial precursor and energy source and is notorious for leakage in the built environment (Weller, *et al.* 2020). Identification of a methane sensing protein and signal transduction pathway in a model system like *M. alcaliphilum* can be leveraged into potential biosensor technologies. This could result in a bacterial phenotype harnessed for applications that are a pressing interest to industry and consumers such as natural gas leak abatement.

4.5 References

Adler, J. (1973). A method for measuring chemotaxis and use of the method to determine optimum conditions for chemotaxis by *Escherichia coli*. Journal of General Microbiology **74**:77-91.

Baker, M.D., Wolanin, P.M., Stock, J.B. (2005) Signal transduction in bacterial chemotasis. BioEssays **28**:9-22.

Colin, R., Drescher, K., Sourjik, V. (2019). Chemotactic behavior of *E. coli* at high cell density. Nature Communications **10**:5329.

Danilova, O., Suzina, N., van de Kamp, J., Svenning, M.M., Bodrossy, L., Dedysh, S.N. (2016). A new cell morphotype among methane oxidizers: a spiral-shaped obligately microaerophilic methanotroph from northern low-oxygen environments. ISME Journal **10**:2734–2743 https://doi.org/10.1038/ismej.2016.48.

Falke, J.J., Bass, R.B., Butler, S.L., Chervitz, S.A., Danielson, M.A. (1997). The two-component signaling pathway of bacterial chemotaxis: a molecular view of signal transduction by receptors, kinases, and adaptation enzymes. Annual Reviews Cell and Develomental Biology **13**:457-512. doi: 10.1146/annurev.cellbio.13.1.457

Li, C., Boileau, A.J., Kung, C., Adler, J. (1988). Osmotaxis in *Escherichia coli*. Proceedings of the National Academy of Sciences **85**:9451-9455.

Levit, M.N. and Stock, J.B. (2002). Receptor methylation controls themagnitude of stimulus-responsecoupling in bacterial chemotaxis. J.Biol. Chem. 277, 36760–36765.

Ortega, D., Subramanian, P., Mann, P., Kjaer, A., Watts, K., Pirbadian, S., Collins, D., Kooger, R., Kalyuzhnaya, M., Pilhofer, M., Ringgaard, S., Briegel, A., Jensen, G. (2020). Repurposing a chemosensory macromolecular machine. Nature Communications.

Tengerdy, R.P., Nagy, J.G., Martin, B. (1967). Quantitative measurement of bacterial growth by the reduction of tetrazolium salts. Applied Microbiology **15**(4):954-955.

Wadhams, G., Armitage, J. (2004) Making sense of it all: Bacterial chemotaxis. Nat Rev Mol Cell Bio. 5, 1024–1037.

Watari, N., Larson, R.G. (2010). The hydrodynamics of a run-and-tumble bacteria propelled by polymorphic helical flagella. Biophysics Journal **98**(1):12-17. doi: 10.1016/j.bpj.2009.09.044.

Watts, K.J., Taylor, B.L, Johnson, M.S. (2011). PAS/poly-HAMP signalling in Aer-2, a soluble haem-based sensor. Molecular Microbiology **79**(3):686-699.

Weller, Z.D., Hamburg, S.P., von Fischer, J.C. (2020). A national estimate of methane leakage from pipeline amins in natural gas local distribution systems. Environmental Science Technology **54**(14):8958-8967.

Wuichet, K., Zhulin, I. (2010) Origins and diversification of a complex signal transduction system in prokaryotes. Sci Signal. 3, ra50.

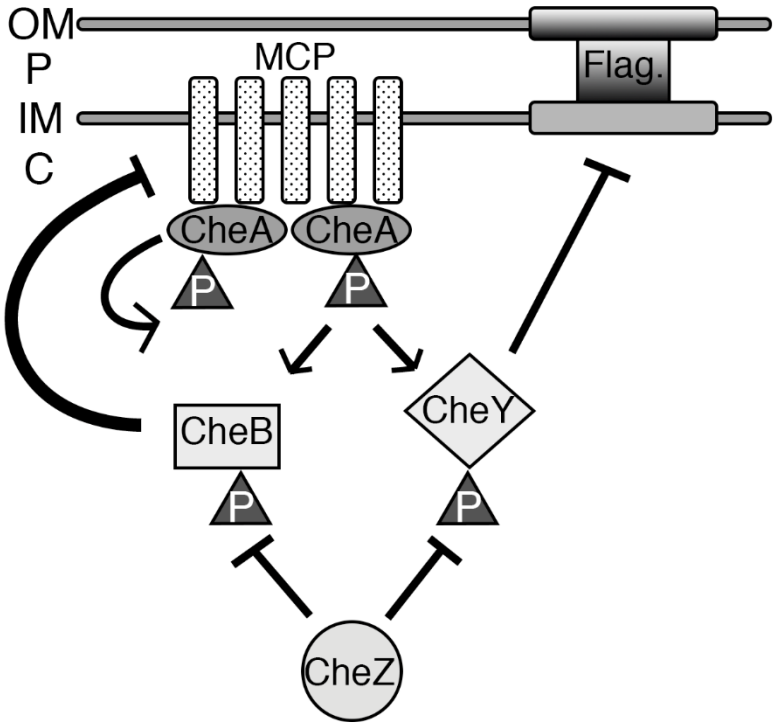

Figure 4.1: Schematic of signal transduction for chemotaxis including in *M. alcaliphilum* $20Z^{R}$.

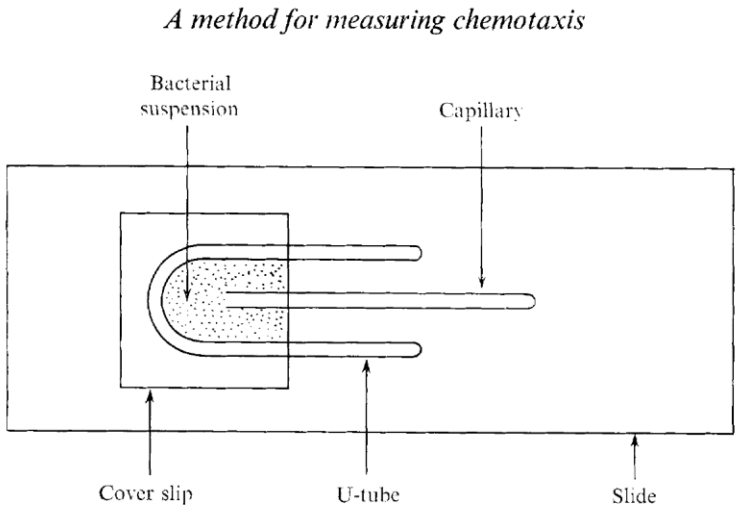

Figure 4.2: Adler's method for measuring chemotaxis in motile bacteria

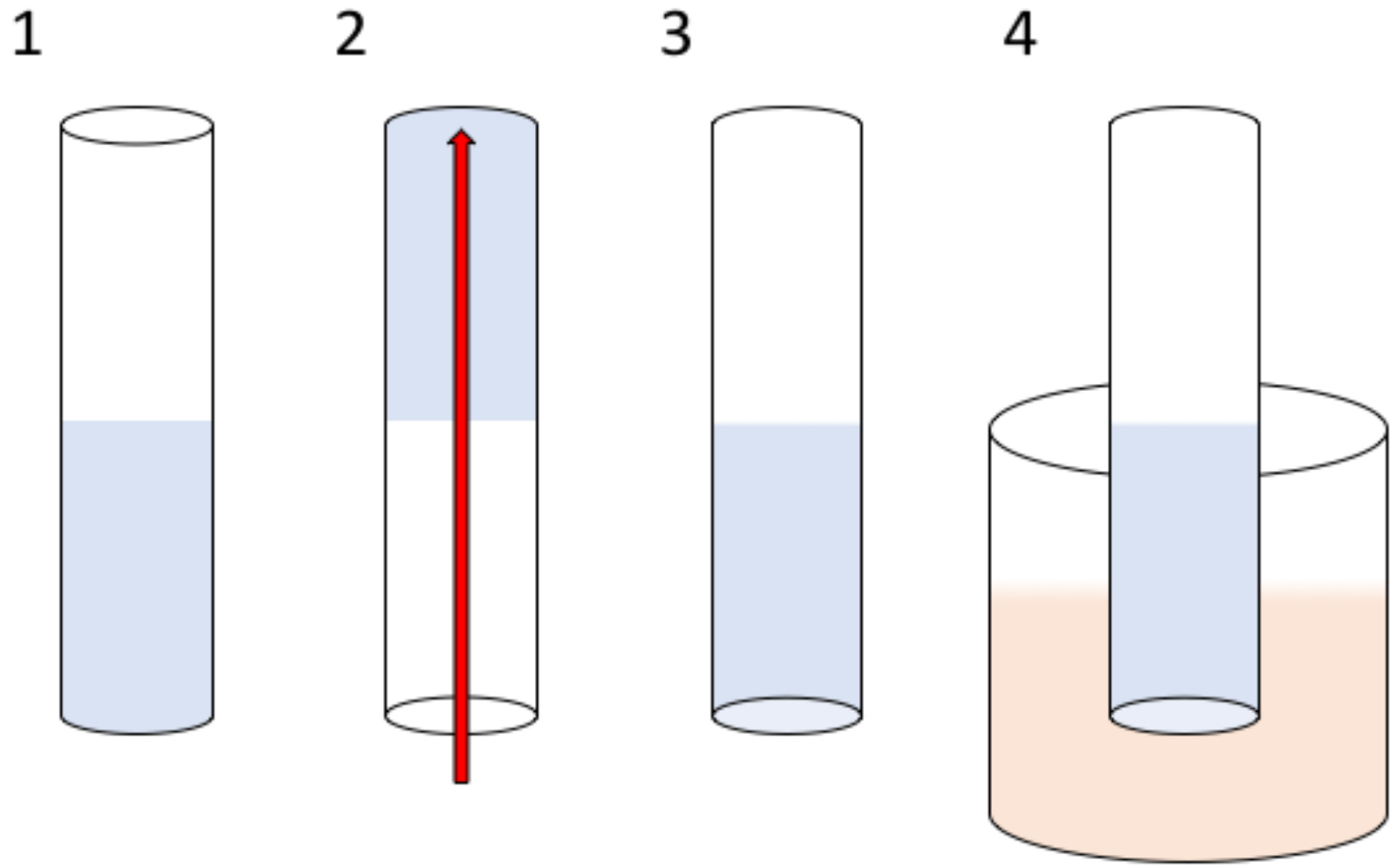

Figure 4.3: Modified method for measuring chemotaxis in methanotrophic bacteria.

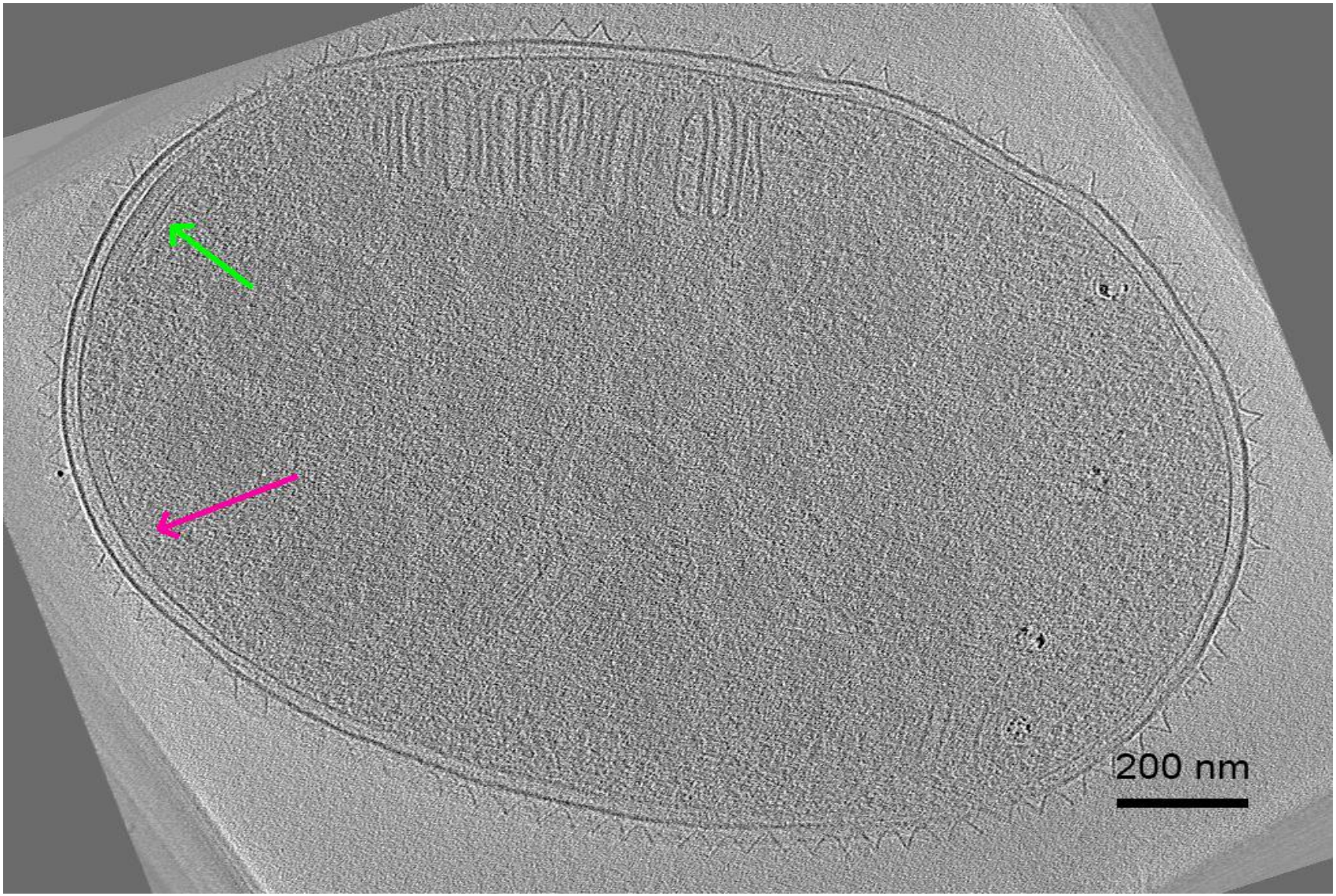

Figure 4.4: Electron cryotomograph of *M. alcaliphilum* 20Z^{R} showing chemotaxis sensor arrays.

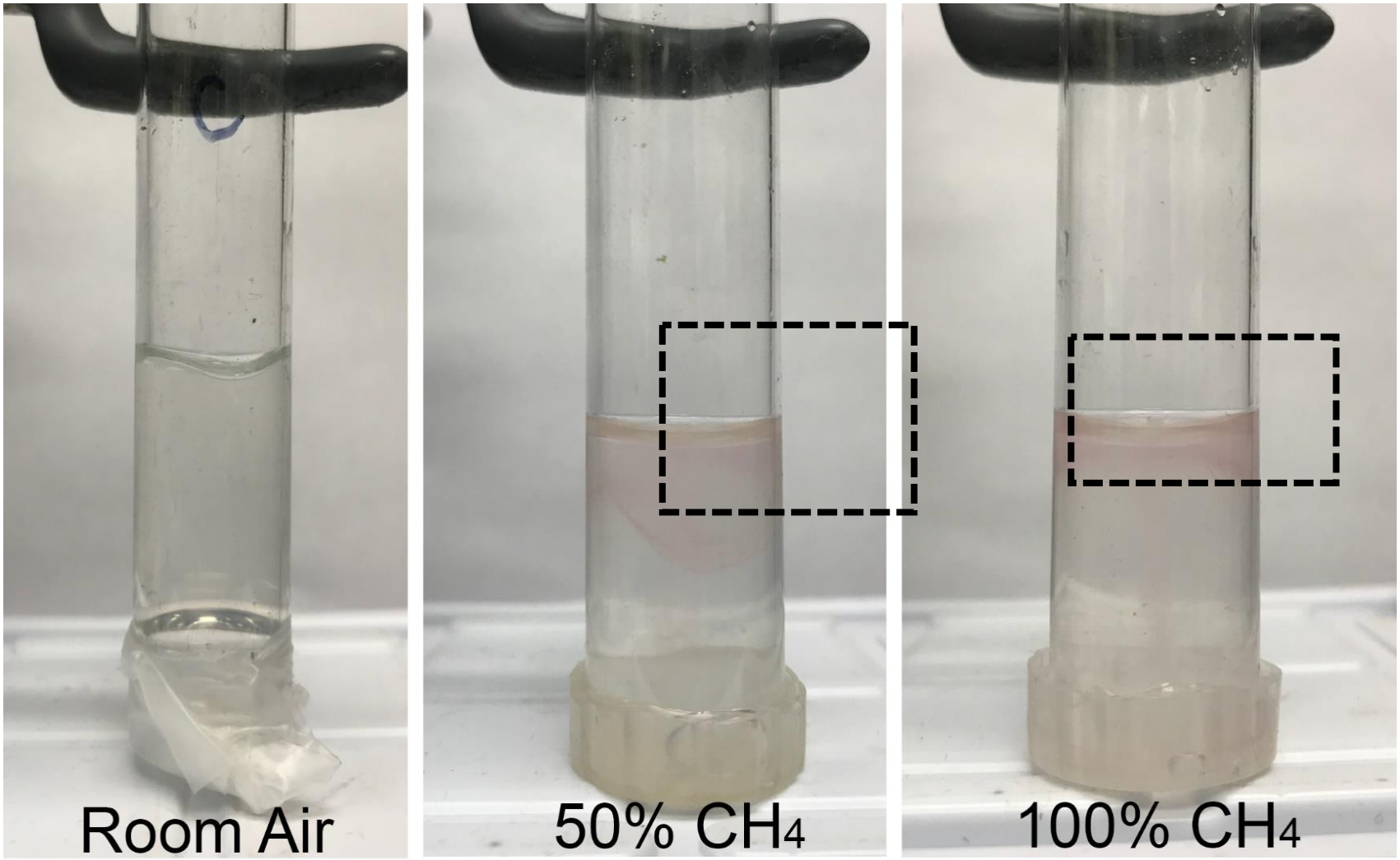

Figure 4.5: Chemotaxis Assay for wildtype *M. alcaliphilum* 20Z^{R}

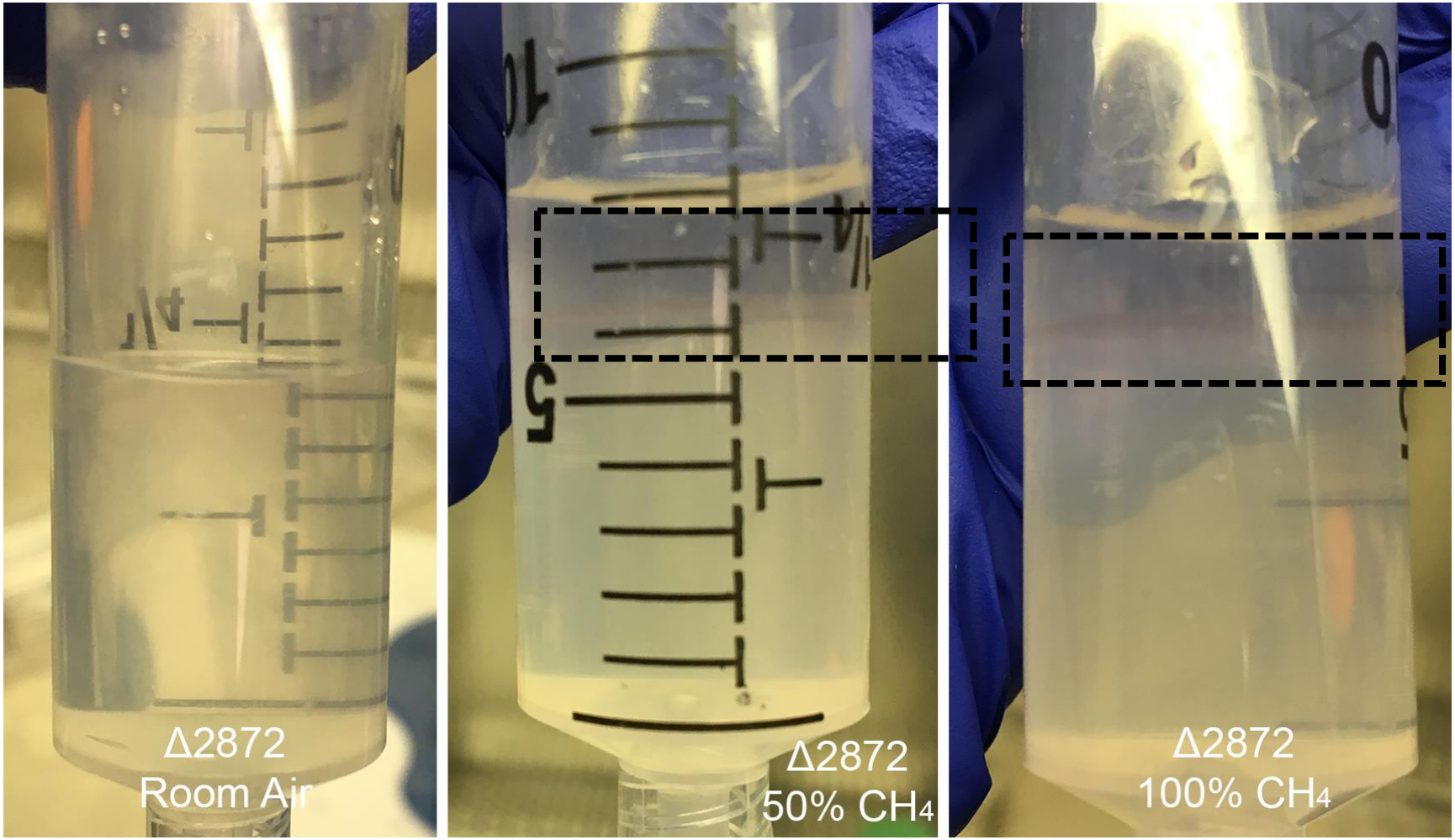

Figure 4.6: Chemotaxis assay in *M. aciliphilum* 20Z^{R} ΔMALCv4_2872

Table 4.1: F-Type clusters of identified chemotaxis genes

Chemotaxis Cluster I (F7)					
Label	Gene	Start	End	Length	Name
MALCv4_2869	cheY	3290769	3291131	363	Putative chemotaxis protein CheY
MALCv4_2870	cheA	3291296	3293338	2043	Chemotaxis protein CheA
MALCv4_2871	cheW	3293343	3293864	522	Chemotaxis protein CheW
MALCv4_2872		**3293907**	**3296270**	**2364**	**Methyl-accepting chemotaxis sensory transducer with Pas/Pac sensor**
MALCv4_2873	cheW	3296404	3296901	498	Chemotaxis protein CheW
MALCv4_2874		3296898	3297281	384	protein of unknown function
MALCv4_2875	cheR	3297284	3298147	864	Chemotaxis protein methyltransferase
MALCv4_2876	cheD	3298144	3298782	639	Chemotaxis protein CheD
MALCv4_2877	cheB	3298793	3299833	1041	Chemotaxis response regulator protein-glutamate methylesterase
MALCv4_2878		**3299844**	**3301049**	**1206**	**Methyl-accepting chemotaxis sensory transducer**
MALCv4_2879		3301098	3301406	309	conserved protein of unknown function (STAS domain-containing protein)
MALCv4_2880		3302502	3303464	963	protein of unkown function
MALCv4_2881		**3303561**	**3304181**	**621**	**Methyl-accepting chemotaxis protein**
Chemotaxis Cluster II (F8)					
Label	Gene	Start	End	Length	Name
MALCv4_2939		**3375856**	**3377889**	**2034**	**Methyl-accepting chemotaxis sensory transducer**
MALCv4_2940	cheW	3377914	3378480	567	CheW protein
MALCv4_2941	cheA	3378858	3381065	2208	CheA signal transduction histidine kinase
Chemotaxis Cluster III (F6)					
Label	Gene	Start	End	Length	Name
MALCv4_3148		3652000	3652377	378	Conserved protein of unknown function (DUF2802 domain-containing protein)
MALCv4_3149		3652377	3652550	174	Conserved protein of unknown function
MALCv4_3150	cheW	3652608	3653084	477	CheW
MALCv4_3151		3653260	3653979	720	Putative CheW protein
MALCv4_3153		3654892	3655785	894	putative flagellar motor protein MotD
MALCv4_3154	motA	3655952	3656719	768	Motility protein A
MALCv4_3155	cheB	3656719	3657822	1104	Chemotaxis response regulator protein-glutamate methylesterase 2
MALCv4_3156	cheA	3658130	3660415	2286	CheA signal transduction histidine kinase
MALCv4_3157	cheZ	3660426	3661151	726	Chemotaxis phosphatase, CheZ
MALCv4_3158	cheY	3661166	3661540	375	Chemotaxis protein CheY

Table 4.2: Z-score transformations of chemotaxis genes from proteome of starved cells.

Protein_Protein	Description_Description	Cyto_Cult_rep1	Cyto_Cult_rep2	Cyto_Fed_rep1	Cyto_Fed_rep2	Cyto_Starv_rep1	Cyto_Starv_rep2	Mem_Cult_Frac1_rep1	Mem_Cult_Frac1_rep2	Mem_Cult_Frac2_rep1	Mem_Cult_Frac2_rep2	Mem_Cult_Frac3_rep1	Mem_Cult_Frac3_rep2	Mem_Fed_Frac1_rep1	Mem_Fed_Frac1_rep2	Mem_Fed_Frac2_rep1	Mem_Fed_Frac2_rep2	Mem_Fed_Frac3_rep1	Mem_Starv_Frac1_rep1	Mem_Starv_Frac1_rep2	Mem_Starv_Frac2_rep2	Mem_Starv_Frac3_rep1	Mem_Starv_Frac3_rep2	MemPel_Cult_rep1	MemPel_Cult_rep2	MemPel_Fed_rep1	MemPel_Fed_rep2	MemPel_Starv_rep1	MemPel_Starv_rep2	Press_Cult_rep1	Press_Cult_rep2	Press_Fed_rep1	Press_Fed_rep2	Press_Starv_rep1	Press_Starv_rep2
gi|351716819|emb|CCE22484.1|	Methyl-accepting chemotaxis protein	1.4	1.9	1.8	1.4	0.8	1.6	0	-0.2	-0.2	-0.5	-0.3	-1	-0.7	-0.5	-0.6	-0.5	-0.2	-1.3	-1.2	-1.3	-1.1	-1	-0.2	-0.7	-0.7	-0.8	-0.8	-0.7	1.6	0.4	0.8	0.3	1.6	0.8
gi|351717017|emb|CCE22682.1|	Chemotaxis protein	1.9	1.1	1.6	2.5	1.1	0.5	-1.2	-1.2	-0.9	-0.6	-0.3	-1.2	-0	-0.3	-1.2	-0.9	-1.2	-0.9	0.2	-0.6	0.2	-0	-0.6	-1.2	-0.6	-0.6	0.2	0.5	-0	1.1	0.5	-0.6	1.3	1.3
gi|351717018|emb|CCE22683.1|	Chemotaxis protein methyltransferase	-0.4	1.6	1.6	-0.4	-0.4	-0.4	-0.4	-0.4	-0.4	-0.4	-0.4	-0.4	-0.4	-0.4	-0.4	-0.4	-0.4	-0.4	1.6	-0.4	4.3	-0.4	-0.4	-0.4	-0.4	-0.4	1.6	-0.4	-0.4	-0.4	-0.4	-0.4	-0.4	-0.4
gi|351717054|emb|CCE22719.1|	putative methyltransferase CheR	0.6	-0	1.3	0.4	-0.2	-0.4	-0.6	-0.6	-0.6	-0.5	-0.6	-0.5	-0.6	-0.5	-0.4	-0.4	-0.5	-0.5	-0.5	0.9	3.2	3.4	-0.6	-0.6	-0.6	-0.5	1.1	0.1	-0.6	-0.5	0.1	-0.6	0.4	0.4
gi|351717936|emb|CCE23601.1|	Chemotaxis protein PomA	0.9	0.6	-0.9	-1.2	-1.5	-1.2	0.6	0.9	1.8	0.9	1.8	1.2	-0	-0	0.3	-0	-0.3	-0.3	-0.3	-0.6	-0.9	-0	1.2	1.5	-0	-0.6	-0.6	-0.9	1.2	0.9	-0	-1.5	-1.5	-1.5
gi|351718398|emb|CCE24069.1|	Methyl-accepting chemotaxis protein	2.8	2.6	1.3	1.5	0.5	0.8	0.2	-0.5	-0.8	-0.8	-1	-1	-0.8	-0.3	-0.8	-0.8	-0	0.5	-0.5	-0.5	-0.5	-1	-0.5	-0.8	-0.8	-1	-0.3	-0.5	0.2	0.8	1.3	0.2	0.5	0.2
gi|351718461|emb|CCE24132.1|	putative chemotaxis protein, methyltransferase domain CheR	-0.5	-0.5	-0.5	-0.5	-0.5	-0.5	1.1	-0.5	-0.5	-0.5	-0.5	-0.5	-0.5	-0.5	-0.5	-0.5	1.1	-0.5	-0.5	1.1	3.2	1.1	1.1	-0.5	3.2	-0.5	-0.5	-0.5	-0.5	-0.5	-0.5	-0.5	-0.5	-0.5
gi|351718547|emb|CCE24218.1|	MCP methyltransferase/methylesterase, CheR/CheB	2.7	2.7	-0.4	2.7	-0.4	-0.4	-0.4	-0.4	-0.4	-0.4	-0.4	-0.4	-0.4	-0.4	-0.4	-0.4	-0.4	-0.4	-0.4	-0.4	-0.4	-0.4	-0.4	-0.4	-0.4	-0.4	-0.4	-0.4	2.7	-0.4	-0.4	-0.4	-0.4	-0.4
gi|351718861|emb|CCE24535.1|	Putative chemotaxis protein CheY	1.4	1.4	-0.5	-1.1	0.8	0.8	0.2	-2.4	0.8	-1.1	-1.1	0.2	0.2	1.4	0.2	0.2	0.2	-0.5	1.4	0.2	0.2	1.4	0.2	0.2	-0.5	-0.5	0.8	0.8	-2.4	0.2	0.2	-1.1	-0.5	-1.1
gi|351718864|emb|CCE24538.1|	Methyl-accepting chemotaxis sensory transducer with Pas/Pac sensor	1.4	1.5	1.6	0.7	1.2	0	-0.8	-1	0.9	0.1	1	0.9	0.2	-0.2	0.8	0.4	-1.5	-1.6	-1.1	-1.3	-0.3	0.1	0	0.7	-0.1	0.4	-0.2	-0.3	0.3	1.4	-0.1	-2.1	-1.4	-1.6
gi|351718865|emb|CCE24539.1|	Chemotaxis protein CheW	0.4	-1.2	-0.4	1.2	-1.2	0.4	-0.4	-1.2	0.4	0.4	1.2	-0.4	-1.2	-0.4	0.4	1.2	-1.2	1.2	2.8	-0.4	-1.2	-0.4	-0.4	0.4	1.2	-1.2	1.2	-1.2	-0.4	-0.4	0.4	1.2	0.4	-1.2
gi|351718867|emb|CCE24541.1|	Chemotaxis protein methyltransferase	2.5	4.1	0.8	0.8	-0.5	-0.5	-0.5	-0.5	-0.5	-0.5	-0.5	-0.5	0.8	0.8	-0.5	-0.5	-0.5	-0.5	-0.5	-0.5	-0.5	-0.5	-0.5	-0.5	-0.5	0.8	-0.5	-0.5	-0.5	0.8	-0.5	0.8	-0.5	-0.5
gi|351718868|emb|CCE24542.1|	Chemotaxis protein CheD	-0.9	-0.9	0	-0.9	-0.9	-0.9	0	2.6	1.3	1.3	1.3	0	0	1.3	0	0	1.3	-0.9	1.3	-0.9	0	0	0	0	-0.9	1.3	-0.9	1.3	-0.9	-0.9	-0.9	-0.9	-0.9	-0.9
gi|351718870|emb|CCE24544.1|	Methyl-accepting chemotaxis sensory transducer	1.4	2.1	2.1	1.9	1.2	0.7	-0.3	-0.4	0.4	-0.2	-0.1	0.3	0.1	-0.3	0.1	-0.7	-0.7	-1.3	-1.2	-1.2	-1.7	-1.2	0.4	0.8	0.1	-0.4	-0.9	-0.8	0.5	1	0.3	-1.4	-0.6	0.1
gi|351718873|emb|CCE24547.1|	Methyl-accepting chemotaxis protein	2.4	2.4	1.4	0.4	0.4	0.4	-0.1	0.4	-0.6	-0.6	-2	-0.6	1.4	0.9	-0.6	0.4	-1.6	-1.1	-0.6	-1.1	-1.1	-0.1	0.4	0.4	-0.6	-0.6	-0.6	-0.1	1.4	0.4	-0.6	-0.1	-0.1	-0.6
gi|351718931|emb|CCE24605.1|	Methyl-accepting chemotaxis sensory transducer	2.1	1.6	1.3	1.9	0.3	0.8	0.5	1	-0.5	0.2	-0.1	-0.3	-1	-0.8	-0.3	-0.8	-1	-1.3	-1	-1.3	-1.2	-1.3	-0.1	0.2	-0.3	-0.5	-1.1	-1	1.3	1.3	0.8	0.6	0.1	-0.3
gi|351718932|emb|CCE24606.1|	CheW protein	2.1	2.5	1.8	1.4	0.3	0.3	-1.1	-0.8	-1.1	-1.1	-0.5	-0.1	-0.8	-1.1	-0.8	0.6	-1.1	-0.8	-0.5	-0.5	0.3	0.3	-0.8	-0.5	-1.1	-0.8	1	-0.1	0.6	0.6	1.4	0.3	-0.1	0.3
gi|351719124|emb|CCE24798.1|	putative methyl-accepting chemotaxis sensory transducer	1.8	2.3	2.4	2.1	0.6	0.9	0.2	-0.1	-0.3	-0.5	0.2	0.1	0.1	-0.3	0.4	-0.3	-1.1	-1.1	-0.5	-1.8	-1.7	-1	-0.3	-0.3	-0.3	-0.6	-0.8	-0.8	0.4	0.1	0.7	-0.1	-0.3	0.1
gi|351719127|emb|CCE24801.1|	putative chemoreceptor glutamine deamidase CheD 1	-0.5	1.9	-0.5	-0.5	-0.5	-0.5	-0.5	-0.5	-0.5	-0.5	-0.5	-0.5	-0.5	1.9	-0.5	-0.5	-0.5	-0.5	-0.5	-0.5	-0.5	1.9	-0.5	-0.5	-0.5	-0.5	1.9	1.9	-0.5	1.9	1.9	-0.5	-0.5	-0.5
gi|351719141|emb|CCE24815.1|	CheW	0.9	0.9	2.3	1.8	1.6	1.9	-0.8	-0.8	-0.8	-0.6	-0.9	-1.1	-1.1	-0.3	-0.8	-0.6	-0.9	-0.8	0.3	-0.8	-0.6	-0.9	-0.6	-0.5	-0.3	-0.5	-0.3	-0.2	0.6	1.3	1.5	0.1	0.9	0.4
gi|351719142|emb|CCE24816.1|	putative CheW protein	-0.5	-0.5	-0.5	1.8	-0.5	-0.5	1.8	-0.5	-0.5	-0.5	1.8	-0.5	-0.5	-0.5	1.8	1.8	-0.5	-0.5	-0.5	-0.5	-0.5	1.8	-0.5	-0.5	-0.5	-0.5	-0.5	-0.5	-0.5	-0.5	1.8	-0.5	-0.5	1.8
gi|351719145|emb|CCE24819.1|	Motility protein A	1.5	1.5	0	-1.1	-1.1	0	0	0	0	1.5	0	1.5	0	1.5	0	-1.1	-1.1	-1.1	0	-1.1	-1.1	-1.1	1.5	1.5	0	0	0	0	0	0	1.5	-1.1	-1.1	-1.1
gi|351719147|emb|CCE24821.1|	CheA signal transduction histidine kinase	1.8	1.2	1.9	2	1	1.9	-0.7	-0.8	-0.8	-0.6	-0.8	-0.7	-0.7	-0.6	-0.8	-0.5	-0.9	-0.7	-0.5	-0.9	-0.8	-0.4	-0.4	-0.7	-0.6	-0.4	-0.4	-0.5	0.6	0.6	0.6	-0.4	1.9	0.9
gi|351719148|emb|CCE24822.1|	Chemotaxis phosphatase, CheZ	1.1	1.3	2.4	2.1	1.7	2	-0.7	-0.6	-0.7	-0.5	-0.7	-0.7	-0.7	-0.5	-0.7	-0.7	-0.7	-0.7	-0.6	-0.7	-0.7	-0.7	-0.6	-0.6	-0.7	-0.6	-0.6	-0.6	0.4	0.2	0.5	-0.5	1.2	1.3
gi|503914225|ref|WP_014148219.1|	MULTISPECIES: chemotaxis protein CheB	-0.2	-0.2	-0.2	-0.2	-0.2	-0.2	-0.2	-0.2	-0.2	-0.2	-0.2	-0.2	-0.2	-0.2	-0.2	-0.2	-0.2	-0.2	-0.2	-0.2	-0.2	-0.2	-0.2	-0.2	-0.2	-0.2	-0.2	-0.2	-0.2	-0.2	-0.2	3.9	3.9
gi|503915306|ref|WP_014149300.1|	chemotaxis protein CheA	2.8	2.2	1.6	3.1	0.3	1	-0.6	-0.6	-0.6	-0.8	-0.8	-0.6	-0.3	-0.3	-0.6	-0.6	-0.8	-0.3	-0.3	0	-0.3	0.3	-0.6	-0.3	-0.8	-0.6	-0.3	-0.6	-0.3	0.6	-0.6	-0.3	-0.3	-0.3
gi|503915377|ref|WP_014149371.1|	chemotaxis protein CheA	3.2	2.1	1.8	1.5	0.5	1.5	-0.7	-0.5	-0.6	-0.3	-0.3	-0.6	-0.7	-0.7	-0.7	-0.7	-0.7	-0.6	-0.6	-0.6	-0.7	-0.7	-0.3	-0.2	-0.7	-0.6	-0.3	-0.7	0.5	0.8	0.3	0.1	0.3	0.5
gi|503915568|ref|WP_014149562.1|	chemotaxis response regulator protein-glutamate methylesterase	0.7	0	-1.1	-0.6	-1.1	0	-1.1	-1.1	0.7	-1.1	0	0	1.9	-0.6	1.3	1.3	-1.1	0	0.7	-1.1	-0.6	1.9	-0.6	-0.6	0	1.9	0.7	1.9	-0.6	-0.6	0.7	-1.1	-0.6	-0.6
gi|503915586|ref|WP_014149580.1|	chemotaxis response regulator protein-glutamate methylesterase	-0.2	-0.2	-0.2	-0.2	-0.2	-0.2	-0.2	-0.2	-0.2	-0.2	-0.2	-0.2	-0.2	-0.2	-0.2	-0.2	-0.2	-0.2	-0.2	-0.2	3.9	3.9	-0.2	-0.2	-0.2	-0.2	-0.2	-0.2	-0.2	-0.2	-0.2	-0.2	-0.2	-0.2
gi|503915589|ref|WP_014149583.1|	chemotaxis protein CheY	0.9	0.4	2.7	2.7	-0	0.4	0.4	-0.9	-0.5	-0.9	-0	-1.3	0.9	-0	-0.5	-0	-0	1.3	1.3	-0.5	-0.5	-0	-1.7	-0.9	-0.9	-1.3	-0	-0	-0	-0	-0.5	-1.3	-0	0.4
gi|503916166|ref|WP_014150160.1|	methyl-accepting chemotaxis sensory transducer	0.5	0.8	0.2	-0.2	-1.2	-1.1	0.5	0.7	1.8	1.4	1.5	2.8	0.5	0.1	1.3	-0.3	-0	-0.6	-0.5	-0.8	-0.9	-0.3	0.2	-0	0.5	-0.6	-0.5	-0.8	0.1	-0.2	-0.8	-1.3	-1.2	-1.8
gi|802897967|ref|WP_046061245.1|	chemotaxis protein	1.3	1.2	0.7	0.9	1.2	-0.8	-0.5	0.1	1.3	0.6	1	0.1	1.3	-0	0.4	0.4	-1.1	-0.9	-0.9	-1.5	-1.5	-0.9	0.7	0.6	0.3	0.1	-0.8	-1.1	1.2	0.6	0.9	-1.9	-1.6	-1.4
gi|802899170|ref|WP_046061566.1|	chemotaxis protein CheR	0.3	0.1	-0.2	-0.3	-0.7	-0.7	-0.5	-0.7	-0.3	-0.7	-0.2	-0.3	-0.1	-0.3	-0.3	0.1	-0.1	-0.7	-0.7	0.3	4.5	2.7	-0.3	-0.5	-0.1	0.1	0.3	0.6	-0.2	-0.5	-0.1	-0.6	-0.1	0.2
gi|802899177|ref|WP_046061573.1|	chemotaxis protein CheB	1	4.8	1	1	1	-0.4	-0.4	-0.4	-0.4	-0.4	-0.4	-0.4	-0.4	-0.4	-0.4	-0.4	-0.4	-0.4	-0.4	-0.4	-0.4	-0.4	-0.4	-0.4	-0.4	-0.4	1	1	-0.4	-0.4	-0.4	-0.4	-0.4	-0.4
gi|802899199|ref|WP_046061595.1|	chemotaxis protein CheW	1.3	0.5	0.5	-0.2	-0.9	-0.2	2	1.3	-0.9	-0.2	1.3	-0.9	-0.2	2	-0.2	-0.2	-0.9	2	0.5	-0.2	-0.9	-0.9	0.5	-1.4	-0.9	-0.2	-0.9	1.3	-0.9	0.5	-0.9	-0.9	-1.4	0.5

Chapter 4, in part references data published by Ortega, D., Subramanian, P., Mann, P., Kjaer, A., Watts, K., Pirbadian, S., Collins, D., Kooger, R., Kalyuzhnaya, M., Pilhofer, M., Ringgaard, S., Briegel, A., Jensen, G. as “Repurposing a chemosensory macromolecular machine” (2020) in Nature Communications. The dissertation author was a contributing investigator and author of this material.

FUTURE OUTLOOK

Through many decades of study of methanotrophs their diversity and impacts on a global scale has been revealed. Their metabolism has demonstrated pathways and reactions which are the starting point for biotechnology based on the consumption of greenhouse gases like methane or other C_1-compounds like methanol. They will continue to be a model system for examining new aspects of cell biology as the research of my dissertation shows that multi-omics and structural studies paired with phenotypic analysis can continue to explore unknown properties of the methanotrophs.

Making room for the model

Previous research methods show the importance of modeling at the organismal level for methanotrophs. Incorporating this data while integrating structural changes and growth performance will create comprehensive models for *M. alcaliphilum* $20Z^R$ to test in new growth conditions. Systems level analysis in the future should incorporate all these types of data, paying special attention to the structural uniqueness of a model organism. These will involve incorporating the amounts of membranes within cells and the spatial volumes they occupy compared to the free cytosol. This would be an important constraint on the rates of reactions and potential number of enzymes or ribosomes available in the cell. This dissertation should also stress the importance of culture conditions on the outcomes of cell performance beyond the data gathered from multi-omics approaches. It is shown to be relevant in *M. alcaliphilum* $20Z^R$ that trace minerals can have a dramatic effect on cell structure resulting in shifts in metabolic capability. Some of the data suggested by experiments in Chapter 2 revealed a state of

possible overflow metabolism during some growth conditions. Using *M. alcaliphilum* as a model system it may be possible to refine the explanation for overflow metabolism.

Holistically it should be understood that cells must accomplish more than reactions in which substrate is converted to product. The cell must also assemble proteins which constitute the enzymes of these pathways and must transport enzymes to where reactions take place within the cell; in the case of *M. alcaliphilum* this would require navigating the volume of the intracytoplasmic membrane network. It becomes increasingly complex when multiple constraints are considered as a model system *M. alcaliphilum* would be ideal for examining these constraints because of the known changes to structure controlled by culture conditions. During overflow metabolism cells will excrete and incompletely catabolized substrate into formate for example. Presumably this excretion is a result of fast-growing cells balancing multiple factors within them. The overflow metabolic phenotype be based on two potential models: 1) The available real estate for metabolism is limited or 2) The constraint of biosynthetic costs limits reaction efficiency.

If the real estate hypothesis is correct cell volume including free cytosol in the volume occupied by ICMs constrains the space in which reactions can occur. This real estate is not solely in the dimension of volume but potentially also is the 2-dimensional real estate of the membrane plane, which is increased by the icms as well. The real estate of the cell is quantifiably for $20Z^R$ using some of the data presented in Chapter 2. The alternative hypothesis for cells entering overflow metabolism is related to protein biosynthesis which stipulates the synthetic costs of enzymes and proteins is not equal between pathways. The constraints of this hypothesis are related to the availability of

protein synthesis machinery including the number of ribosomes, the unequal availability of tRNA depending on protein codon usage and considering the ICM network may be related to required transport costs of proteins to reaction sites either in the periplasm or within the membranes of the cell.

A future synthesis of this data is called for including a model which can explain overflow metabolism in controlled states for *M. alcaliphilum* and can account for these two alternative hypotheses. It will include structural data to constrain rates of reactions as the cell constitutes multiple compartments based on examinations by electron microscopy. This future model would have to account for the complex flux of carbon through *M. alcaliphilum*. The core metabolic pathway is known in *M. alcaliphilum* but the division of biomass to sites such as membranes and cytosolic granules of glycogen will have to be accounted for in a comprehensive model of explaining overflow metabolism. In this way we should make room for a model of *M. alcaliphilum* which accounts for the space occupied in cells which does not participate in reactions overall but impacts synthetic costs and free real estate.

Membranes in two, three, and four dimensions

An area lacking definitive answers revealed by my research and through the many decades of ultrastructural examinations of methanotrophs is the formation of the intracytoplasmic membrane network. Previous studies as explained in Chapter 2 showed substrates such as CH_4 and O_2 to be important for the formation of the ICM network but in *M. alcaliphilum* my work demonstrates that micronutrients and minerals are the cause of the formation of such a dramatic structural feature change in the cell. A model system such as *M. alcaliphilum* would be ideal for studying at the individual cell

level the formation of the ICM network, which is key for methane oxidation by using a technique such as electron cyromicroscopy. This would enable the study of the formation of the ICMs at the level of resolution to definitively show the origination of ICMS from the site of the cell membrane.

This is of particular interest to me due to the similarities of ICMs to the mitochondrion. It should be addressed whether there are specific proteins involved with the gatekeeping of intracytoplasmic membranes as in the mitochondria; the mitochondrial contact site and cristae organizing system dubbed MICOS (Hessenberger, *et al.* 2017). It is not known in methanotrophs if there exists such a gatekeeping protein which regulates the diffusion or insertion of membrane proteins such as pMMO or the complexes of the electron transport chain into the ICM 2D plane. Such gatekeepers exist within the MICOS complex (Stoldt, *et al.* 2019); some proteins in the *M. alcaliphilum* 20Z^R genome show homology to one member Mic60. Discovery of such a complex may be important for future metabolic engineering of customized ICMs or for bestowing the much-admired *E. coli* with membrane complexes akin to ICMs for industrial fermentation.

Another aspect that is unclear and of interest for further study is if the ICM network truly forms vesicles or if the space of the lumen is continually connected with the periplasmic milieu. If the spaces within the ICMs are contiguous with the periplasm it would represent a huge change to the surface area to volume ratio presumed for a cell of this size. It would also pose numerous problems for protein export and targeting of molecules to the actual periplasm versus the ICM vesicular lumen, such as the enzymes involved in peptidoglycan synthesis. If these hypothetical ICM lumens are

distinct vesicles, they represent a novel compartment for the biochemistry of the cell which complicates models of the 3D space in the cell. Distinct lumens would constitute a nano-domain of the cell akin to the matrix of the mitochondrion. ICM vesicles with embedded complexes of the electron transport chain may create acidic compartments as protons are pumped into a confined volume not contiguous with the periplasm. This may provide a mechanism for an alkaliphilic organisms such as *M. alcaliphilum* to establish a proton gradient by the electron transport chain without neutralization from the ambient pH of culturing conditions.

Besides identifying a potential gatekeeper of the ICMs it should be determined how their position is regulated and maintenance through cell division occurs, such as segregation of ICMs to daughter cells. Is the division of ICMs to daughter cells always equal or does an asymmetry exist for the next generation in which they must synthesize more membranes (and proteins) than their sibling cell? It should be determined if cytoskeletal protein associations are important for controlling ICM positions throughout the cell, as is increasingly clear in bacterial that cytoskeletal proteins determine cell shape (Jamin, *et al.* 2018). The life cycle of the ICMs is also not understood; they must undergo some turnover, but no mechanism is understood in methanotrophs which accounts for the 4D lifespan of ICMs. Defective proteins or changes to lipid composition would require the membranes deep within the network of the cells ICM to undergo remodeling in composition overtime compared to newly synthesized regions of the network.

Seen in electron micrographs of Chapter 2 pre-existing granules within the cell are surrounded by sheets of intracytoplasmic membranes. Examinations with electron

cryotomography would reveal if any templating or organization of the formation of ICMs occurs from such preexisting structures within the cell. There are additional inclusions seen within the cell that are frequently much more electron-dense than any surrounding part of the cell and vary in diameter but are common features within methanotrophs. These dark bodies are only postulated in composition due to characteristics in electron micrographs to be composed of chemicals with many organic double-bonds such as unsaturated lipids. These warrant further examination for their exact composition, if they indeed represent storage of unsaturated fats in the cell it may facilitate extraction or be manipulated for production purposes. Taken together intracytoplasmic membrane network still has many unanswered questions to be answered in 2-, 3-, and 4-dimensions.

Is there more beneath the Surface (layer protein)?

The surface layer protein is the most intriguing of readily apparent features in methanotrophs. No definitive identifiable function based on this research and others has been able to determine precisely what benefit they serve. Their regulation indicates potential involvement in the acquisition of metals such as copper but requires further experiments to determine if they have any ability to bind to free metals outside of the cell. While I cannot surmise an exact role of the surface layer protein based on the mutants generated, it is not outside of reasoning that inadequate conditions were tested. The SLP also warrants additional structural characterization through crystallization of purified protein, characterization by atomic force microscopy, modeling by electron cryotomography or through electron diffraction modeling by microED.

Methods such as these may reveal if metal binding sites exist in the SLP and potentially capture bound metals to the protein.

A possible function may also be related to life in the environment, which does not exist in the lab - predation. Hypothetically the SLP may serve as a barrier to bacteriophages which would naturally predate a methanotroph in the nature. Mutants for the SLP would be an ideal candidate for the screening of bacteriophage libraries isolated from the environment towards *M. alcaliphilum*. Results from such an experiment would yield additional genetic tools for the engineering of *M. alcaliphilum* if lytic or lysogenic bacteriophages were identified. It is also possible the SLP itself could be a receptor for an unknown bacteriophage but no known bacteriophages of *M. alcaliphilum* 20Z^R have been discovered. This potential function for the SLP is in line with evidence that the SLPs in *Caulobacter* functions to deter predators such as *Bdellovibrio*, which are hindered from entering host cells by the surface layer protein RsaA (Awram & Smit, 1998). This potentially ecological function of the surface layer protein should be addressed by prospecting for predators, from viruses and bacteria to protists, isolated from similar haloalkali environments to *M. alcaliphilum* 20Z^R.

Nose and Noise

No definitive protein sensor responsible for methane-taxis in *M. alcaliphilum* was identified in my work, but still awaits discovery of the true receptor for this phenotype. This would truly be an exciting result as it could generate numerous technologies based on a native biosensor for methane. As referenced in the introduction to my dissertation, methane leaks are an increasingly disastrous problem from scales of consumer to community. A novel biosensor could not prevent large-scale leakage but distributing

information on the presence of low-level methane leaks would constitute savings for consumers and energy distributors. Such a biosensor would be the first of its kind for the detection of relevant gases and could utilize engineered genetic circuits downstream of the receptor like luciferase to signal the presence of methane. Presumably such a sensing system also exists in organisms capable of oxidizing larger alkanes such as ethane and propane like species identified within Deltaproteobacteria. In this way we can look towards the 'nose' of methanotrophs as indicators for the problems which arise from the integration of fossil fuels into the economy.

Many genes remain to be tested in *M. alcaliphilum* and as mentioned in Chapter 4, a high throughput method may be required to identify the function of some of these in methane sensing. I would propose the creation of mutant libraries either through chemical mutagenesis or transposon insertion. These libraries could easily be purified for mutants capable or incapable of methane-taxis and insertion sites or genetic lesions identified through sequencing to pinpoint the gene. Presumably multiple false positives would be generated such as mutants of the flagellar apparatus or in parts of the signal transduction pathway sharing crosstalk between other receptor systems. Both outcomes are likely, as non-motile bacteria and non-chemotactic bacteria would have the same phenotype in the assay. Similarly, mutants in regulatory roles of the signal transduction cascade may result in decrease sensitivity of the system or excessive inhibition which may have the same phenotypes despite not being involved in sensing of the substrate tested. This sort of 'noise' is surmountable with a model system that is amenable to genetic manipulations beyond random lesions. To overcome such a limitation for random mutagenesis I propose a contemporary approach of targeted mutagenesis at

multiple hit sites using a CRISPR system. With a sequenced genome and known CRISPR based technologies demonstrated in methanotrophs, adapting this technique to *M alcaliphilum* is possible. It may be feasible to potentially generate multiple mutants simultaneously using the native CRISPR system in *M. alcaliphilum* or a heterologous CRISPR system to target putative methane sensing gene targets rapidly. By bringing new molecular techniques to a classical phenotype such as chemotaxis the hurdles of noise to identifying the ‘nose’ of *M. alcaliphilum* can be reduced or eliminated.

References

Awram, P., & Smit, J. (1998). The *Caulobacter crescentus* paracrystalline S-layer protein is secreted by an ABC transporter (type I) secretion apparatus. *Journal of bacteriology*, *180*(12), 3062–3069. https://doi.org/10.1128/JB.180.12.3062-3069.1998

Hessenberger, M., Zerbes, R.M., Rampelt, H., Kunz, S., Xavier, A.H., Purfuerst, B., Lilie, H., Pfanner, N., van der Laan, M., Daumke, O. (2017). Regulated membrane remodeling by Mic60 controls formation of mitochondrial crista junctions. Nature Communications **8**:15258.

Jamin, N., Garrigos, M., Jaxel, C., Frelet-Barrand, A., Orlowski, S. (2018). Ectopic neo-formed intracellular membranes in *Escherichia coli*: a response to membrane protein-induced stress involving membrane curvature and domains. Biomolecules **8**(3): 88. https://doi.org/10.3390/biom8030088

Stoldt, S., Stephan, T, Jans, D.C., Brueser, C., Lange, F., Keller-Findeisen, J., Riedel, D., Hell, S.W., Jakobs, S. (2019). Mic60 exhibits a coordinated clustered distribution along and across yeast and mammalian mitochondria. Proceedings of the National Academy of Sciences **116**(20):9853-9858.